

# EXCHANGEABILITY OF GNN REPRESENTATIONS WITH APPLICATIONS TO GRAPH RETRIEVAL

005 **Anonymous authors**

006 Paper under double-blind review

## ABSTRACT

011 In this work, we discover a probabilistic symmetry, called exchangeability, in  
 012 graph neural networks (GNNs). Specifically, we show that the trained node em-  
 013 bedding computed using a large family of graph neural networks, learned under  
 014 standard optimization tools, are exchangeable random variables. This implies that  
 015 the probability density of the node embeddings remains invariant with respect to a  
 016 permutation applied on their dimension axis. This results in identical distribution  
 017 across the elements of the graph representations. Such a property enables approxi-  
 018 mation of transportation-based graph similarities by Euclidean similarities between  
 019 the sorted embedding elements in fixed dimension. This allows us to propose a  
 020 unified locality-sensitive hashing (LSH) framework that supports diverse relevance  
 021 measures for graphs, *e.g.*, subgraph matching, graph edit distance, *etc.* Experiments  
 022 show that our method provides more effective LSH than baselines.

## 1 INTRODUCTION

025 In their seminal work, [Hecht-Nielsen \(1990\)](#) first demonstrated that the output of multi-layer per-  
 026 ceptrons (MLPs) remains invariant under suitable permutations of the weight matrices across layers.  
 027 Since then, such weight-space symmetries have been widely recognized, and have resurfaced with  
 028 the advent of deep learning ([Neyshabur et al., 2015b](#); [Freeman et al., 2016](#); [Brea et al., 2019](#)). Recent  
 029 works ([Bui Thi Mai et al., 2020](#); [Godfrey et al., 2022](#)) characterized such symmetries for different  
 030 activation functions. Beyond academic interest, weight space symmetries underpin several practical  
 031 advances: for example, they enhance model training ([Neyshabur et al., 2015b](#)), equivariant architec-  
 032 ture design ([Cohen et al., 2016](#); [Maron et al., 2019](#); [Navon et al., 2023](#)), enable model merging ([Peña  
 033 et al., 2022](#); [Ainsworth et al., 2022](#)), motivate data augmentation ([Schürholt et al., 2021](#)), *etc.* They  
 034 also yield deeper characterizations of geometry and loss landscapes ([Brea et al., 2019](#); [Simsek et al.,  
 035 2021](#); [Entezari et al., 2021](#)). These works focus on algebraic symmetry largely for MLPs, and treat  
 036 them in isolation from training. This leaves unaddressed the probabilistic symmetry structures that  
 037 emerge naturally during standard training, starting with random model initialization.

038 **Our contributions** Instead of working on well-explored algebraic symmetries, we analyze the  
 039 probabilistic symmetries within trained embedding vectors which appear to exist in a broad class  
 040 of neural architectures. We move beyond simple MLPs and extend to the more complex setting of  
 041 graph neural networks (GNNs). As will gradually unfold, such an analysis for GNNs has significant  
 042 implications for applications including locality-sensitive hashing and efficient neural graph retrieval.

043 — *Characterization of exchangeability:* We establish a new property of GNNs: under standard  
 044 conditions, the elements of node embeddings computed by a trained GNN are exchangeable random  
 045 variables, where the randomness is induced by the initialization of model parameters. Let  $\mathbf{x}(u) \in \mathbb{R}^D$   
 046 denote the embedding of node  $u$ , produced by a trained GNN. Then, the joint distribution of its  
 047 components  $\mathbf{x}(u)[1], \dots, \mathbf{x}(u)[D]$  is invariant under any permutation of the embedding dimensions  
 048  $d \in [D]$ . This has a significant consequence: the components  $\mathbf{x}(u)[1], \dots, \mathbf{x}(u)[D]$  are identically  
 049 distributed random variables. Therefore, when averaged across multiple random seeds, the expected  
 050 embedding matrix  $\mathbb{E}[\mathbf{x}(u)]_{u \in V}$  collapses to a rank one matrix.

051 We would like to highlight that, we show such exchangeability holds for a wide spectrum of GNNs and  
 052 graph transformers; and several optimizers, *e.g.*, SGD, Adam. In view of GNNs’ known propensity  
 053 for spatial oversmoothing ([Roth et al., 2024](#)) and recent discoveries of output rank collapse of  
 054 transformers ([Dong et al., 2023](#); [Naderi et al., 2025](#)), and sequential state space models ([Joseph et al.,  
 055 2025](#)), this result is of independent interest.

—*Applications to graph retrieval:* In neural graph retrieval, the goal is to find corpus graphs  $C = \{G_c\}$  most relevant to a query graph  $G_q$ . Recent studies (Jain et al., 2024; Zhuo et al., 2022; Fey et al., 2020) make it clear that optimal transport-based (also called transportation-based) relevance distance between node embeddings performs significantly better than single-vector aggregation and graph kernels (Roy et al., 2022; Zhuo et al., 2022). Exchangeability enables efficient graph retrieval in two steps:

(1) Approximating transportation similarity with 1-D Euclidean approximations: Consider embeddings in one dimension ( $D = 1$ ). In this case, the transportation distance between two sets can be solved exactly by sorting the points in each set and matching them in order. For example, suppose we use a GNN to produce one-dimensional embeddings  $x(u) \in \mathbb{R}$ . Then, given two graphs  $G_q$  and  $G_c$ , each with  $n$  nodes, the transportation distance between their embedding sets is  $\text{Transport}(\{x^{(q)}(u)\}, \{x^{(c)}(u)\}) = \|\text{SORT}(\{x^{(q)}(u)\}) - \text{SORT}(\{x^{(c)}(u)\})\|$ . In higher dimensions ( $D > 1$ ), however, computing transportation-based distance (or transportation-based similarity) is substantially more complex, with exact algorithms scaling for  $n$  nodes as  $O(n^3)$  and often requiring  $O(n^2)$  approximations such as Sinkhorn iterations. Exchangeability provides a way around this: since embedding coordinates are identically distributed, each dimension yields a concentrated estimate of the underlying transportation-based similarity. Instead of solving the full high-dimensional transportation-based similarity, we approximate it by aggregating  $D$  simple Euclidean similarities across dimensions, thereby reducing “transportation distance between high dimensional vector sets” to an estimate based on per-dimension sorted orders, which is more amenable to indexing.

(2) Locality sensitive hashing (LSH) for graphs: LSH enables sublinear-time retrieval by hashing similar objects into the same bucket (Gionis et al.; Indyk et al., 1998; Charikar, 2002). Exchangeability lets us approximate costly transportation-based similarity with simple Euclidean similarity across embedding dimensions, making existing LSH schemes directly applicable. Notably, LSH for asymmetric transportation-based similarity has remained unexplored; our approximation provides the first principled approach, leveraging Roy et al. (2023). This yields a unified LSH framework that supports diverse graph relevance measures, from subgraph matching to graph edit distance with general costs.

## 2 PRELIMINARIES

**Notation** For a graph  $G = (V, E)$ , we denote  $\mathbf{A}$  as its  $n \times n$  adjacency matrix. We write  $[\cdot]_+ = \max\{\cdot, 0\}$  as the hinge or ReLU function,  $\mathcal{P}_n$  as the set of  $n \times n$  permutation matrices and  $[n] = \{1, \dots, n\}$  for any integer  $n$ . We denote  $\mathbf{P}$  and  $\pi$  to indicate  $n$  and  $D$  dimensional permutation matrices, respectively, which are applied on the nodes and their embedding vectors respectively.  $[\bullet] \in \{0, 1\}$  is indicator function. In the context of graph retrieval, we denote a query graph as  $G_q$ , a corpus graph as  $G_c$  with  $|V_q| = |V_c| = n$  after padding with suitable number of nodes; and, the set of corpus graphs as  $C$ . We also use  $\mathbf{A}_q$  and  $\mathbf{A}_c$  to denote their  $n \times n$  adjacency matrices. We use  $p(\cdot)$  to denote the density of any random variable. Given a group  $\mathcal{G}$ , a function  $f$  is  $\mathcal{G}$ -equivariant ( $\mathcal{G}$ -invariant) if  $f(gx) = gf(x)$  (resp.,  $f(gx) = f(x)$ ) for all  $g \in \mathcal{G}$ .

**Node embedding computation using GNN** Given the number of message passing steps (or layers)  $K$  and the dimension of node embeddings  $D$ , a graph neural network ( $\text{GNN}_\theta$ ) computes node embeddings  $\mathbf{x}_k(u) = \text{GNN}_\theta(G) \in \mathbb{R}^D$  for  $u \in V$  using  $K$  message passing steps. For brevity, we drop  $K$  to write  $\mathbf{x}(u) = \mathbf{x}_K(u)$ . We compute the embedding matrices  $\mathbf{X} \in \mathbb{R}^{n \times D}$  as  $\mathbf{X} = [\mathbf{x}(u)]_{u \in [n]}$ .  $\mathbf{X}[:, d] \in \mathbb{R}^n$  denotes the  $d$ -th column of  $\mathbf{X}$ . The operator  $\text{SORT}(\cdot)$  sorts an input vector in decreasing order. In the context of graph retrieval, we denote  $\mathbf{x}^{(q)}(u)$  and  $\mathbf{x}^{(c)}(u')$  to denote embeddings of node  $u \in [n]$  and  $u' \in [n]$  in the query and corpus graphs  $G_q$  and  $G_c$ , respectively. Similarly, we use  $\mathbf{X}^{(q)} = [\mathbf{x}^{(q)}(u)]_{u \in [n]} \in \mathbb{R}^{n \times D}$  and  $\mathbf{X}^{(c)} = [\mathbf{x}^{(c)}(u')]_{u' \in [n]} \in \mathbb{R}^{n \times D}$  to denote the embedding matrices.

The parameters  $\theta$  of the GNN are learned by minimizing a task specific loss function, which we denote as  $\text{loss}(\theta)$ . We assume that weights in  $\theta$  are initialized via iid sampling from popular distributions, and then some popular gradient-based update recipes are used for training.

**Exchangeability** Exchangeability implies that the joint density of the elements within a vector is permutation invariant with respect to the ordering of the elements.

**Definition 1** (Exchangeability (Aldous, 1985)). *Let  $\mathbf{Y}_d \in \mathbb{R}^n$  be random vectors for  $d \in [D]$ . We say  $\mathbf{Y}_1, \dots, \mathbf{Y}_D$  are exchangeable, if for all permutations  $\pi : [D] \rightarrow [D]$ , the probability density*

108    *functions of the sequence of vectors  $\{\mathbf{Y}_1, \dots, \mathbf{Y}_D\}$  is the same as that of  $\{\mathbf{Y}_{\pi(1)}, \dots, \mathbf{Y}_{\pi(D)}\}$ , i.e.,*  
 109     $p_{\mathbf{Y}_1, \dots, \mathbf{Y}_D}(\mathbf{y}_1, \dots, \mathbf{y}_D) = p_{\mathbf{Y}_{\pi(1)}, \dots, \mathbf{Y}_{\pi(D)}}(\mathbf{y}_1, \dots, \mathbf{y}_D)$  *for all realizations:  $\mathbf{Y}_d = \mathbf{y}_d$  for  $d \in [D]$ .*  
 110

111    **Order statistics** For a vector  $\mathbf{a}$ , we denote its order statistics by  $\text{SORT}(\mathbf{a})$ , obtained by sorting its  
 112    entries in decreasing order. For the node embedding matrix  $\mathbf{X}$ , we will frequently use  $\text{SORT}(\mathbf{X}[:, d])$ —  
 113    the order statistics of the  $d$ -th embedding dimension across all nodes.

114    **Overview of our analysis** (1) Distinct from algebraic symmetry, we characterize a new type  
 115    of probabilistic symmetry in the node embeddings  $\mathbf{X}$  of a graph  $G$ , which is computed using a  
 116    trained GNN starting with random model initialization. Specifically, we show that  $\mathbf{X}[:, 1], \dots, \mathbf{X}[:, D]$   
 117    are exchangeable random variables, where the randomness is induced by the initialization of the  
 118    model. (2) Given a query–corpus graph pair  $(G_q, G_c)$ , we exploit this property to approximate  
 119    the transportation-based similarity between  $\mathbf{X}^{(q)}$  and  $\mathbf{X}^{(c)}$  using Euclidean similarity between the  
 120    order statistics  $\text{SORT}(\mathbf{X}^{(q)}[:, d])$  and  $\text{SORT}(\mathbf{X}^{(c)}[:, d])$  for  $d \in [D]$ . (3) Building upon the proposal  
 121    of Roy et al. (2023), we develop a unified LSH (Charikar, 2002) method for several graph relevance  
 122    measures using the Fourier transform on the order statistics vectors. We further show that the resulting  
 123    algorithm is a valid LSH for the original transportation-based graph similarity.

### 124    3 EXCHANGEABILITY OF GNN REPRESENTATIONS

126    In this section, we characterize the probabilistic symmetry of node representations, explicitly  
 127    incorporating the effect of model training. Specifically, given the node representation matrix  
 128     $\mathbf{X} = [\mathbf{x}(u)]_{u \in [n]} \in \mathbb{R}^{n \times D} = \text{GNN}_\theta(G)$ , we show that  $\mathbf{X}[:, 1], \dots, \mathbf{X}[:, D]$  are exchangeable random  
 129    variables (Definition 1) across the axis of the embedding dimension, where  $\mathbf{X}[:, d] = [\mathbf{x}(u)[d]]_{u \in [n]}$ .  
 130    We first describe the setting for our analysis, followed by a high level explanation on why exchange-  
 131    ability will hold. Finally, we present the formal characterization.

#### 132    3.1 SETTING

134    We provide the four components of our settings. We emphasize that they are presented primarily for  
 135    technical completeness. They are not restrictive and, in fact, capture a broad class of settings.

136    **(1) Broad class of GNN architectures** We consider the a wide variety of GNN architectures, which  
 137    are listed in Appendix F. This list includes gated GNN (Gilmer et al., 2017), GIN (Xu et al., 2019),  
 138    GAT (Veličković et al., 2018), GCN (Kipf et al., 2017). Our analysis is likely to extend beyond these  
 139    cases, and also applies to graph transformers (Appendix F).

140    **(2) IID initialization of the parameters within a layer** The entries of the parameter matrix within  
 141    each layer are initialized in an i.i.d manner. This covers standard model initialization schemes,  
 142    including Kaiming (He et al., 2015) and Xavier initialization (Glorot et al., 2010).

143    **(3) Permutation invariance of loss function** We consider loss functions that are invariant to  
 144    permutations of elements in the node embedding vectors. This condition holds naturally in several  
 145    settings, including graph retrieval. Here, the loss, whether binary cross-entropy or pairwise ranking,  
 146    depends on the similarity between  $(G_q, G_c)$  via the transportation plan between  $\mathbf{X}^{(q)}$  and  $\mathbf{X}^{(c)}$ .  
 147    Since this similarity is invariant under permutations of embedding elements, the loss is likewise  
 148    permutation-invariant. This also applies to link prediction, when the similarity between nodes  $u$  and  
 149     $v$  is computed as the dot product  $\mathbf{x}(u)^\top \mathbf{x}(v)$ , which is permutation invariant w.r.t. elements of  $\mathbf{x}$ .

150    **(4) Broad class of optimizers** Our results hold for a broad class of gradient-based optimizers, *viz.*,  
 151    SGD (Zhang, 2004), Adam (Kingma et al., 2015), *etc.*

#### 152    3.2 WHY EXCHANGEABILITY HOLDS: A HIGH LEVEL EXPLANATION

154    **Exchangeability among initialized model parameters** Training begins with i.i.d. initialization of  
 155    the parameter matrices. Formally, consider a weight matrix  $\Theta$  whose entries are drawn i.i.d. from a  
 156    common distribution. Its joint distribution is invariant to column permutations: for any permutation  
 157    matrix  $\pi$ ,  $p(\Theta) = p(\Theta\pi)$ . When  $\Theta$  is applied to an input row vector  $\mathbf{x}$ , the output  $\mathbf{x}' = \mathbf{x}\Theta$  is  
 158    *equivariant* to column permutations of  $\Theta$ :  $\Theta \mapsto \Theta\pi \implies \mathbf{x}' \mapsto \mathbf{x}'\pi$ . Although permuting  $\Theta$   
 159    changes the values of  $\mathbf{x}'$ , an i.i.d. initialization ensures that all permutations are equally likely, so the  
 160    distribution of  $\mathbf{x}'$  is invariant:  $p(\mathbf{x}') = p(\mathbf{x}'\pi)$ . This statistical symmetry is precisely what we mean  
 161    by exchangeability of hidden units at initialization. Nonlinear activations  $\sigma$ , such as sigmoid or tanh,  
 being identical and applied pointwise, preserve this symmetry.

162 **Exchangeability in MLP Training** Consider a two-layer MLP with weights  $\Psi, \Theta$  and nonlinear  
 163 activations  $\sigma$ , which maps an input row feature vector  $\text{feat}$  to an output representation  $\mathbf{x}$  via  
 164  $\mathbf{x} = \sigma(\sigma(\text{feat} \Psi) \Theta)$ . As discussed, at initialization ( $t = 0$ ), exchangeability holds by construction:  
 165 the entries of  $\Theta_0$  ( $\Theta$  at  $t = 0$ ) are i.i.d., so  $p(\Theta_0) = p(\Theta_0 \pi)$ , and consequently  $p(\mathbf{x}) = p(\mathbf{x} \pi)$ .

166 As noted in Section 3.1 (3), the loss function is invariant to permutations of the embedding dimensions.  
 167 With all other randomness fixed by seeding, permuting the columns of  $\Theta_0$  yields identical losses  
 168 and hence equivariant gradients. Consequently, the training trajectories are permutation-equivariant:  
 169 for any  $\pi$ ,  $\Theta_0 \mapsto \Theta_0 \pi \implies \Theta_t \mapsto \Theta_t \pi$  for all epochs  $t$ . Combining  $p(\Theta_0) = p(\Theta_0 \pi)$  at  
 170 initialization, with permutation-equivariant training dynamics, we obtain  $p(\Theta_t) = p(\Theta_t \pi)$  and  
 171 hence  $p(\mathbf{x}) = p(\mathbf{x} \pi)$  for all  $t \geq 0$ .

### 173 3.3 FORMAL CHARACTERIZATION OF EXCHANGEABILITY

174 **Overview** Here, we seek to establish the afore-mentioned arguments for GNN to prove the ex-  
 175 changeability of the elements of the node embeddings. We prove this using four steps:

176 (1) **Permutation induced parameter transformation on GNN** (Lemma 2): Given  $\text{GNN}_\theta$  with par-  
 177 ameter set  $\theta$ , consider any permutation  $\pi \in \mathcal{P}_D$ . We show that there exists a bijective transfor-  
 178 mation  $\Gamma_\pi$  on  $\theta$  such that, for  $\theta' = \Gamma_\pi(\theta)$ , the elements of the node embeddings are permuted by  $\pi$ , *i.e.*,  
 179  $\mathbf{X} \mapsto \mathbf{X} \pi$ . We refer to  $\Gamma_\pi$  as a permutation-inducing transformation corresponding to  $\pi$ .

180 (2) **Gradient equivariance** (Lemma 3): We show that the gradient of loss is equivariant with respect  
 181 to a permutation inducing transformation  $\Gamma_\pi$ .

182 (3) **Invariance of the probability density of model parameters** (Lemma 4): We show that at any  
 183 stage of training, the model parameters are exchangeable—the probability density of the parameters  
 184  $\theta$  remains invariant to the transformation  $\Gamma_\pi$ .

185 (4) **Result on exchangeability** (Theorem 5): Using (1–3), we show that  $\mathbf{X}[:, 1], \dots, \mathbf{X}[:, D]$  are  
 186 exchangeable.

187 **Warmup: Constructing  $\Gamma_\pi$  for 2-layer MLP** We are given an MLP of the form  $\mathbf{x} =$   
 188  $\sigma(\sigma(\text{feat} \Psi) \Theta)$ . If we want to reorder  $\mathbf{x}$  by a given permutation  $\pi$ , we will transform  $\Theta \mapsto \Theta \pi$ ,  
 189 which will result in  $\mathbf{x} \mapsto \mathbf{x} \pi$ . Equivalently, suppose we write  $\theta = [\Psi^\top, \Theta]$ , then, we can introduce a  
 190 bijection  $\Gamma_\pi$  by  $\Gamma_\pi(\theta) := \theta \text{Diag}(\mathbb{I}, \pi)$ , which will result in output equivariance  $\mathbf{x} \mapsto \mathbf{x} \pi$ .

191 **Permutation induced parameter transformation on GNN** Constructing a similar transformation  
 192  $\Gamma_\pi$  is more involved for GNNs. The difficulty stems from the iterative message passing protocol:  
 193 permutations of parameters in one layer propagate through neighborhood aggregations, which can  
 194 entangle the symmetry across layers and makes it hard to identify  $\Gamma_\pi$  for popular GNNs, *e.g.*, gated  
 195 GNN (Li et al., 2016), (Gilmer et al., 2017) which is widely used in graph retrieval (Li et al., 2019;  
 196 Roy et al., 2022; Jain et al., 2024). Nevertheless, in the following, we formally establish that such  
 197 transformations can indeed be derived for GNNs (proven in Appendix E).

198 **Lemma 2.** *Given a graph  $G$  and a GNN architecture  $\text{GNN}_\theta$  described in Appendix F, let the*  
 199 *node embedding matrix of  $G$  be  $\mathbf{X} = \text{GNN}_\theta(G) \in \mathbb{R}^{n \times D}$ . Then, for any permutation matrix*  
 200  *$\pi \in \mathcal{P}_D$ , there exists a bijective transformation  $\Gamma_\pi$  with  $|\text{Det}(\partial \Gamma_\pi(\theta) / \partial \theta)| = 1$  such that  $\mathbf{X} \pi =$*   
 201  *$\text{GNN}_{\Gamma_\pi(\theta)}(G)$ . We call  $\Gamma_\pi$  a model transformation induced by permutation  $\pi$ .*

202 Given this characterization, we seek to reduce the problem of establishing exchangeability to estab-  
 203 lishing probabilistic symmetries in the model parameters  $\theta$  with respect to the transformation  $\Gamma_\pi$ .

204 **Equivariance of gradient under permutation induced parameter transformation** Since the  
 205 loss function is invariant to any permutation  $\pi$  of the node embeddings, it is also invariant to the  
 206 transformation  $\Gamma_\pi$  on  $\theta$  (Lemma 2). As a result, the corresponding loss landscape exhibits symmetry  
 207 under  $\Gamma_\pi$ . This symmetry, in turn, implies an equivariance property for the gradient, as formalized  
 208 below (proven in Appendix E).

209 **Lemma 3** (Gradient equivariance). *Given the setting described in Section 3.1. Let  $\Gamma_\pi$  be the*  
 210 *transformation on the GNN parameters  $\theta$ , induced by a permutation  $\pi$ , as introduced in Lemma 2.*  
 211 *We denote the loss function as  $\text{loss}(\theta)$ . Then the gradient of the loss  $\nabla_\theta \text{loss}(\theta)$  is equivariant under*  
 212 *transformation  $\Gamma_\pi$  of the parameters  $\theta$ .*

213 **Invariance of probability density of model parameters under the transformation  $\Gamma_\pi$**  Suppose  
 214 we shuffle the initial parameters within a layer. Then, from the gradient equivariance property  
 215 (Lemma 3) the resultant trajectory  $\{\theta_t \mid t \geq 0\}$  of  $\theta$  at different epochs  $t$ , will undergo an equivariant

transformation with respect to a permutation-induced bijection  $\Gamma_\pi$ . Since  $p(\theta_0) = p(\Gamma_\pi(\theta_0))$ , the observation will lead to invariance of the probability density of  $\theta_t$  for  $t \geq 0$  too, as stated below (proven in Appendix E).

**Lemma 4** (Invariance of density of  $\Gamma_\pi(\theta)$ ). *Given the setting described in Section 3.1. Let  $\{\theta_t \mid t \geq 0\}$  be the trajectory of the parameter  $\theta$  of a GNN across different training epochs  $t \geq 0$ . Then, we have:  $p(\theta_t) = p(\Gamma_\pi(\theta_t))$  for all  $t \geq 0$ .*

**Key results on exchangeability** Using Lemmas 2–4, we can show our key exchangeability results, stated as follows (proven in Appendix E).

**Theorem 5** (Exchangeability of embedding elements). *Given the setting described in Section 3.1. Then,  $\mathbf{X} = \text{GNN}_\theta(G)$  are exchangeable random variables, where the randomness is induced by the model initialization prior to training. That is,  $p(\mathbf{X}) = p(\mathbf{X}\pi)$ .*

Note that the above theorem can also be generalized for a joint distribution over multiple graphs. For example, in graph retrieval, is necessary to compute the joint distribution of the embeddings of the query and corpus graph pairs  $(G_q, G_c)$ . In such cases, we have the following result (proven in Appendix E).

**Proposition 6.** *Given two graphs  $G_q, G_c$ , let the settings in Section 3.1 hold true. Specifically, let us assume that the loss function be invariant to simultaneous permutations of the embeddings  $\mathbf{X}^{(q)} = \text{GNN}_\theta(G_q)$  and  $\mathbf{X}^{(c)} = \text{GNN}_\theta(G_c)$ . Then,  $\mathbf{Y} = [\mathbf{X}^{(q)}; \mathbf{X}^{(c)}] \in \mathbb{R}^{2n \times D}$  satisfies  $p(\mathbf{Y}) = p(\mathbf{Y}\pi)$ .*

**Scope of the result** We imposed a few simplifying assumptions only for brevity. In fact, our exchangeability results continue to hold even when these conditions are not explicitly met, including architectures that incorporate more complex operations such as normalization layers. Moreover, our results remain valid even when the loss itself is not permutation-invariant. This is because such losses may still exhibit invariance under a joint transformation consisting of (i) a permutation of intermediate representations; and, (ii) a corresponding permutation-induced transformation of the parameters in the subsequent layer (Appendix E.1.6).

## 4 APPLICATIONS TO GRAPH RETRIEVAL

**Graph retrieval** In graph retrieval, we are given a large number of corpus graphs  $C = \{G_c\}$  and the goal is to *efficiently* find out top- $b$  graphs that are relevant to a given query  $G_q$ . In a typical real-world application, the corpus database contains large number of graphs, necessitating efficient indexing and retrieval mechanisms, akin to other retrieval tasks. In this section, we exploit exchangeability to design a locality-sensitive hashing (LSH) method (Gionis et al.; Indyk et al., 1998; Charikar, 2002) that accommodates a wide variety of transportation-based graph distance measures in a unified framework. This would allow us to return the set of relevant items in a query time that is sublinear in the number of corpus items  $|C|$ .

We proceed in two steps: (1) We leverage our results on exchangeability (Theorem 5 and Proposition 6) to approximate the transportation-based graph similarity using Euclidean similarity, which is suited for LSH. (2) We build upon the proposal of (Roy et al., 2023) to design LSH for such approximate Euclidean similarity, which is also a valid LSH for the true transportation-based Euclidean similarity.

### 4.1 USE OF EXCHANGEABILITY TO DERIVE SIMILARITY OF GRAPHS IN EUCLIDEAN SPACE

**Transportation-based relevance distance between graphs** It is well established in the literature (Roy et al., 2022; Zhuo et al., 2022; Fey et al., 2020; Jain et al., 2024; Bommakanti et al., 2024) that transport distance between sets of node embeddings across query and corpus graphs results in better accuracy than graph kernels or pooled single-vector representation. These works have proposed different notions of transportation distances, *e.g.*, hinge distance for subgraph matching (Roy et al., 2022), graph edit distance (Jain et al., 2024; Zhuo et al., 2022, GED), *etc*. We unify these distances under a common relevance distance, computed using a function  $\rho$  convex, potentially asymmetric and decomposable between dimensions, *i.e.*,  $\rho(\mathbf{x}) = \sum_{d \in [D]} \rho(\mathbf{x}[d])$ .

$$\Delta(G_c, G_q) = \min_{\mathbf{P} \in \mathcal{P}_n} \sum_{u, u'} \sum_{d \in [D]} \rho(\mathbf{x}^{(q)}(u)[d] - \mathbf{x}^{(c)}(u')[d]) \cdot \mathbf{P}[u, u'] \quad (1)$$

If  $\rho(\bullet) = [\bullet]_+$ , then  $\Delta(G_c, G_q)$  captures the hinge distance for subgraph isomorphism (Roy et al., 2022); if  $\rho(\bullet) = e_\ominus \times [\bullet]_+ + e_\oplus \times [-\bullet]_+$  for some  $e_\ominus, e_\oplus > 0$ , then  $\Delta(G_c, G_q)$  captures GED, where  $e_\ominus$  and  $e_\oplus$  denote the costs of edge deletion and addition, respectively (Jain et al., 2024).

**Distance to similarity** Suppose the elements of the node embeddings are bounded by  $x_{\max}$ . Given cost function  $\rho$ , we compute  $\rho_{\max} = \max_{x, x' \in [-x_{\max}, x_{\max}]} \rho(x - x')$ . We define a score function  $s(x) = \rho_{\max} - \rho(x)$ , which converts the transportation-based distance in Eq. (1) to the following transportation-based similarity measure.

$$\text{sim}(G_c, G_q) = \max_{P \in \mathcal{P}_n} \sum_{u, u'} \sum_{d \in [D]} s(\mathbf{x}^{(q)}(u)[d] - \mathbf{x}^{(c)}(u')[d]) \cdot P[u, u']. \quad (2)$$

**Approximation of transportation-based similarity into Euclidean similarity** Owing to the random initialization of the parameters  $\theta$ ,  $\mathbf{x}^{(q)}(u)$  and  $\mathbf{x}^{(c)}(u')$  are random variables, which makes  $\text{sim}(G_c, G_q)$  a random scalar. Now,  $\text{sim}(G_c, G_q)$  is not amenable to indexing and search. To tackle this, we approximate this similarity using a simpler Euclidean similarity  $\text{sim}_d(G_c, G_q)$ , focusing on a single dimension  $d$ . This approximate similarity is also a random variable, due to the parameter initialization, but more amenable to approximate nearest neighbor search. As we will see shortly,  $\text{sim}_d(G_c, G_q)$  serves as a scaled approximation of  $\text{sim}(G_c, G_q)$  with high probability.

Proposition 6 suggests that the node embedding pairs of  $G_q$  and  $G_c$  are exchangeable across dimensions *i.e.*, if  $\mathbf{Y} = [\mathbf{X}^{(q)}; \mathbf{X}^{(c)}]$ , then we have:  $p(\mathbf{Y}) = p(\mathbf{Y}\pi)$  for any permutation  $\pi$ . This means that the elements of the embeddings have an identical distribution across different dimensions. This also yields an identical distribution in the output of the score function  $s(\cdot)$  across different embedding dimensions. This, in turn, allows us to approximate the score by evaluating it in any one dimension  $d$ :

$$\text{sim}_d(G_c, G_q) = \max_{P \in \mathcal{P}_n} \sum_{u, u'} s(\mathbf{x}^{(q)}(u)[d] - \mathbf{x}^{(c)}(u')[d]) \cdot P[u, u'] \quad (3)$$

By restricting Eq. (3) to a single dimension  $d \in [D]$ , the problem reduces to transportation cost between scalars. This — together with the property that  $s(\cdot)$  is concave (as  $\rho$  is convex) — allows us to simplify Eq. (3) (Appendix E) into a similarity function between the order statistics or the sorted vector of the node embedding elements in a fixed dimension. Specifically, we compute the order statistics:  $\text{SORT}(\mathbf{X}^{(q)}[:, d])$  and  $\text{SORT}(\mathbf{X}^{(c)}[:, d])$  and express the similarity function for dimension  $d$  in Eq. (3) as the similarity between these order statistics:

$$\text{sim}_d(G_c, G_q) = s(\text{SORT}(\mathbf{X}^{(q)}[:, d]) - \text{SORT}(\mathbf{X}^{(c)}[:, d])) \quad (4)$$

As the distance function  $\rho$  is decomposable  $\rho(\mathbf{x}) = \sum_d \rho(\mathbf{x}[d])$ , the score function satisfies:  $s(\mathbf{x}) = \sum_d s(\mathbf{x}[d])$ . Hence, we overload  $s(\bullet)$  as a function on scalars in Eq. (3), as well as vectors in Eq. (4).

As exchangeability results in an identical distribution of the above similarity across the dimension  $d$ , we will have the following concentrations (Proven in Appendix E):

**Proposition 7.** For any  $\epsilon > 0, \delta > 0$ , setting  $D > \frac{1}{\epsilon^2 \delta}$  ensures that, for some  $\beta_0 = O_D(1)$ , we have:

$$\Pr \left( \left| \text{sim}(G_c, G_q)/D - \text{sim}_d(G_c, G_q) \right| \leq \epsilon \right) \geq 1 - \beta_0 \delta. \quad (5)$$

## 4.2 LOCALITY SENSITIVE HASHING OF GRAPHS

**Locality sensitive hashing** Locality Sensitive Hashing (LSH) maps queries and corpus items to the same bucket with high probability when they are similar, and with low probability otherwise (Gionis et al.; Indyk et al., 1998; Charikar, 2002; Neyshabur et al., 2015a). This enables retrieving relevant graphs from  $\{G_c\}$  by searching only within the bucket where  $G_q$  gets hashed.

**Why will existing approaches not work?** If  $s(\cdot)$  in Eq. (4) were a symmetric Euclidean distance, we could directly apply existing LSH methods, such as grid-based projections for  $L_1$  (Andoni et al., 2006) or line projections for  $L_2$  (Datar et al., 2004). However, various common graph similarities are inherently asymmetric (refer to the examples below Eq. (1)). To address this limitation, we propose a new framework for LSH of graphs, starting with the definition of asymmetric-LSH for graphs under a general similarity measure (Neyshabur et al., 2015a).

**Definition 8.** Given  $Q, C$ , the domain of query and corpus graphs and a similarity measure  $\text{sim} : C \times Q \rightarrow \mathbb{R}$ . A distribution over mappings  $\mathcal{F} : Q \rightarrow \mathbb{N}$  and  $\mathcal{H} : C \rightarrow \mathbb{N}$  is called a  $(S_0, \gamma S_0, p, p')$ -

324 asymmetric LSH (ALSH) if, with  $p > p'$  and  $\gamma \in (0, 1)$ , the following conditions are satisfied.

325 (1)  $\Pr_{f \sim \mathcal{F}, h \sim \mathcal{H}}(f(G_q) = h(G_c)) \geq p$ , if  $\text{sim}(G_c, G_q) \geq S_0$ , (6)  
 326 (2)  $\Pr_{f \sim \mathcal{F}, h \sim \mathcal{H}}(f(G_q) = h(G_c)) \leq p'$ , if  $\text{sim}(G_c, G_q) \leq \gamma S_0$ .

328 **Intuition behind our approach** Suppose we estimate two vectors  $\widehat{\mathbf{T}}_{q,d}$  and  $\widehat{\mathbf{T}}_{c,d}$ , such that the  
 329 Euclidean similarity for dimension  $d$  in Eq. (4) can be expressed as  $\text{sim}_d(G_q, G_c) \propto \cos(\widehat{\mathbf{T}}_{q,d}^\top \widehat{\mathbf{T}}_{c,d})$ .  
 330 Then, the random hyperplane projections given by  $f(G_q) = \text{sign}(\mathbf{w}^\top \widehat{\mathbf{T}}_{q,d})$  and  $h(G_c) =$   
 331  $\text{sign}(\mathbf{w}^\top \widehat{\mathbf{T}}_{c,d})$  with  $\mathbf{w} \sim \mathcal{N}(0, I)$ , will be a valid LSH for  $\text{sim}_d$  (Charikar, 2002; Neyshabur et al.,  
 332 2015a). Since this Euclidean similarity is only a scaled approximation of the transportation-based  
 333 similarity  $\text{sim}(G_c, G_q)$  (Proposition 7), the same random hyperplane projection is a valid LSH for  
 334  $\text{sim}(G_c, G_q)$ . Hence, we now focus on obtaining such vectors  $\widehat{\mathbf{T}}_{q,d}$  and  $\widehat{\mathbf{T}}_{c,d}$  whose inner product  
 335 approximates  $\text{sim}_d$ .

336 **GRAPHHASH: Our approach for LSH for graphs** In their seminal work, Rahimi et al. (2007)  
 337 showed that kernels of the form  $\kappa(\mathbf{x} - \mathbf{x}')$  can be approximated using a product of finite-dimensional  
 338 Fourier features. Our approximate similarity  $\text{sim}_d(G_c, G_q) = s(\text{SORT}(\mathbf{X}^{(q)}[:, d]) - \text{SORT}(\mathbf{X}^{(c)}[:, d]))$   
 339 has a similar structure. However,  $s(\cdot)$  is generally not a kernel, because the underlying distance  
 340 measure can involve complex asymmetric structure (see examples following Eq. (1)). Hence, their  
 341 method cannot be directly applied. Roy et al. (2023) extended the approach to hinge-based similarities.  
 342 We build on their idea and generalize it to arbitrary graph similarity functions. Specifically, we  
 343 express  $\text{sim}_d(G_c, G_q)$  as an integral over dot products of two real vectors.

344 **Proposition 9.** For each  $u \in [n]$ , there exist vectors  $\mathbf{F}_{q,d}(\iota\omega_u)$ ,  $\mathbf{F}_{c,d}(\iota\omega_u) \in \mathbb{R}^4$  with different  
 345 Fourier frequency  $\omega_u$  for each node  $u$ , such that:  $\text{sim}_d(G_c, G_q)$  (Eq. (4)) can be expressed as:

$$\text{sim}_d(G_c, G_q) = \sum_{u \in [n]} \int_{\omega_u \in \mathbb{R}} \mathbf{F}_{q,d}(\iota\omega_u)^\top \mathbf{F}_{c,d}(\iota\omega_u) d\omega_u \quad (7)$$

349 To approximate the above integral into finite terms, we design the frequency sampling distribution  
 350 as  $p(\omega_u) \propto |S(\iota\omega_u)|$ , where  $S(\iota\omega)$  is the Fourier transform of the scoring function  $s(\bullet)$  when  
 351 applied on scalars. Given  $\omega = [\omega_1, \dots, \omega_n]$ , we use  $\mathbf{T}_{\bullet,d}(\omega) = [\mathbf{F}_{\bullet,d}(\iota\omega_u)/\sqrt{p(\omega_u)}]_{u \in [n]}$  to obtain  
 352 an equivalent expression for Eq. (7), as follows:

$$\text{sim}_d(G_c, G_q) = \mathbb{E}_{\omega_1, \dots, \omega_n \sim p(\bullet)} [\mathbf{T}_{q,d}(\omega)^\top \mathbf{T}_{c,d}(\omega)] \quad (8)$$

353 We prove it in Appendix E. One can show that  $\|\mathbf{T}_{q,d}(\omega)\|_2 = \|\mathbf{T}_{c,d}(\omega)\|_2$  for all  $G_q$  and  $G_c$ . Next,  
 354 we draw  $\{\omega^{(m)}\} \stackrel{iid}{\sim} p(\omega)$  to compute  $\widehat{\mathbf{T}}_{\bullet,d} \in \mathbb{R}^{4nM} \stackrel{\Delta}{=} [\mathbf{T}_{\bullet,d}(\omega^{(m)})]_{m \in [M]}$ , which will give:

$$\text{sim}_d(G_c, G_q) \propto \cos(\widehat{\mathbf{T}}_{q,d}^\top \widehat{\mathbf{T}}_{c,d}) \quad (9)$$

355 **Overall routine (GRAPHHASH)** Finally, we use the random hyperplane method to compute hash  
 356 codes  $f(G_q)$  and  $h(G_c)$ . Given  $\dim_T$ , the dimension of  $\widehat{\mathbf{T}}_{\bullet,d}$  and  $\dim_h$ , the size of a hashcode,  
 357 we first draw  $\mathbf{W} \in \mathbb{R}^{\dim_h \times \dim_T}$  with  $\mathbf{W}[r, t] \stackrel{iid}{\sim} \mathcal{N}(0, 1)$  and then set  $h^{(d)}(G_c) = \text{sign}(\mathbf{W}^\top \widehat{\mathbf{T}}_{c,d})$   
 358 (Algorithm 1). During query execution, we return top- $b$  corpus graphs  $\{G_c\}$  which belong to the  
 359 hash bucket  $f^{(d)}(G_q)$  where,  $f^{(d)}(G_q) = \text{sign}(\mathbf{W}^\top \widehat{\mathbf{T}}_{q,d})$  (Algorithm 2). The family of these hash  
 360 functions gives a valid LSH. We call our method as GRAPHHASH. We provide LSH guarantees for  
 361 GRAPHHASH in Appendix E.

---

362 **Algorithm 1** Indexing phase of GRAPHHASH

---

363 **Require:** Corpus  $\{G_c\}$ , score function  $s(\bullet)$   
 364 frequency samples  $\{\omega^{(m)}\}$ .  
 365 1:  $\mathbf{W}[i, j] \sim \mathcal{N}(0, 1)$ ,  $i \in [\dim_h]$ ,  $j \in [\dim_T]$ .  
 366 2: **for all**  $G_c$  and  $d \in [D]$  **do**  
 367 3: Use  $s(\cdot)$  to compute  $\mathbf{F}_{c,d}(\iota\omega_u^{(m)})$  from  
 368  $\text{SORT}(\mathbf{X}^{(c)}[:, d])$  for all  $d, m$   
 369 4: Compute  $\widehat{\mathbf{T}}_{c,d}$  from  
 370  $\{\mathbf{F}_{c,d}(\iota\omega_u^{(m)})\}$  and  $\{p_\lambda(\omega_u^{(m)})\}$   
 371 5:  $h^{(d)}(G_c) = \text{sign}(\mathbf{W}^\top \widehat{\mathbf{T}}_{c,d})$   
 372 6: Store  $G_c$  in the bucket indexed by  $h^{(d)}(G_c)$   
 373 7: Store  $\mathbf{W}$  for use in the query phase

---



---

374 **Algorithm 2** Query phase of GRAPHHASH

---

375 **Require:** Query  $G_q$ , stored hyperplanes  $\mathbf{W}$ ,  
 376 frequency samples  $\{\omega^{(m)}\}_{m=1}^M$   
 377 1:  $\mathcal{R} \leftarrow \emptyset$   
 378 2: **for**  $d \in [D]$  **do**  
 379 3: Given  $s(\cdot)$ , compute  $\mathbf{F}_{q,d}(\iota\omega_u^{(m)})$  from  
 380  $\text{SORT}(\mathbf{X}^{(q)}[:, d])$  for all  $d, m$   
 381 4: Compute  $\widehat{\mathbf{T}}_{q,d}$  from  
 382  $\{\mathbf{F}_{q,d}(\iota\omega_u^{(m)})\}$  and  $\{p_\lambda(\omega_u^{(m)})\}$   
 383 5:  $f^{(d)}(G_q) = \text{sign}(\mathbf{W}^\top \widehat{\mathbf{T}}_{q,d})$   
 384 6:  $\mathcal{R} \leftarrow \mathcal{R} \cup \{G_c : G_c \in \text{Bucket}(f^{(d)}(G_q))\}$   
 385 7: **Return** Top- $b$  graphs from  $\mathcal{R}$

---

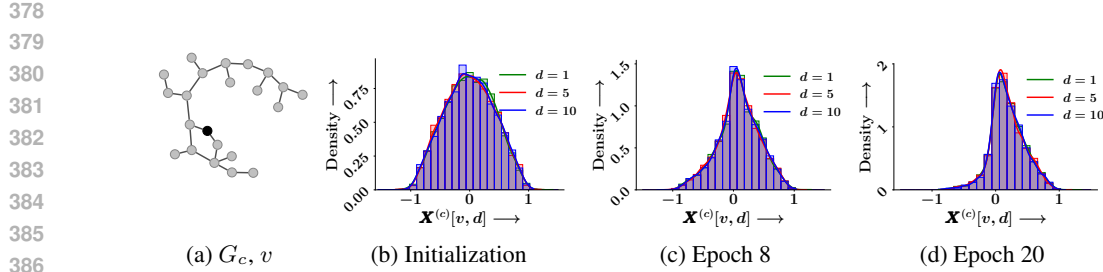


Figure 1: Empirical probability density of  $\mathbf{X}^{(c)}[v, d]$  the highlighted node  $v$  in the example corpus graph  $G_c$  in `cox2`, obtained using 5000 independently trained instances of the GNN model for Subgraph Matching based graph retrieval. Panels (b)–(d) show the density of  $\mathbf{X}^{(c)}[v, d]$  after model initialization and different stages of training.

## 5 EXPERIMENTS

We organize our experiments in two parts: first, we empirically validate the exchangeability property of GNN-based graph embeddings (Theorem 5); second, we evaluate the retrieval effectiveness of GRAPHHASH across multiple datasets. Appendix H shows additional experiments.

### 5.1 EMPIRICAL VALIDATION OF EMBEDDING EXCHANGEABILITY

**Validation using marginal distribution** We verify a necessary condition of exchangeability in the following experiments: identical marginal distribution of the embedding elements for a fixed node across independently initialized and trained models. For this setup, we train 5,000 independently initialized GNN models on a small subset of the `cox2` dataset, consisting of 1,024 query-corpus graph pairs. Each model is trained for 20 epochs using the Adam optimizer with an embedding size  $D = 10$ , by minimizing a ranking loss for a subgraph matching based graph retrieval task. For each trained model, we extract the embedding vector for a fixed, node  $v$  from one graph  $G_c$  and record the scalar values  $\mathbf{X}^{(c)}[v, d]$  for  $d \in [D]$ . This yields an empirical distribution of  $\mathbf{X}^{(c)}[v, d]$  across model instances for each  $d \in [D]$ .

Figure 1 shows the empirical probability density of  $\mathbf{X}^{(c)}[v, d]$  for three representative dimensions  $d = 1, 5, 10$ , at three points in training: initialization, epoch 8, and epoch 20. We observe that the distributions remain identical across the embedding dimensions throughout training. This validates the necessary condition of our result that the embedding dimensions are exchangeable under random initialization and remain so despite backpropagation, non-convex losses.

**Direct test for exchangeability** The marginal distributions do not capture more complex dependencies between dimensions, which is why we make use of the maximum mean discrepancy to quantify the gap between the distribution of  $\mathbf{X}$  and  $\mathbf{X}\pi$ . We sample 100 different permutations and compute the estimator of  $\text{MMD}^2$  for each permutation, and report the average over these 100 observations. Note that estimator of  $\text{MMD}^2$  can be negative. Table 2 shows that the MMD values are extremely small for `cox2` dataset for both GED and subgraph matching (SM). These results strongly support that  $p_{\mathbf{X}}$  and  $p_{\mathbf{X}\pi}$  are close.

**Rank of  $\mathbb{E}[\mathbf{X}]$**  Another consequence of exchangeability is that the expectation of the graph embedding matrix  $\mathbb{E}[\mathbf{X}]$  is rank one. Consequently, we expect the leading singular value of the sample mean graph embedding matrix to be significantly larger than the rest. Figure 3 shows how the ratio  $\frac{\sigma_1^2}{\sum_i \sigma_i^2}$  varies over multiple runs, where  $\sigma_1, \dots, \sigma_n$  are the singular values of  $\mathbb{E}[\mathbf{X}]$ , sorted in decreasing order. We observe that this fraction converges to one, which indicates that the rank of the embedding matrix is 1.

cox2 (GED)	$-3.89 \times 10^{-5} \pm 2.69 \times 10^{-5}$
cox2 (SM)	$-1.18 \times 10^{-6} \pm 3.28 \times 10^{-5}$

Table 2: Estimator for unbiased  $\text{MMD}^2$  for  $p_{\mathbf{X}}$  and  $p_{\mathbf{X}\pi}$  for `cox2` dataset

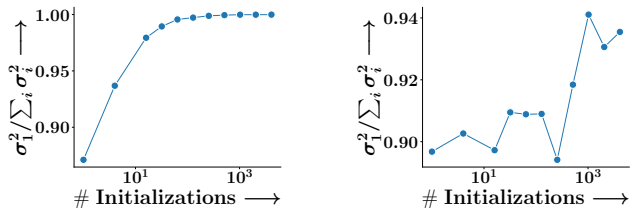
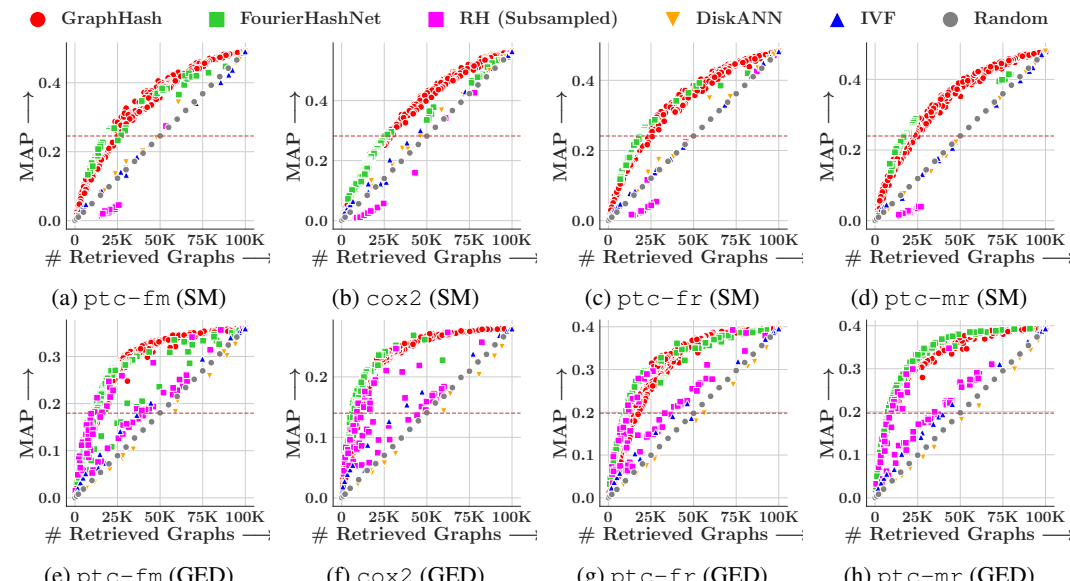
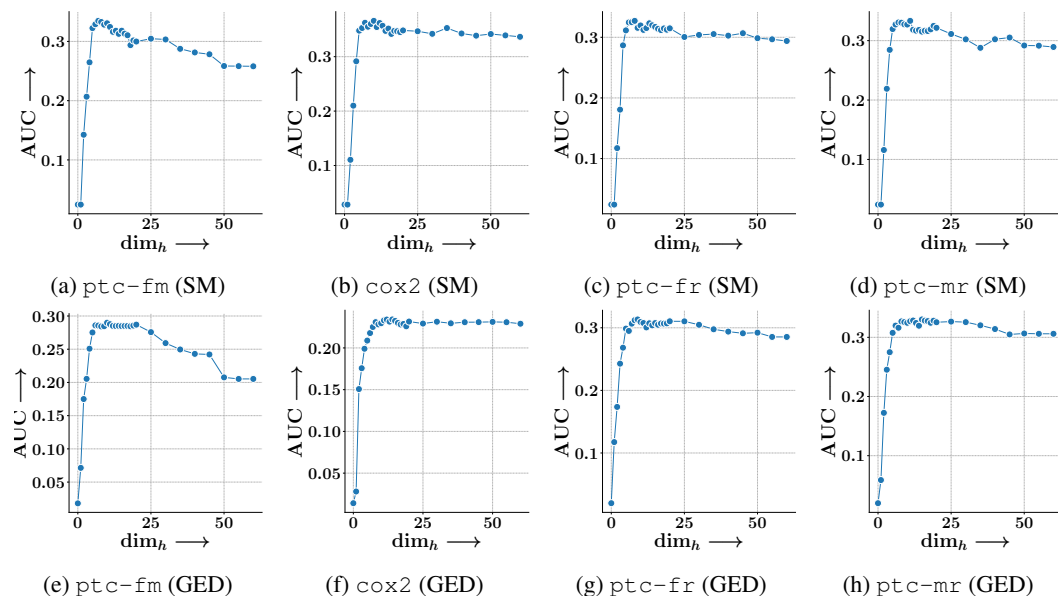


Figure 3: The relative size of the top singular value of the mean (trained) embedding across model initializations.

432 5.2 EVALUATION OF GRAPHHASH’S RETRIEVAL PERFORMANCE  
433434 We evaluate GRAPHHASH against existing baselines on four datasets to assess retrieval accuracy-  
435 efficiency trade-offs across indexing strategies.436 **Setup** We construct retrieval datasets using four real-world benchmarks from the TUDatasets (Mor-  
437 rris et al., 2020): `ptc-fr`, `ptc-fm`, `cox2`, and `ptc-mr`. Each dataset consists of 500 query graphs  
438 and a corpus of 100,000 graphs, following related work (Roy et al., 2022; Lou et al., 2020). We  
439 generate binary relevance labels under two asymmetric graph similarity signals: **(1) Subgraph**  
440 **Matching (SM):** Relevance is determined using the VF2 subgraph matching algorithm (Hagberg  
441 et al., 2020). Here, we set binary relevance  $\text{rel}(G_c, G_q) = \llbracket G_q \subset G_c \rrbracket$ , where  $\llbracket \bullet \rrbracket$  is the indicator  
442 function. **(2) GED:** We use the GEDLIB toolkit (Blumenthal et al., 2019) to compute edit distances  
443 with asymmetric costs  $e_{\oplus} = 1$  (insertion) and  $e_{\ominus} = 2$  (deletion), followed by thresholding to obtain  
444 binary relevance. Here, we set  $\text{rel}(G_c, G_q) = \llbracket \text{GED}(G_c, G_q) \leq \tau \rrbracket$ , where  $\tau$  is a threshold. For each  
445 supervision type, we train a separate transport-based scoring model using the relevance distances for  
446 Subgraph Matching and for GED. The model is trained using a pairwise ranking loss (Roy et al., 2022;  
447 Jain et al., 2024) of the form  $\sum_q \sum_{c:\text{rel}(G_c, G_q)=1, c':\text{rel}(G_{c'}, G_q)=0} [\Delta(G_c, G_q) - \Delta(G_{c'}, G_q) + \gamma]_+$   
448 where  $\gamma$  is a fixed margin, and  $\Delta(\cdot, \cdot)$  denotes the transport-based relevance distance (Eq. (1)). We  
449 evaluate retrieval performance using both MAP and NDCG. The analysis presented below focuses on  
450 MAP, while NDCG results and additional experiments are in Appendix H.  
451452 We benchmark GRAPHHASH against five competitive ANN methods adapted to graph retrieval. These  
453 include single-vector and multi-vector indexing paradigms. **(I) FourierHashNet (Roy et al., 2023):** It  
454 implements an LSH tailored for shift-invariant asymmetric distances by projecting graph embeddings  
455 into the Fourier space. Each graph  $G_{\bullet}$  is represented as a single vector  $\mathbf{z}_{\bullet} = \frac{1}{|V_{\bullet}|} \sum_{u \in V_{\bullet}} \mathbf{x}(u)$ ,  
456 where  $\mathbf{X} = [\mathbf{x}(u)]_{u \in [n]}$ . **(II) Random Hyperplanes (RH) (Charikar, 2002; Indyk et al., 1997):**  
457 It serves as a classic LSH baseline, where we directly hash mean pooled graph representations using  
458 random linear projections. **(III) IVF (Douze et al., 2024):** It follows the FAISS-based ColBERT-  
459 style approach, constructing a dense inverted index over the collection of corpus node embeddings,  
460 and probes with individual query node vectors, followed by aggregating the hits at the graph level.  
461 **(IV) DiskANN (Simhadri et al., 2023)** follows a similar multi-vector setup but leverages an HNSW  
462 index over corpus node embeddings. Lastly, we include a **Random** baseline that retrieves a uniformly  
463 sampled subset of corpus graphs. Appendix G contains additional details about the setup.481 Figure 4: Trade-off between mean average precision (MAP) and number of retrieved graphs, for  
482 GRAPHHASH, FourierHashNet (Roy et al., 2023), Random Hyperplane (RH) (Charikar, 2002; Indyk  
483 et al., 1997), IVF (Douze et al., 2024), DiskANN (Simhadri et al., 2023) and Random, across all  
484 datasets. Top row: Retrieval based on Subgraph Matching (SM); Bottom row: Retrieval based on  
485 GED. Horizontal red line denotes 50% of exhaustive MAP. Our method shows a better trade-off than  
486 others in majority of the cases.

486 **Results** We vary hyperparameters in each method to produce different retrieval set sizes, yielding  
 487 MAP vs. # retrieved graphs trade-offs shown in Figure 4. The key observations are as follows.  
 488 **(1)** GRAPHHASH consistently outperforms all baselines across both Subgraph Matching (SM)  
 489 and Graph Edit Distance (GED), with FourierHashNet emerging as the next-best method overall.  
 490 **(2)** FourierHashNet fails to span the full selectivity spectrum, particularly on SM tasks—most notably  
 491 on ptc-fr and ptc-mr, where its MAP plateaus below 50% of the exhaustive MAP. **(3)** RH  
 492 hashing performs reasonably well on GED, occasionally matching GRAPHHASH in MAP. However,  
 493 it exhibits high variance at fixed selectivity levels, complicating hyperparameter tuning. On SM tasks,  
 494 RH performs worse than random, which is expected since cosine similarity over pooled vectors is  
 495 ill-suited to the asymmetric nature of containment queries. **(4)** DiskANN and IVF, despite using  
 496 multi-vector indexing, perform poorly due to their reliance on symmetric similarity metrics like  $L_2$   
 497 and cosine, which are incompatible with the asymmetric transport-based supervision. **(5)** Random  
 498 sampling yields substantially lower MAP compared to both GRAPHHASH and FourierHashNet,  
 499 highlighting the non-trivial structure captured by learned or LSH-based methods.  
 500

501 Next, we vary  $\text{dim}_h$  (number of hash bits) and obtain different trade-off curve between MAP and #no  
 502 of retrieved graphs. We plot the variation of AUC against  $\text{dim}_h$ , which shows at around  $\text{dim}_h = 10$ ,  
 503 we obtain an optimal trade-off.  
 504



510  
 511 Figure 5: Performance of GRAPHHASH across different choices for  $\text{dim}_h$ , the size of the hashcode.  
 512 We summarize the trade-off plot between MAP and the number of retrieved graphs by computing  
 513 the area under the curve after normalizing the x-axis. We observe that the optimal size is around  
 514  $\text{dim}_h = 10$  across datasets and tasks.  
 515

## 516 6 CONCLUSIONS

517 Taking a step beyond existing notions of algebraic symmetries in neural architectures and losses, we  
 518 introduce the property of exchangeability over neural graph embeddings. We show that this property  
 519 is exhibited by a broad class of graph neural networks across a broad class of loss functions and  
 520 optimizers. We utilize this property to obtain a concentration bound for reducing transport problems  
 521 on node embeddings, culminating in GRAPHHASH, a unified and theoretically grounded framework  
 522 for approximate graph retrieval using general transport-based distances. We experimentally validate  
 523 exchangeability, and GRAPHHASH consistently outperforms strong baselines in retrieval performance  
 524 under both subgraph matching and edit distance supervision. Future work might explore other  
 525 consequences of the phenomenon on learning and training dynamics. It may be worthwhile to extend  
 526 the framework to similarities over a richer class of similarity functions between three dimensional  
 527 molecular structures, 3D objects, etc.  
 528

540 ETHICS STATEMENT

541

542 This work makes an algorithmic contribution and uses only publicly available, non-proprietary graph  
 543 datasets under their original licenses. No human subjects or sensitive data are involved. We believe  
 544 our results advance understanding of graph retrieval without raising additional ethical concerns.

545

546 REPRODUCIBILITY STATEMENT

547

548 We provide code, configuration files, and dataset splits to fully reproduce all experiments. Hyper-  
 549 parameters, training settings, and evaluation protocols are documented, and scripts are included  
 550 to regenerate the reported figures and tables. In addition, all theorems are stated formally with  
 551 accompanying proofs in the appendix to allow independent verification of our theoretical claims.

552

553 REFERENCES

554

555 Samuel K Ainsworth, Jonathan Hayase, and Siddhartha Srinivasa. Git re-basin: Merging models  
 556 modulo permutation symmetries. *arXiv preprint arXiv:2209.04836*, 2022.

557

558 David J. Aldous. *Exchangeability and related topics*, pp. 1–198. Springer Berlin Heidelberg, 1985.  
 559 ISBN 9783540393160. doi: 10.1007/bfb0099421. URL <http://dx.doi.org/10.1007/BFb0099421>.

560

561 Alexandr Andoni and Piotr Indyk. Near-optimal hashing algorithms for approximate nearest neighbor  
 562 in high dimensions. In *Proceedings of the 47th Annual IEEE Symposium on Foundations of  
 563 Computer Science (FOCS '2006)*, pp. 459–468, 2006.

564

565 Alexandr Andoni, Piotr Indyk, and Robert Krauthgamer. Earth mover distance over high-dimensional  
 566 spaces. In *Proceedings of the 19th ACM-SIAM Symposium on Discrete Algorithms (SODA '2008)*,  
 567 pp. 343–352, 2008.

568

569 Alexandr Andoni, Khanh Do Ba, Piotr Indyk, and David Woodruff. Efficient sketches for earth-mover  
 570 distance, with applications. In *Proceedings of the 50th Annual IEEE Symposium on Foundations  
 571 of Computer Science (FOCS '2009)*, 2009.

572

573 Yunsheng Bai, Hao Ding, Song Bian, Ting Chen, Yizhou Sun, and Wei Wang. Simgnn: A neural  
 574 network approach to fast graph similarity computation. In *Proceedings of the Twelfth ACM  
 575 International Conference on Web Search and Data Mining*, pp. 384–392, 2019.

576

577 Benjamin Bloem-Reddy, Yee Whye, et al. Probabilistic symmetries and invariant neural networks.  
 578 *Journal of Machine Learning Research*, 21(90):1–61, 2020.

579

580 David B. Blumenthal, Sébastien Bougleux, Johann Gamper, and Luc Brun. Gedlib: A c++ library  
 581 for graph edit distance computation. In Donatello Conte, Jean-Yves Ramel, and Pasquale Foggia  
 582 (eds.), *Graph-Based Representations in Pattern Recognition*, pp. 14–24, Cham, 2019. Springer  
 583 International Publishing. ISBN 978-3-030-20081-7.

584

585 Deyu Bo, Chuan Shi, Lele Wang, and Renjie Liao. Specformer: Spectral graph neural networks meet  
 586 transformers. 2023.

587

588 Salomon Bochner and Komaravolu Chandrasekharan. *Fourier transforms. (AM-19), volume 19.*  
 589 Annals of Mathematics Studies. Princeton University Press, Princeton, NJ, July 1949.

590

591 Aditya Bommakanti, Harshith R Vonteri, Konstantinos Skitsas, Sayan Ranu, Davide Mottin, and  
 592 Panagiotis Karras. Fugal: Feature-fortified unrestricted graph alignment. *Advances in Neural  
 593 Information Processing Systems*, 37:19523–19546, 2024.

594

595 Johann Brea, Berfin Simsek, Bernd Illing, and Wulfram Gerstner. Weight-space symmetry in  
 596 deep networks gives rise to permutation saddles, connected by equal-loss valleys across the loss  
 597 landscape. *arXiv preprint arXiv:1907.02911*, 2019.

598

599 Xavier Bresson and Thomas Laurent. Residual gated graph convnets. *arXiv preprint*, 2017.

600

601 Phuong Bui Thi Mai and Christoph Lampert. Functional vs. parametric equivalence of relu networks.  
 602 In *8th International Conference on Learning Representations*, 2020.

594 Hongyun Cai, Vincent W Zheng, and Kevin Chen-Chuan Chang. A comprehensive survey of graph  
 595 embedding: Problems, techniques, and applications. *IEEE transactions on knowledge and data  
 596 engineering*, 30(9):1616–1637, 2018.

597

598 Moses S. Charikar. Similarity estimation techniques from rounding algorithms. In *Proceedings  
 599 of the Thiry-Fourth Annual ACM Symposium on Theory of Computing*, STOC '02, pp. 380–388.  
 600 Association for Computing Machinery, 2002. ISBN 1581134959. doi: 10.1145/509907.509965.  
 601 URL <https://doi.org/10.1145/509907.509965>.

602 Xi Chen, Rajesh Jayaram, Amit Levi, and Erik Waingarten. An improved analysis of the quadtree for  
 603 high-dimensional emd. 2020.

604

605 Xi Chen, Rajesh Jayaram, Amit Levi, and Erik Waingarten. New streaming algorithms for high  
 606 dimensional emd and mst. In *Proceedings of the 54th Annual ACM SIGACT Symposium on Theory  
 607 of Computing*, pp. 222–233, 2022.

608 Taco Cohen and Max Welling. Group equivariant convolutional networks. In *International conference  
 609 on machine learning*, pp. 2990–2999. PMLR, 2016.

610

611 John M. Danskin. *The Theory of Max-Min and its Application to Weapons Allocation Problems*.  
 612 Springer Berlin Heidelberg, 1967. ISBN 9783642460920. doi: 10.1007/978-3-642-46092-0. URL  
 613 <http://dx.doi.org/10.1007/978-3-642-46092-0>.

614 Mayur Datar, Nicole Immorlica, Piotr Indyk, and Vahab S. Mirrokni. Locality-sensitive hashing  
 615 scheme based on p-stable distributions. In *Proceedings of the 20th ACM Symposium on Computa-  
 616 tional Geometry (SoCG '2004)*, pp. 253–262, 2004.

617

618 Michaël Defferrard, Xavier Bresson, and Pierre Vandergheynst. Convolutional neural networks on  
 619 graphs with fast localized spectral filtering. In *Advances in Neural Information Processing Systems  
 620 (NeurIPS)*, 2016.

621 Ishan Deshpande, Ziyu Zhang, and Alexander G Schwing. Generative modeling using the sliced  
 622 wasserstein distance. In *Proceedings of the IEEE conference on computer vision and pattern  
 623 recognition*, pp. 3483–3491, 2018.

624

625 Yihe Dong, Jean-Baptiste Cordonnier, and Andreas Loukas. Attention is not all you need: Pure  
 626 attention loses rank doubly exponentially with depth, 2023. URL <https://arxiv.org/abs/2103.03404>.

627

628 Matthijs Douze, Alexandre Guzhva, Chengqi Deng, Jeff Johnson, Gergely Szilvassy, Pierre-Emmanuel  
 629 Mazaré, Maria Lomeli, Lucas Hosseini, and Hervé Jégou. The faiss library. *arXiv preprint  
 630 arXiv:2401.08281*, 2024.

631

632 Jian Du, Shanghang Zhang, Guanhong Wu, José MF Moura, and Soummya Kar. Topology adaptive  
 633 graph convolutional networks. *arXiv preprint arXiv:1710.10370*, 2017.

634

635 John Duchi, Elad Hazan, and Yoram Singer. Adaptive subgradient methods for online learning and  
 636 stochastic optimization. *Journal of Machine Learning Research*, 12:2121–2159, 2011.

637

638 Chi Thang Duong. *Graph Embedding for Retrieval*. PhD thesis, EPFL, 2022.

639

640 David Duvenaud, Dougal Maclaurin, Jorge Aguilera-Iparraguirre, Rafael Gómez-Bombarelli, Tim-  
 641 othy Hirzel, Alán Aspuru-Guzik, and Ryan P. Adams. Convolutional networks on graphs for  
 642 learning molecular fingerprints. 2015.

643

644 Rahim Entezari, Hanie Sedghi, Olga Saukh, and Behnam Neyshabur. The role of permutation  
 645 invariance in linear mode connectivity of neural networks. *arXiv preprint arXiv:2110.06296*, 2021.

646

647 Matthias Fey, Jan Eric Lenssen, Christopher Morris, Jonathan Masci, and Nils M. Kriege. Deep  
 648 graph matching consensus. In *8th International Conference on Learning Representations, ICLR  
 2020, Addis Ababa, Ethiopia, April 26-30, 2020*. OpenReview.net, 2020. URL <https://openreview.net/forum?id=HyeJf1HKvS>.

648 C Daniel Freeman and Joan Bruna. Topology and geometry of half-rectified network optimization.  
 649 *arXiv preprint arXiv:1611.01540*, 2016.  
 650

651 Johannes Gasteiger, Aleksandar Bojchevski, and Stephan Günnemann. Predict then propagate: Graph  
 652 neural networks meet personalized pagerank. *arXiv preprint arXiv:1810.05997*, 2018.  
 653

654 Emma J Gerritse, Faegheh Hasibi, and Arjen P de Vries. Graph-embedding empowered entity  
 655 retrieval. In *Advances in Information Retrieval: 42nd European Conference on IR Research, ECIR  
 2020, Lisbon, Portugal, April 14–17, 2020, Proceedings, Part I* 42, pp. 97–110. Springer, 2020.  
 656

657 Justin Gilmer, Samuel S Schoenholz, Patrick F Riley, Oriol Vinyals, and George E Dahl. Neural  
 658 message passing for quantum chemistry. In *International conference on machine learning*, pp.  
 659 1263–1272. PMLR, 2017.  
 660

661 Aristides Gionis, Piotr Indyk, and Rajeev Motwani. Similarity search in high dimensions via hashing.  
 662 In *Proceedings of the 25th International Conference on Very Large Data Bases (VLDB '1999)*.  
 663

664 Xavier Glorot and Yoshua Bengio. Understanding the difficulty of training deep feedforward neural  
 665 networks. In *Proceedings of the thirteenth international conference on artificial intelligence and  
 666 statistics*, pp. 249–256. JMLR Workshop and Conference Proceedings, 2010.  
 667

668 Charles Godfrey, Davis Brown, Tegan Emerson, and Henry Kvinge. On the symmetries of deep  
 669 learning models and their internal representations. *arXiv preprint arXiv:2205.14258*, 2022.  
 670

671 Aric Hagberg and Drew Conway. Networkx: Network analysis with python. *URL: https://networkx.  
 672 github. io*, 2020.  
 673

674 Will Hamilton, Zhitao Ying, and Jure Leskovec. Inductive representation learning on large graphs. In *Advances  
 675 in Neural Information Processing Systems (NeurIPS)*, 2017.  
 676

677 Kaiming He, Xiangyu Zhang, Shaoqing Ren, and Jian Sun. Delving deep into rectifiers: Surpassing  
 678 human-level performance on imagenet classification. In *Proceedings of the IEEE international  
 679 conference on computer vision*, pp. 1026–1034, 2015.  
 680

681 Robert Hecht-Nielsen. On the algebraic structure of feedforward network weight spaces. In *Advanced  
 682 Neural Computers*, pp. 129–135. Elsevier, 1990.  
 683

684 Piotr Indyk. Algorithms for dynamic geometric problems over data streams. In *Proceedings of the  
 685 36th ACM Symposium on the Theory of Computing (STOC '2004)*, pp. 373–380, 2004.  
 686

687 Piotr Indyk and Rajeev Motwani. Approximate nearest neighbors: Towards removing the curse  
 688 of dimensionality. In *Proceedings of the 30th ACM Symposium on the Theory of Computing  
 (STOC '1998)*, pp. 604–613, 1998.  
 689

690 Piotr Indyk and Nitin Thaper. Fast color image retrieval via embeddings. In *Workshop on Statistical  
 691 and Computational Theories of Vision (at ICCV)*, 2003.  
 692

693 Piotr Indyk, Rajeev Motwani, Prabhakar Raghavan, and Santosh Vempala. Locality-preserving  
 694 hashing in multidimensional spaces. In *Proceedings of the twenty-ninth annual ACM symposium  
 695 on Theory of computing*, pp. 618–625, 1997.  
 696

697 Eeshaan Jain, Indradymna Roy, Saswat Meher, Soumen Chakrabarti, and Abir De. Graph edit  
 698 distance with general costs using neural set divergence. In *The Thirty-eighth Annual Conference  
 699 on Neural Information Processing Systems*, 2024.  
 700

701 Rajesh Jayaram, Erik Waingarten, and Tian Zhang. Data-dependent lsh for the earth mover's distance.  
 702 In *Proceedings of the 56th Annual ACM Symposium on Theory of Computing*, pp. 800–811, 2024.  
 703

704 Federico Arangath Joseph, Jerome Sieber, Melanie Zeilinger, and Carmen Amo Alonso. Lambda-  
 705 skip connections: the architectural component that prevents rank collapse. In *The Thirteenth  
 706 International Conference on Learning Representations*, 2025. *URL https://openreview.  
 707 net/forum?id=1yJP5TVWiH*.  
 708

702 Diederik P. Kingma and Jimmy Ba. Adam: A method for stochastic optimization.  
 703 *CoRR*, abs/1412.6980, 2014. URL <https://api.semanticscholar.org/CorpusID:6628106>.

705 Diederik P. Kingma and Jimmy Ba. Adam: A method for stochastic optimization. In *International Conference on Learning Representations (ICLR)*, 2015.

708 Thomas N. Kipf and Max Welling. Semi-supervised classification with graph convolutional networks.  
 709 In *International Conference on Learning Representations (ICLR)*, 2017.

710 Soheil Kolouri, Kimia Nadjahi, Umut Simsekli, Roland Badeau, and Gustavo Rohde. Generalized sliced wasserstein distances. *Advances in neural information processing systems*, 32, 2019.

713 Devin Kreuzer, Dominique Beaini, Will Hamilton, Vincent Létourneau, and Prudencio Tossou.  
 714 Rethinking graph transformers with spectral attention. *Advances in Neural Information Processing Systems*, 34:21618–21629, 2021.

716 Juho Lee, Yoonho Lee, Jungtaek Kim, Adam R. Kosiorek, Seungjin Choi, and Yee Whye Teh.  
 717 Set transformer: A framework for attention-based permutation-invariant neural networks. In *International Conference on Machine Learning (ICML)*, 2019.

720 Yujia Li, Daniel Tarlow, Marc Brockschmidt, and Richard Zemel. Gated graph sequence neural  
 721 networks. In *International Conference on Learning Representations (ICLR)*, 2016.

722 Yujia Li, Chenjie Gu, Thomas Dullien, Oriol Vinyals, and Pushmeet Kohli. Graph matching networks  
 723 for learning the similarity of graph structured objects. In *International conference on machine learning*, pp. 3835–3845. PMLR, 2019. URL <https://arxiv.org/abs/1904.12787>.

726 Zihao Li, Yuyi Ao, and Jingrui He. Sphere: Expressive and interpretable knowledge graph embedding  
 727 for set retrieval. In *Proceedings of the 47th International ACM SIGIR Conference on Research and Development in Information Retrieval*, pp. 2629–2634, 2024.

730 Zhaoyu Lou, Jiaxuan You, Chengtao Wen, Arquimedes Canedo, Jure Leskovec, et al. Neural subgraph  
 731 matching. *arXiv preprint arXiv:2007.03092*, 2020.

732 Haggai Maron, Heli Ben-Hamu, Nadav Shamir, and Yaron Lipman. Invariant and equivariant graph  
 733 networks. In *7th International Conference on Learning Representations, ICLR*, 2019.

735 Christopher Morris, Nils M. Kriege, Franka Bause, Kristian Kersting, Petra Mutzel, and Marion  
 736 Neumann. Tudataset: A collection of benchmark datasets for learning with graphs, 2020.

738 Alireza Naderi, Thiziri Nait Saada, and Jared Tanner. Mind the gap: a spectral analysis of rank  
 739 collapse and signal propagation in attention layers, 2025. URL <https://arxiv.org/abs/2410.07799>.

741 Aviv Navon, Aviv Shamsian, Idan Achituv, Ethan Fetaya, Gal Chechik, and Haggai Maron. Equivariant  
 742 architectures for learning in deep weight spaces. In *International Conference on Machine Learning*, pp. 25790–25816. PMLR, 2023.

744 Behnam Neyshabur and Nathan Srebro. On symmetric and asymmetric lshs for inner product search.  
 745 In *International Conference on Machine Learning*, pp. 1926–1934. PMLR, 2015a.

747 Behnam Neyshabur, Russ R Salakhutdinov, and Nati Srebro. Path-sgd: Path-normalized optimization  
 748 in deep neural networks. *Advances in neural information processing systems*, 28, 2015b.

750 Hamid Palangi, Li Deng, Yelong Shen, Jianfeng Gao, Xiaodong He, Jianshu Chen, Xinying Song,  
 751 and Rabab Ward. Deep sentence embedding using long short-term memory networks: Analysis  
 752 and application to information retrieval. *IEEE/ACM Transactions on Audio, Speech, and Language Processing*, 24(4):694–707, 2016.

754 Fidel A Guerrero Peña, Heitor Rapela Medeiros, Thomas Dubail, Masih Aminbeidokhti, Eric  
 755 Granger, and Marco Pedersoli. Re-basin via implicit sinkhorn differentiation. *arXiv preprint arXiv:2212.12042*, 2022.

756 Ali Rahimi and Benjamin Recht. Random features for large-scale kernel machines. *Advances in*  
 757 *neural information processing systems*, 20, 2007.

758

759 Ladislav Rampášek, Michael Galkin, Vijay Prakash Dwivedi, Anh Tuan Luu, Guy Wolf, and Do-  
 760 minique Beaini. Recipe for a general, powerful, scalable graph transformer. *Advances in Neural*  
 761 *Information Processing Systems*, 35:14501–14515, 2022.

762

763 Rishabh Ranjan, Siddharth Grover, Sourav Medya, Venkatesan Chakaravarthy, Yogish Sabharwal,  
 764 and Sayan Ranu. Greed: A neural framework for learning graph distance functions. In *Advances in*  
 765 *Neural Information Processing Systems 36: Annual Conference on Neural Information Processing*  
 766 *Systems 2022, NeurIPS 2022, November 29-Decemer 1, 2022*, 2022.

767

768 Andreas Roth and Thomas Liebig. Rank collapse causes over-smoothing and over-correlation in  
 769 graph neural networks, 2024. URL <https://arxiv.org/abs/2308.16800>.

770

771 Indradymna Roy, Venkata Sai Baba Reddy Velugoti, Soumen Chakrabarti, and Abir De. Interpretable  
 772 neural subgraph matching for graph retrieval. In *Proceedings of the AAAI conference on artificial*  
 773 *intelligence*, volume 36, pp. 8115–8123, 2022.

774

775 Indradymna Roy, Rishi Agarwal, Soumen Chakrabarti, Anirban Dasgupta, and Abir De. Locality  
 776 sensitive hashing in fourier frequency domain for soft set containment search. *Advances in Neural*  
 777 *Information Processing Systems*, 36:56352–56383, 2023.

778

779 Yuki Saito, Takuma Nakamura, Hirotaka Hachiya, and Kenji Fukumizu. Exchangeable deep neural  
 780 networks for set-to-set matching and learning. In *European Conference on Computer Vision*, pp.  
 781 626–646. Springer, 2020.

782

783 Filippo Santambrogio. *Optimal transport for applied mathematicians*, volume 87. Springer, 2015.

784

785 Konstantin Schürholt, Dimche Kostadinov, and Damian Borth. Self-supervised representation learning  
 786 on neural network weights for model characteristic prediction. *Advances in Neural Information*  
 787 *Processing Systems*, 34:16481–16493, 2021.

788

789 Hamed Shirzad, Ameya Velingker, Balaji Venkatachalam, Danica J Sutherland, and Ali Kemal Sinop.  
 790 Exphormer: Sparse transformers for graphs. In *International Conference on Machine Learning*,  
 791 pp. 31613–31632. PMLR, 2023.

792

793 Harsha Vardhan Simhadri, Ravishankar Krishnaswamy, Gopal Srinivasa, Suhas Jayaram Subramanya,  
 794 Andrija Antonijevic, Dax Pryce, David Kaczynski, Shane Williams, Siddarth Gollapudi, Varun  
 795 Sivashankar, Neel Karia, Aditi Singh, Shikhar Jaiswal, Neelam Mahapatro, Philip Adams, Bryan  
 796 Tower, and Yash Patel. DiskANN: Graph-structured indices for scalable, fast, fresh and filtered  
 797 approximate nearest neighbor search, 2023. URL <https://github.com/Microsoft/DiskANN>.

798

799 Berfin Simsek, François Ged, Arthur Jacot, Francesco Spadaro, Clément Hongler, Wulfram Gerstner,  
 800 and Johanni Brea. Geometry of the loss landscape in overparameterized neural networks: Symme-  
 801 tries and invariances. In *International Conference on Machine Learning*, pp. 9722–9732. PMLR,  
 802 2021.

803

804 Kiran K. Thekumpampil, Chong Wang, Sewoong Oh, and Li-Jia Li. Attention-based graph  
 805 neural network for semi-supervised learning, 2018. URL <https://arxiv.org/abs/1803.03735>.

806

807 Tijmen Tieleman and Geoffrey Hinton. Neural networks for machine learning, lecture 6.5—rmsprop.  
 808 <http://www.cs.toronto.edu/~hinton/coursera/lecture6/lec6.pdf>, 2012.  
 809 Coursera lecture slides.

810

811 Titouan Vayer, Rémi Flamary, Romain Tavenard, Laetitia Chapel, and Nicolas Courty. Sliced  
 812 gromov-wasserstein. *arXiv preprint arXiv:1905.10124*, 2019.

813

814 Petar Veličković, Guillem Cucurull, Arantxa Casanova, Adriana Romero, Pietro Liò, and Yoshua  
 815 Bengio. Graph attention networks. In *International Conference on Learning Representations*  
 816 (*ICLR*), 2018.

810 Quan Wang, Zhendong Mao, Bin Wang, and Li Guo. Knowledge graph embedding: A survey of  
 811 approaches and applications. *IEEE transactions on knowledge and data engineering*, 29(12):  
 812 2724–2743, 2017.

813

814 Felix Wu, Tianyi Zhang, Amauri Holanda de Souza Jr., Christopher Fifty, Tao Yu, and Kilian Q.  
 815 Weinberger. Simplifying graph convolutional networks. *arXiv preprint*, 2019.

816 Qitian Wu, Wentao Zhao, Zenan Li, David Wipf, and Junchi Yan. Nodeformer: A scalable graph  
 817 structure learning transformer for node classification, 2023. URL <https://arxiv.org/abs/2306.08385>.

818

819 Wah Chai Wu. On rearrangement inequalities for multiple sequences. 2020. <https://arxiv.org/abs/2002.10514v10>.

820

821 Keyulu Xu, Weihua Hu, Jure Leskovec, and Stefanie Jegelka. How powerful are graph neural  
 822 networks? In *International Conference on Learning Representations (ICLR)*, 2019.

823

824 Chengxuan Ying, Tianle Cai, Shengjie Luo, Shuxin Zheng, Guolin Ke, Di He, Yanming Shen, and  
 825 Tie-Yan Liu. Do transformers really perform badly for graph representation? *Advances in neural  
 826 information processing systems*, 34:28877–28888, 2021.

827

828 Manzil Zaheer, Satwik Kottur, Siamak Ravanbakhsh, Barnabás Póczos, Ruslan Salakhutdinov, and  
 829 Alexander Smola. Deep sets. In *Advances in Neural Information Processing Systems (NeurIPS)*,  
 830 2017.

831

832 Tong Zhang. Solving large scale linear prediction problems using stochastic gradient descent  
 833 algorithms. In *Proceedings of the Twenty-First International Conference on Machine Learning  
 834 (ICML)*, 2004.

835

836 Jianan Zhao, Chaozhuo Li, Qianlong Wen, Yiqi Wang, Yuming Liu, Hao Sun, Xing Xie, and Yanfang  
 837 Ye. Gophormer: Ego-graph transformer for node classification. 2021.

838

839 Xixi Zhou, Yang Gao, Xin Jie, Xiaoxu Cai, Jiajun Bu, and Haishuai Wang. Ease-dr: Enhanced  
 840 sentence embeddings for dense retrieval. In *Proceedings of the 47th International ACM SIGIR  
 841 Conference on Research and Development in Information Retrieval*, pp. 2374–2378, 2024.

842

843 Hao Zhu and Piotr Koniusz. Simple spectral graph convolution. In *ICLR*, 2021.

844

845 Wei Zhuo and Guang Tan. Efficient graph similarity computation with alignment regularization.  
 846 *Advances in Neural Information Processing Systems*, 35:30181–30193, 2022.

847

848

849

850

851

852

853

854

855

856

857

858

859

860

861

862

863

# 864 Exchangeability of GNN Representations

## 865 with Applications to Graph Retrieval

### 866 (Appendix)

## 867 CONTENTS

871	<b>A Broader Impact</b>	<b>18</b>
872	<b>B Limitations</b>	<b>18</b>
873	<b>C LLM Usage</b>	<b>18</b>
874	<b>D Related work</b>	<b>18</b>
875	<b>E Proofs and other technical details</b>	<b>20</b>
876	E.1 Proofs of the results of exchangeability presented in Section 3	20
877	E.1.1 Proof of Lemma 2	21
878	E.1.2 Proof of Lemma 3	23
879	E.1.3 Proof of Lemma 4	24
880	E.1.4 Proof of Theorem 5 and Proposition 6	25
881	E.1.5 Equivariance of the Update Step	27
882	E.1.6 Additional Results on Exchangeability	31
883	E.2 Proofs of the technical results in Section 4	33
884	E.2.1 Proof of Proposition 7	33
885	E.2.2 Proof of the fact that Eq. (3) and Eq. (4) are equivalent	35
886	E.2.3 Auxiliary Results used to prove Lemmas in Appendix E.2	36
887	E.2.4 Proofs of LSH results	38
888	E.2.5 Auxiliary results used to prove results in this subsection E.2.4	43
889	<b>F List of GNNs</b>	<b>45</b>
890	F.1 Graph Neural Network	45
891	F.2 Graph Transformers	47
892	F.3 Set-based Neural Network	49
893	<b>G Additional details about experiments</b>	<b>50</b>
894	G.1 Datasets	50
895	G.2 Embedding model architecture	50
896	G.3 Fourier-map and hashcode training	51
897	G.4 Baselines	51
898	G.5 Evaluation Metrics	52
899	G.6 Hardware and Licenses	53
900	<b>H Additional Experiments</b>	<b>54</b>
901	H.1 Additional Exchangeability Results	54
902	H.2 Further Evaluation of GRAPHHASH’s Retrieval Performance	55
903	H.2.1 MAP on Equal-Cost GED	55
904	H.2.2 Evaluation using NDCG	56
905	H.2.3 Clarification on RH (Subsampled)	57
906	H.2.4 Evaluation on Larger Graphs	59
907	H.2.5 Evaluation on larger corpus	59
908	H.2.6 Ablation Studies	60
909	H.2.7 Comparison of $\text{sim}$ and $\text{sim}_d$	63
910	H.2.8 Evaluation of LSH Methods under Aligned Scoring Functions	64

918 **A BROADER IMPACT**  
919920 Our work is the first of its kind within the space of distributional symmetries in neural architectures,  
921 as it moves the focus towards the distribution of embeddings over randomness in initialization. Our  
922 work may also be adapted to other classes of neural networks. Probabilistic symmetries may have  
923 other consequences to training and learning dynamics, like our concentration bound.924 GRAPHHASH also offers an efficient way to retrieve graphs from a large database of graphs. It can  
925 help in identifying a subset of molecules which is similar to some other molecule, from a large corpus.  
926 It can also help in video or image retrieval by specifically focusing on scene graphs. Thus, our work  
927 has the potential to reduce computational cost and carbon footprint of large search systems.928 **B LIMITATIONS**  
929930 **(1)** We only restrict ourselves to exchangeability as probabilistic symmetry of GNN, which is  
931 symmetry induced by permutations in the weight space. In this work, we do not consider how other  
932 types of symmetry can affect the probability density function of the embeddings. However, our work  
933 can be seen as a stepping stone to characterize such cases. **(2)** It is well known that the exchangeable  
934 sequence  $(Y_1, \dots, Y_D)$  tends to become an i.i.d. sequence as  $D \rightarrow \infty$ . However, this does not apply to  
935 our setting because the values of the embedding elements also depend on  $D$ . It would be interesting  
936 to discover asymptotic characterization of embedding values. **(3)** Exact graph distance involves  
937 solving a quadratic assignment problem, whereas its surrogate used in Eq. (1) approximates graphs  
938 using sets. This gives a first order approximation, which allows us to leverage exchangeability to  
939 approximate transportation distance between two embedding sets using Euclidean distance. One  
940 can provide more accurate approximation using distance between edge embeddings. We did not  
941 provide this formulation in our paper. However, our work can be easily extended to such setting, by  
942 considering joint distribution between node pairs.943 **C LLM USAGE**  
944945 We used an LLM primarily for correction of grammar and polishing text. Very occasionally, we  
946 used it to supplement bibliographic search. No LLM was used to generate ideas, design experiments,  
947 analyze data, implement algorithms, or produce results. We carefully reviewed and revised any  
948 response provided by LLM.949 **D RELATED WORK**  
950951 **Representation learning** Representation using dense embeddings of structured objects has been a  
952 much-studied area of research, e.g. for, sets (Lee et al., 2019; Zaheer et al., 2017), sequences (Palangi  
953 et al., 2016; Zhou et al., 2024), and graphs (Cai et al., 2018; Wang et al., 2017). Relatively fewer  
954 results focus on the question of retrieval using these embeddings (Li et al., 2024; Duong, 2022;  
955 Gerritsen et al., 2020). Prior works on graph retrieval predominantly aggregate node embeddings  
956 from each graph into a single, pre-computable embedding vector (Li et al., 2019; Bai et al., 2019;  
957 Ranjan et al., 2022). This allows for the use of standard indexing methods for vector similarity search.  
958 However, this reduces accuracy due to compressing the entire graph into one embedding.959 **Transportation distance in graphs** More recent techniques for graph embedding employ node-  
960 based vectors and then define relevance scores of the corpus graphs with respect to the query by using  
961 transportation distance between the two sets of vectors (Roy et al., 2022; Zhuo et al., 2022; Fey et al.,  
962 2020). The cost within the transportation framework models various notions of relevance measure,  
963 including asymmetric measures for subgraph matching, graph edit distance with non-uniform costs,  
964 etc., which results in enhanced accuracy, as compared to aggregation to single vectors.965 **Locality sensitive hashing** After obtaining the embedding (or set of embeddings), there still  
966 remains the question of finding out the most relevant object using this representation. For traditional  
967 vector databases, locality sensitive hashing (LSH), Indyk et al. (1998) pioneered a celebrated method  
968 for approximate near neighbor search. The benefit of LSH over comparable techniques, e.g., IVF, and  
969 graph-based techniques, e.g., HNSW, is the faster indexing time while giving comparable or slightly  
970 worse recall times.971 **LSH for transportation distance** A key contribution of the current work is to propose an LSH for  
972 transportation distance, in context of GNN. Nearest neighbor methods has been studied extensively in

972 the theory community (Indyk et al., 2003; Andoni et al., 2009; Chen et al., 2022; 2020; Indyk, 2004;  
 973 Andoni et al., 2008; Jayaram et al., 2024). They first embed a set similarity into Euclidean space with  
 974 some distortion factor, and then use this reduction to design an LSH. However, the similarity measure  
 975 in these existing works is always symmetric, whereas in graph retrieval, it is often asymmetric, such  
 976 as in subgraph matching or Graph Edit Distance (GED) with non-uniform costs.

977 **Sliced Wasserstein distance** While transportation distance is computationally expensive, recent  
 978 studies have explored approximations that are cheaper (Kolouri et al., 2019; Deshpande et al., 2018;  
 979 Vayer et al., 2019). The most well-known one, perhaps, is the *sliced Wasserstein* (SW) distance,  
 980 which is the average of the Wasserstein distance over multiple 1D random projections. Deshpande  
 981 et al. (2018) show the efficacy of the SW distance for GAN training. Kolouri et al. (2019) demonstrate  
 982 the connection of SW distance to the Radon transform, and Vayer et al. (2019) propose *sliced Gromov*  
 983 *Wasserstein*, a similar approximation for the Gromov-Wasserstein distance, also used for optimal  
 984 transport. However, none of them study the question of efficient retrieval under such distances, or the  
 985 connection with dimension exchangeability of representations produced by common neural networks.

986 Transportation distance has also been studied in the average case: Jayaram et al. (2024) give a  
 987  $O(\log n)$  approximate data-dependent LSH in the distributional case. In our setting, this problem is  
 988 tackled by showing the exchangeability of embedding dimensions of GNNS. Our result is incom-  
 989 parable to (Jayaram et al., 2024), since their posited distribution is not exchangeable, and our set  
 990 of exchangeable distributions is broader than what (Jayaram et al., 2024) assumed. The notion of  
 991 exchangeability has been studied before for neural networks, but in different contexts and toward  
 992 different goals. Set transformers famously utilized permutation invariance to give set embeddings,  
 993 exchangeable networks for set-to-set matching were described by Saito et al. (2020), while Bloem-  
 994 Reddy et al. (2020) characterized invariant network architectures for a particular symmetry property,  
 995 including exchangeability, of the input. However, none of these results have characterized the ex-  
 996 changeability property of the embedding dimensions, as is done in our work. In Introduction, we have  
 997 already mentioned works that recognized various symmetries of loss surfaces with respect to hidden  
 998 units of some standard networks. In those works, such symmetry is usually an impediment to fast  
 999 optimization, remedied by advanced optimization techniques. In contrast, we use such symmetries to  
 establish exchangeability, in the service of efficient LSH indexes.

1000  
 1001  
 1002  
 1003  
 1004  
 1005  
 1006  
 1007  
 1008  
 1009  
 1010  
 1011  
 1012  
 1013  
 1014  
 1015  
 1016  
 1017  
 1018  
 1019  
 1020  
 1021  
 1022  
 1023  
 1024  
 1025

1026 

## E PROOFS AND OTHER TECHNICAL DETAILS

1027  
1028 In this section, we present the proofs of the technical results presented in Section 3 and Section 4.  
10291030  
1031 

### E.1 PROOFS OF THE RESULTS OF EXCHANGEABILITY PRESENTED IN SECTION 3

  
10321033 Here, we prove Lemma 2, Lemma 3, Lemma 4, Theorem 5 and Proposition 6. To achieve this goal,  
1034 we first restate the setting:1035 **(1) Broad class of GNN architectures** We consider the a wide variety of GNN architectures, which  
1036 are enlisted in Appendix F. This list encompasses a wide range of GNN architectures, including gated  
1037 GNN (Gilmer et al., 2017), GIN (Xu et al., 2019), GAT (Veličković et al., 2018), GCN (Kipf et al.,  
1038 2017). Note that, our analysis is likely to extend beyond these cases, and can also be applied in Graph  
1039 transformers, as shown in Appendix F1040 **(2) IID intialization of the parameters within a layer** The entries of the parameter matrix  $\Theta^{(\ell)}$   
1041 in each layer of are initialized in an i.i.d manner. Parameters across different layers are initialized  
1042 independently, but not necessarily identically. This covers standard model initialization schemes,  
1043 such as Kaiming initialization (He et al., 2015) and Xavier initialization (Glorot et al., 2010), both of  
1044 which yield i.i.d. initialization of the parameters within a layer.1045 **(3) Permutation invariance of loss function** We consider the loss function is invariant to the  
1046 permutations of elements in the node embeddings. This holds naturally in several settings including  
1047 our graph retrieval. Here, the loss, whether binary cross-entropy or pairwise ranking, depends on the  
1048 similarity between  $(G_q, G_c)$  via the transportation plan between  $\mathbf{X}^{(q)}$  and  $\mathbf{X}^{(c)}$  (Roy et al., 2022;  
1049 Zhuo et al., 2022). Since this similarity is invariant under permutations of embedding elements, the  
1050 loss is likewise permutation-invariant. In link prediction, the similarity between two nodes  $u$  and  $v$  is  
1051 often computed as the dot product  $\mathbf{x}(u)^\top \mathbf{x}(v)$ , which is invariant to permutations of the elements of  
1052  $\mathbf{x}$ . Consequently, the associated loss is also permutation-invariant.1052 **(4) Broad class of optimizers** The optimizer for training can be SGD (Zhang, 2004),  
1053 Adam (Kingma et al., 2015), etc. This pertains to standard optimizers, which are routinely em-  
1054 ployed across learning settings.1055 **Additional Notation** We further introduce supplementary notation.1056  
1057 **(1)** We use  $\Theta_t^{(\ell)}$  to denote the parameter matrix of the  $\ell$ -th layer at the  $t^{\text{th}}$  update step. We shall  
1058 index our weights using the set  $[\ell_{\max}] = \{0, 1, \dots, \ell_{\max}\}$ , which shall implicitly cover each of the  
1059 components (embedding initialization, message passing and update step). We will typically use  $\ell$  to  
1060 denote the layer index.1061 **(2)**  $\Theta_{<t}^{(\ell)}$  denotes the *collection* of parameters  $\Theta_{\text{iter}}^{(\ell)}$  for  $\text{iter} = 0, 1, \dots, t - 1$ .1062 **(3)**  $\theta_{<t}$  denotes the collection of all parameters  $\theta_{\text{iter}}$  for  $\text{iter} = 0, 1, \dots, t - 1$ .1063 **(4)**  $\Gamma_\pi^{(\ell)}$  is a transformation on the parameters of the  $\ell$ -th layer.  $\Gamma_\pi$  is a global transformation on  
1064 all parameters. We take  $\Gamma_\pi$  to be separable across layers (this holds for the permutation-based  
1065 transformations considered by us). That is,  $\Gamma_\pi$  may be written as  $\Gamma_\pi = \bigoplus_{\ell \in [\ell_{\max}]} \Gamma_\pi^{(\ell)}$ . This means  
1066 that  $\Gamma_\pi(\theta) = \left( \Gamma_\pi^{(\ell)}(\Theta^{(\ell)}) \mid \ell \in [\ell_{\max}] \right)$ .1067 **(5)**  $\mathcal{I}_2$  refers to the domain of the parameters, which is  $\mathbb{R}^p$  where  $p$  is the number of parameters in  
1068 the network.1069 **(6)** We refer to the loss function at the  $t^{\text{th}}$  update step as  $\text{loss}_t$ , which a function of the parameters of  
1070 the network, i.e.,  $\text{loss}_t(\theta)$ ; thus the index  $t$  encodes the batching/data used for that update step. When  
1071 it is clear from context, we may write  $\text{loss}_t(\theta_t)$  simply as  $\text{loss}_t$ .1072 **(7)**  $\delta_{\Delta, (k, l)}$  is defined as the matrix of appropriate dimensions with all zeros except for a  $\Delta$  at the  
1073  $(k, l)$ -th position. Note that this is different from Dirac delta function  $\delta(\bullet)$  — we will alert the reader  
1074 if we use  $\delta$  as Dirac delta function.1075 **(8)** We denote the gradient of the loss function with respect to the parameters  $\theta_t$  as the collection  
1076  $\text{grad}_t \triangleq (\text{grad}_t^{(\ell)} \mid \ell \in [\ell_{\max}])$ , where  $\ell$  is the layer index. Here,  $\text{grad}_t^{(\ell)}$  is a matrix of the same  
1077 dimensions as  $\Theta_t^{(\ell)}$  which has the corresponding gradients. As set by earlier convention,  $\text{grad}_{<t}^{(\ell)}$   
1078 denotes the collection of gradients  $\text{grad}_{\text{iter}}^{(\ell)}$  for  $\text{iter} = 0, 1, \dots, t - 1$ , and  $\text{grad}_{<t}$  denotes the  
1079 collection of all gradients  $\text{grad}_{\text{iter}}$  for  $\text{iter} = 0, 1, \dots, t - 1$ .

1080  
1081

## E.1.1 PROOF OF LEMMA 2

1082  
1083  
1084  
1085  
1086

**Lemma 2.** Given a graph  $G$  and a GNN architecture  $\text{GNN}_\theta$  enlisted in Appendix F, let the node embedding matrix of  $G$  be  $\mathbf{X} = \text{GNN}_\theta(G) \in \mathbb{R}^{n \times D}$ . Then, for any permutation matrix  $\pi \in \mathcal{P}_D$ , there exists a bijective transformation  $\Gamma_\pi$  with  $|\text{Det}(\partial\Gamma_\pi(\theta)/\partial\theta)| = 1$  such that  $\mathbf{X}\pi = \text{GNN}_{\Gamma_\pi(\theta)}(G)$ . We call  $\Gamma_\pi$  as a permutation induced transformation, for  $\pi$ .

1087  
1088  
1089  
1090

**Proof:** *Overview.* In this section, we focus on two architectures, which covers the intricacy involved in designing the permutation inducing transformation. For other GNN architectures, we provide the reader with building blocks for transformations involving other common GNN layers in Appendix F.

1091  
1092

In this proof, we consider the GNN in the form of gated GNN used by Li et al. (2016); Gilmer et al. (2017).

1093  
1094  
1095  
1096

*Architecture.* Given integers  $K$  and  $D$ , a graph neural network ( $\text{GNN}_\theta$ ) computes node embeddings  $\mathbf{x}_k(u) \in \mathbb{R}^D$  for  $u \in V$  using  $K$  message passing steps. Here, we initialize  $\mathbf{x}_0(u)$  using node features  $\text{feat}(u)$  and keep updating  $\mathbf{x}_k$  using two neural networks  $\text{upd}_\theta$  and  $\text{msg}_\theta$  having parameters  $\theta$ .

1097  
1098  
1099  
1100

$$\mathbf{x}_0(u) = \text{init}_\theta(\text{feat}(u)), \quad (10)$$

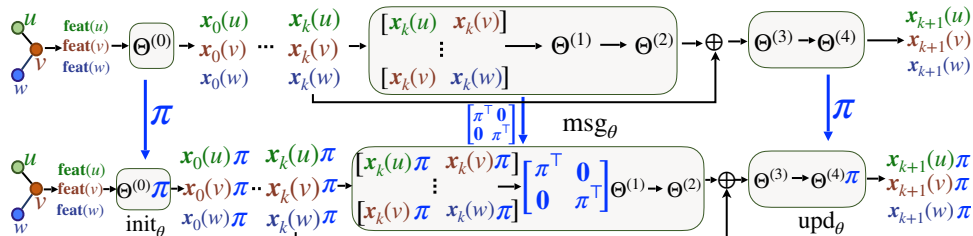
$$\mathbf{x}_{k+1}(u) = \text{upd}_\theta(\mathbf{x}_k(u), \sum_{v:(u,v) \in E} \text{msg}_\theta(\mathbf{x}_k(u), \mathbf{x}_k(v))), \quad \text{for } k < K. \quad (11)$$

1101

In the above:  $\text{init}_\theta, \text{msg}_\theta$  are multilayer perceptron (MLP) networks of the form of  $\text{Linear}^{(\ell_{\max})} \circ \sigma^{(\ell_{\max}-1)} \circ \dots \circ \sigma^{(1)} \circ \text{Linear}^{(1)}$ , where  $\text{Linear}^{(\ell)}$  is a linear layer and  $\sigma^{(\ell)}$  is an activation function that applies pointwise.  $\text{upd}_\theta$  can be (a) an MLP network or, (b) one layer of GRU (Gilmer et al., 2017). In the current analysis, we omit step index  $t$ , since we are focusing on only one step.

1105

**Gated GNN with MLP based  $\text{upd}_\theta$ :** *Proof Sketch.* In particular, we assume that each of

1106  
1107  
1108  
1109  
1110  
1111  
1112  
1113  
11141115  
1116  
1117  
1118  
1119  
1120  
1121  
1122

$\text{init}_\theta, \text{msg}_\theta, \text{upd}_\theta$  is a simple MLP with 1, 2, and 2 layers, respectively. The figure shows initialization and recursive propagation from layer  $k$  to  $k+1$ . To induce the transformation  $\mathbf{x}_K(u) \mapsto \mathbf{x}_K(u)\pi$ , we modify the final layer of  $\text{upd}_\theta$  as  $\Theta^{(4)} \mapsto \Theta^{(4)}\pi$ , which also changes all intermediate outputs of  $\text{upd}_\theta$ :  $\mathbf{x}_k(u) \mapsto \mathbf{x}_k(u)\pi$ . This change affects  $\text{msg}_\theta$  inputs. We undo the “side-effect” by transforming  $\Theta^{(1)}$  to  $\text{Diag}(\pi^\top, \pi^\top)\Theta^{(1)}$ . Finally, we update  $\Theta^{(0)} \mapsto \Theta^{(0)}\pi$  to ensure that the initial input to  $\text{msg}_\theta$ , namely  $\mathbf{x}_0(u)\pi$ , aligns with the transformed flow. Since the rest of the network remains unchanged, this transformation is agnostic to the depths of init, msg, and upd, affecting only the last layers of init and upd and the first layer of msg.

1123  
1124  
1125  
1126  
1127  
1128

*Detailed Proof.* Firstly, we re-index the network weights for readability, as — **(I)** init: Let the last weight of init be  $\Theta^{(\ell_0)}$ . **(II)** msg: Given  $(u, v) \in E$ , and the propagation layer  $k$ , let  $\bar{\mathbf{X}}_k^{(0)} = [\mathbf{x}_k^\top(u), \mathbf{x}_k^\top(v)]$  be the input to the message propagation layer after the node embeddings are concatenated according to the edges in the graph. The weight matrix in the first propagation layer of msg is  $\Theta^{(\ell_1)}$ . Let  $\bar{\mathbf{X}}_k^{(\ell_1)}$  be the output of  $\Theta^{(\ell_1)}$ , i.e.,  $\bar{\mathbf{X}}_k^{(\ell_1)} = \bar{\mathbf{X}}_k^{(0)}\Theta^{(\ell_1)}$  **(III)** upd: Let the final layer of upd be  $\Theta^{(\ell_2)}$ . The transformation is defined as follows:

1129  
1130  
1131  
1132  
1133

$$\Gamma_\pi^{(\ell_0)}(\Theta^{(\ell_0)}) = \Theta^{(\ell_0)}\pi, \quad (12)$$

$$\Gamma_\pi^{(\ell_1)}(\Theta^{(\ell_1)}) = \begin{bmatrix} \pi^\top & \mathbf{0} \\ \mathbf{0} & \pi^\top \end{bmatrix} \Theta^{(\ell_1)}, \quad (13)$$

$$\Gamma_\pi^{(\ell_2)}(\Theta^{(\ell_2)}) = \Theta^{(\ell_2)}\pi \quad (14)$$

1134 While the remaining transformations are identity, *i.e.*,  $\Gamma_{\pi}^{(\ell)} = \mathbf{I}_{\dim(\Theta^{(\ell)})}$  for all  $\ell \notin \{\ell_0, \ell_1, \ell_2\}$ . We  
 1135 shall show that the output of the network is permuted in columns by  $\pi$ , by tracing the effect of the trans-  
 1136 formation from the input to the output. We show this inductively on the number of propagation steps.  
 1137

1138 *Base case.* For  $k = 0$ . As  $\Theta^{(\ell_0)} \mapsto \Theta^{(\ell_0)}\pi$ , we have:  $\mathbf{X}_0 \mapsto \mathbf{X}_0\pi$ .

1139 *Inductive Step.* Suppose that  $\mathbf{X}_k \mapsto \mathbf{X}_k\pi$  for some  $k$ . Then  $\bar{\mathbf{X}}_k^{(0)} = [\mathbf{x}_k^\top(u), \mathbf{x}_k^\top(v)] \mapsto$   
 1140  $\bar{\mathbf{X}}_k^{(0)} \begin{bmatrix} \pi & \mathbf{0} \\ \mathbf{0} & \pi \end{bmatrix}$  under  $\theta \mapsto \Gamma_{\pi}(\theta)$ .  
 1141

1142 Since we transform  $\Theta^{(\ell_1)} \mapsto \begin{bmatrix} \pi^\top & \mathbf{0} \\ \mathbf{0} & \pi^\top \end{bmatrix} \Theta^{(\ell_1)}$  and  $\bar{\mathbf{X}}_k^{(0)} \mapsto \bar{\mathbf{X}}_k^{(0)} \begin{bmatrix} \pi & \mathbf{0} \\ \mathbf{0} & \pi \end{bmatrix}$ , the quantity  $\bar{\mathbf{X}}_k^{(\ell_1)} \mapsto$   
 1143  $\bar{\mathbf{X}}_k^{(0)} \begin{bmatrix} \pi & \mathbf{0} \\ \mathbf{0} & \pi \end{bmatrix} \begin{bmatrix} \pi^\top & \mathbf{0} \\ \mathbf{0} & \pi^\top \end{bmatrix} \Theta^{(\ell_1)} = \bar{\mathbf{X}}_k^{(0)} \Theta^{(\ell_1)}$  remains unchanged as  $\pi\pi^\top = \mathbf{I}$ .  
 1144

1145 Due to this,  $\bar{\mathbf{X}}_k^{(\ell_1)}$  remains invariant to  $\Gamma_{\pi}$ . Until the final layer of updates, all transformations  $\Gamma_{\pi}^{(\ell)}$   
 1146 are identity and therefore, the resultant intermediate embeddings also remain invariant. At the final  
 1147 layer, we have  $\Theta^{(\ell_2)} \mapsto \Theta^{(\ell_2)}\pi$  (from Eq. (14)). This will give:  $\mathbf{X}_{k+1} \mapsto \mathbf{X}_{k+1}\pi$ .  
 1148

1149 **Gated GNN with GRU based**  $\text{upd}_{\theta}$ : **(I)** Let  $\Theta^{(\ell_0)}, \Theta^{(\ell_1)}, \bar{\mathbf{X}}_k^{(0)}, \bar{\mathbf{X}}_k^{(\ell_1)}$  bear the same  
 1150 meaning as before. **(II)**  $\text{upd}_{\theta}$ : We introduce the hidden state encoding of the GRU:  
 1151  $\bar{\mathbf{X}}_k^{(\text{reset})}, \bar{\mathbf{X}}_k^{(\text{update})}, \bar{\mathbf{X}}_k^{(\text{hidden})}$ . The corresponding weights are indexed by  $\ell_{\text{inp}, \bullet}$  or  $\ell_{\text{hid}, \bullet}$ . Here,  
 1152 the update steps considered in the GRU at the  $k^{\text{th}}$  round of propagation are:  
 1153

$$\bar{\mathbf{X}}_k^{(\text{reset})} = \sigma \left( \mathbf{X}_k \Theta^{(\ell_{\text{inp}, 1})} + \bar{\mathbf{X}}_k^{(\ell_1)} \Theta^{(\ell_{\text{hid}, 1})} \right) \quad (15)$$

$$\bar{\mathbf{X}}_k^{(\text{update})} = \sigma \left( \mathbf{X}_k \Theta^{(\ell_{\text{inp}, 2})} + \bar{\mathbf{X}}_k^{(\ell_1)} \Theta^{(\ell_{\text{hid}, 2})} \right) \quad (16)$$

$$\bar{\mathbf{X}}_k^{(\text{hidden})} = \tanh \left( \mathbf{X}_k \Theta^{(\ell_{\text{inp}, 3})} + (\bar{\mathbf{X}}_k^{(\ell_1)} \odot \bar{\mathbf{X}}_k^{(\text{update})}) \Theta^{(\ell_{\text{hid}, 3})} \right) \quad (17)$$

$$\mathbf{X}_{k+1} = (1 - \bar{\mathbf{X}}_k^{(\text{reset})}) \odot \mathbf{X}_k + \bar{\mathbf{X}}_k^{(\text{reset})} \odot \bar{\mathbf{X}}_k^{(\text{hidden})} \quad (18)$$

1156 We define our transformation as  
 1157

$$\Gamma_{\pi}^{(0)}(\Theta^{(\ell_0)}) = \Theta^{(\ell_0)}\pi \quad \Gamma_{\pi}^{(\ell_1)}(\Theta^{(\ell_1)}) = \begin{bmatrix} \pi^\top & \mathbf{0} \\ \mathbf{0} & \pi^\top \end{bmatrix} \Theta^{(\ell_1)} \quad (19)$$

$$\Gamma_{\pi}^{(\ell_{\text{inp}, \bullet})}(\Theta^{(\ell_{\text{inp}, \bullet})}) = \pi^\top \Theta^{(\ell_{\text{inp}, \bullet})}\pi \quad \Gamma_{\pi}^{(\ell_{\text{hid}, \bullet})}(\Theta^{(\ell_{\text{hid}, \bullet})}) = \Theta^{(\ell_{\text{hid}, \bullet})}\pi \quad (20)$$

1158 While the remaining transformations are identity.  
 1159

1160 Like the previous proof, we trace the computations in the network  
 1161 inductively over the propagation rounds.  
 1162

1163 *Base case.* For  $k = 0$ , this is true just like the previous case.  $\mathbf{X}_0 \mapsto \mathbf{X}_0\pi$  as  $\Theta^{(\ell_0)} \mapsto \Theta^{(\ell_0)}\pi$ .  
 1164

1165 *Inductive Step.* Suppose  $\mathbf{X}_k \mapsto \mathbf{X}_k\pi$  for a value of  $k$ . Then  $\bar{\mathbf{X}}_k^{(0)} = [\mathbf{x}_k^\top(u), \mathbf{x}_k^\top(v)] \mapsto$   
 1166  $\bar{\mathbf{X}}_k^{(0)} \begin{bmatrix} \pi & \mathbf{0} \\ \mathbf{0} & \pi \end{bmatrix}$  under  $\theta \mapsto \Gamma_{\pi}(\theta)$ . Since, we transform  $\Theta^{(\ell_1)} \mapsto \begin{bmatrix} \pi^\top & \mathbf{0} \\ \mathbf{0} & \pi^\top \end{bmatrix} \Theta^{(\ell_1)}$  and  $\bar{\mathbf{X}}_k^{(0)} \mapsto$   
 1167  $\bar{\mathbf{X}}_k^{(0)} \begin{bmatrix} \pi & \mathbf{0} \\ \mathbf{0} & \pi \end{bmatrix}$ , the quantity  $\bar{\mathbf{X}}_k^{(\ell_1)} \mapsto \bar{\mathbf{X}}_k^{(0)} \begin{bmatrix} \pi & \mathbf{0} \\ \mathbf{0} & \pi \end{bmatrix} \begin{bmatrix} \pi^\top & \mathbf{0} \\ \mathbf{0} & \pi^\top \end{bmatrix} \Theta^{(\ell_1)} = \bar{\mathbf{X}}_k^{(0)} \Theta^{(\ell_1)}$  remains un-  
 1168 changed as  $\pi\pi^\top = \mathbf{I}$ .  
 1169

1170 Due to the transformations in Eq. (20), we have: (1)  $\mathbf{X}_k \Theta^{(\ell_{\text{inp}, i})} \mapsto \mathbf{X}_k \pi \pi^\top \Theta^{(\ell_{\text{inp}, i})}\pi =$   
 1171  $\mathbf{X}_k \Theta^{(\ell_{\text{inp}, i})}\pi$ , for each  $i = 1, 2, 3$ ; and, (2)  $\bar{\mathbf{X}}^{(\ell_i)} \Theta^{(\ell_{\text{hid}, i})} \mapsto \bar{\mathbf{X}}^{(\ell)} \Theta^{(\ell_{\text{hid}, i})}\pi$  for each  $i = 1, 2$ .  
 1172

1188 Consequently  $\bar{\mathbf{X}}^{(\text{reset})}, \bar{\mathbf{X}}^{(\text{update})}, \bar{\mathbf{X}}^{(\text{hidden})} \mapsto \bar{\mathbf{X}}^{(\text{reset})}\boldsymbol{\pi}, \bar{\mathbf{X}}^{(\text{update})}\boldsymbol{\pi}, \bar{\mathbf{X}}^{(\text{hidden})}\boldsymbol{\pi}$ , resulting in  
 1189  $\mathbf{X}_{k+1} \mapsto \mathbf{X}_{k+1}\boldsymbol{\pi}$  as follows:

$$1190 \bar{\mathbf{X}}^{(\text{reset})} \mapsto \sigma \left( \mathbf{X}_k \Theta^{(\ell_{\text{inp},1})} \boldsymbol{\pi} + \bar{\mathbf{X}}^{(\ell_1)} \Theta^{(\ell_{\text{hid},1})} \boldsymbol{\pi} \right) \quad (21)$$

$$1192 = \sigma \left( \mathbf{X}_k \Theta^{(\ell_{\text{inp},1})} + \bar{\mathbf{X}}^{(\ell_1)} \Theta^{(\ell_{\text{hid},1})} \right) \boldsymbol{\pi} = \bar{\mathbf{X}}^{(\text{reset})}\boldsymbol{\pi} \quad (22)$$

$$1194 \bar{\mathbf{X}}^{(\text{update})} \mapsto \sigma \left( \mathbf{X}_k \Theta^{(\ell_{\text{inp},2})} \boldsymbol{\pi} + \bar{\mathbf{X}}^{(\ell_1)} \Theta^{(\ell_{\text{hid},2})} \boldsymbol{\pi} \right) \quad (23)$$

$$1196 = \sigma \left( \mathbf{X}_k \Theta^{(\ell_{\text{inp},2})} + \bar{\mathbf{X}}^{(\ell_1)} \Theta^{(\ell_{\text{hid},2})} \right) \boldsymbol{\pi} = \bar{\mathbf{X}}^{(\text{update})}\boldsymbol{\pi} \quad (24)$$

$$1198 \bar{\mathbf{X}}^{(\text{hidden})} \mapsto \tanh \left( \mathbf{X}_k \Theta^{(\ell_{\text{inp},3})} \boldsymbol{\pi} + (\bar{\mathbf{X}}^{(\ell_1)} \odot \bar{\mathbf{X}}^{(\text{update})}\boldsymbol{\pi}) \Theta^{(\ell_{\text{hid},3})} \boldsymbol{\pi} \right) \quad (25)$$

$$1200 = \tanh \left( \mathbf{X}_k \Theta^{(\ell_{\text{inp},3})} + (\bar{\mathbf{X}}^{(\ell_1)} \odot \bar{\mathbf{X}}^{(\text{update})}) \Theta^{(\ell_{\text{hid},3})} \right) \boldsymbol{\pi} = \bar{\mathbf{X}}^{(\text{hidden})}\boldsymbol{\pi} \quad (26)$$

1201 Therefore we will have:

$$1202 \mathbf{X}_{k+1} \mapsto (1 - \bar{\mathbf{X}}^{(\text{reset})}\boldsymbol{\pi}) \odot \mathbf{X}_k \boldsymbol{\pi} + \bar{\mathbf{X}}^{(\text{reset})}\boldsymbol{\pi} \odot \bar{\mathbf{X}}^{(\text{hidden})}\boldsymbol{\pi} \quad (27)$$

$$1204 = \left( (1 - \bar{\mathbf{X}}^{(\text{reset})}) \odot \mathbf{X}_k + \bar{\mathbf{X}}^{(\text{reset})} \odot \bar{\mathbf{X}}^{(\text{hidden})} \right) \boldsymbol{\pi} = \mathbf{X}_{k+1}\boldsymbol{\pi} \quad (28)$$

1206 ■  
 1207

### 1208 E.1.2 PROOF OF LEMMA 3

1210 **Lemma 3.** *Given the setting described in Section 3.1. Let  $\Gamma_{\boldsymbol{\pi}}$  be the transformation on the GNN  
 1211 parameters  $\theta$ , induced by a permutation  $\boldsymbol{\pi} \in \mathbb{R}^D$ , as introduced in Lemma 2. Then the gradient of  
 1212 the loss is equivariant under transformation  $\Gamma_{\boldsymbol{\pi}}$  of the parameters.*

1213 **Proof:** *Outline.* We assume that the loss is differentiable with respect to each parameter. We shall  
 1214 work with a finite difference of  $\Delta$  as a proxy for the gradient. We show that that equivariance holds  
 1215 for this setup. Thus, the equivariance holds in the limiting case  $\Delta \rightarrow 0$ , hence in the case of gradients.

1217 We shall make the following observation in order to prove the lemma: **For every layer, the transformation  
 1218 consists of a permutation of its entries.** This also makes  $\Gamma_{\boldsymbol{\pi}}$  linear.

1219 *Additional Notation to Facilitate the Proof.* Corresponding to each layer  $\ell$  and each scalar  
 1220 parameter  $\Theta_t^{(\ell)}[j, k]$ , we shall consider a perturbation of the parameter by  $\Delta \in \mathbb{R} - \{0\}$ .  
 1221 Within this proof,  $\Delta$  is a perturbation and *not* relevance distance. Finally,  $\delta_{\Delta, (k, l)}$  is defined as the  
 1222 matrix of appropriate dimensions with all zeros except for a  $\Delta$  at the  $(k, l)$ -th position.

1224 We write  $\theta_t +_{\ell} \delta_{\Delta, (j, k)} = \left( \Theta_t^{(\ell')} + \delta_{\Delta, (j, k)} \mathbb{I}[\ell' = \ell] \right)_{\ell' \in [\ell_{\max}]}$ . This indicates the perturbation only  
 1225 at  $(j, k)$ -th entry of  $\Theta_t^{(\ell')}$  at  $\ell' = \ell$ . We define the matrix of discrete differences as  $\mathcal{L}_{t, \Delta}^{(\ell)}$  as

$$1227 \mathcal{L}_{t, \Delta}^{(\ell)}[j, k] = \frac{1}{\Delta} [\text{loss}_t(\theta_t +_{\ell} \delta_{\Delta, (j, k)}) - \text{loss}_t(\theta_t)]. \quad (29)$$

1229 First, we show that when  $\theta_t \mapsto \Gamma_{\boldsymbol{\pi}}(\theta_t)$ , the transformation  $\mathcal{L}_t \mapsto \Gamma_{\boldsymbol{\pi}}(\mathcal{L}_t)$  will hold true. To show this,  
 1230 we derive that for a general  $\ell \in [\ell_{\max}]$ ,  $\mathcal{L}_{t, \Delta}^{(\ell)} \mapsto \Gamma_{\boldsymbol{\pi}}^{(\ell)}(\mathcal{L}_{t, \Delta}^{(\ell)})$ . Let us characterize the permutation on  
 1231 the entries of the parameter corresponding to  $\Gamma_{\boldsymbol{\pi}}^{(\ell)}$  by introducing a permutation map  $\widehat{\pi} : [m] \times [n] \rightarrow$   
 1232  $[m] \times [n]$ . For any  $\Theta_t^{(\ell)}$ , there exists  $\widehat{\pi}$  defined as above, such that:  $\Gamma_{\boldsymbol{\pi}}^{(\ell)}(\Theta_t^{(\ell)})[\widehat{\pi}(j, k)] = \Theta_t^{(\ell)}[j, k]$ .  
 1233 Here,  $\widehat{\pi}$  depends on  $\ell$ . However, we omit this for the sake of readability.

1235 *Proof.* Note the following identities that hold as a consequence:

1236 • For all  $j, k$ , we have:

$$1238 \Gamma_{\boldsymbol{\pi}}^{(\ell)}(\Theta^{(\ell)})[j, k] = \Theta^{(\ell)}[\widehat{\pi}^{-1}(j, k)] \quad (30)$$

1239 • Consider the  $(a, b)^{\text{th}}$  entry of the following matrix:  $\Gamma_{\boldsymbol{\pi}}^{(\ell)} \delta_{\Delta, (j, k)}[a, b] = \delta_{\Delta, (j, k)}[\widehat{\pi}^{-1}(a, b)]$ , which  
 1240 is  $\Delta$  if  $a, b = \widehat{\pi}(j, k)$  and 0, otherwise. Then, by definition of  $\delta_{\Delta, (\bullet, \bullet)}$ , we have:

$$1241 \Gamma_{\boldsymbol{\pi}}^{(\ell)} \delta_{\Delta, (j, k)} = \delta_{\Delta, (\widehat{\pi}(j, k))} \quad (31)$$

The transformation  $\Gamma_\pi$  is linear, which implies that  $\Gamma_\pi(\theta + \ell \delta_{\Delta,(\bullet)}) = \Gamma_\pi(\theta) + \ell \Gamma_\pi^{(\ell)}(\delta_{\Delta,(\bullet)})$ .

Consider the  $(a, b)$ -th entry of  $\widehat{\mathcal{L}}_{t,\Delta}^{(\ell)} = \mathcal{L}_{t,\Delta}^{(\ell)} \Big|_{\theta_t \mapsto \Gamma_\pi(\theta_t)}$  which is the loss:

$$\widehat{\mathcal{L}}_{t,\Delta}^{(\ell)}[a, b] = \frac{1}{\Delta} [\text{loss}_t(\Gamma_\pi(\theta_t) + \ell \delta_{\Delta,(a,b)}) - \text{loss}_t(\Gamma_\pi(\theta_t))] \quad (32)$$

$$= \frac{1}{\Delta} [\text{loss}_t(\Gamma_\pi(\theta_t) + \ell \Gamma_\pi^{(\ell)} \circ \Gamma_\pi^{(\ell)-1} \delta_{\Delta,(a,b)}) - \text{loss}_t(\Gamma_\pi(\theta_t))] \quad (33)$$

$$= \frac{1}{\Delta} [\text{loss}_t(\Gamma_\pi(\theta_t + \ell \Gamma_\pi^{(\ell)-1}(\delta_{\Delta,(a,b)}))) - \text{loss}_t(\Gamma_\pi(\theta_t))] \quad (34)$$

$$= \frac{1}{\Delta} [\text{loss}_t(\theta_t + \ell \Gamma_\pi^{(\ell)-1}(\delta_{\Delta,(a,b)})) - \text{loss}_t(\theta_t)] \quad (\text{as the loss is invariant of } \Gamma_\pi) \quad (35)$$

$$= \frac{1}{\Delta} [\text{loss}_t(\theta_t + \ell \delta_{\Delta,(\widehat{\pi}^{-1}(a,b))}) - \text{loss}_t(\theta_t)] \quad \text{from Eq. (31)} \quad (36)$$

$$= \mathcal{L}_{t,\Delta}^{(\ell)}[\widehat{\pi}^{-1}(a,b)] = \Gamma_\pi^{(\ell)}(\mathcal{L}_{t,\Delta}^{(\ell)})[a,b] \quad \text{from Eq. (30)} \quad (37)$$

Thus,  $\widehat{\mathcal{L}}_{t,\Delta}^{(\ell)} = \Gamma_\pi^{(\ell)}(\mathcal{L}_{t,\Delta}^{(\ell)})$ . Now,  $\lim_{\Delta \rightarrow 0} \mathcal{L}_{t,\Delta}^{(\ell)} = \text{grad}_t^{(\ell)}$ . Hence, we have:

$$\lim_{\Delta \rightarrow 0} \widehat{\mathcal{L}}_{t,\Delta}^{(\ell)} = \lim_{\Delta \rightarrow 0} \Gamma_\pi^{(\ell)}(\mathcal{L}_{t,\Delta}^{(\ell)}) \quad (38)$$

$$= \Gamma_\pi^{(\ell)} \left( \lim_{\Delta \rightarrow 0} \mathcal{L}_{t,\Delta}^{(\ell)} \right) \quad (\Gamma_\pi^{(\ell)} \text{ is a smooth map}) \quad (39)$$

$$= \Gamma_\pi^{(\ell)}(\text{grad}_t^{(\ell)}) \quad (40)$$

Therefore as  $\Theta_t^{(\ell)} \mapsto \Gamma_\pi^{(\ell)}(\Theta_t^{(\ell)})$ , we have  $\text{grad}_t^{(\ell)} \mapsto \Gamma_\pi^{(\ell)}(\text{grad}_t^{(\ell)})$ . Hence,  $\text{grad}_t = [\text{grad}_t^{(\ell)}]_\ell \mapsto [\Gamma_\pi^{(\ell)}(\text{grad}_t^{(\ell)})]_\ell = \Gamma_\pi([\text{grad}_t^{(\ell)}]_\ell) = \Gamma_\pi(\text{grad}_t)$ .  $\blacksquare$

### E.1.3 PROOF OF LEMMA 4

**Lemma 4.** *Given the setting described in Section 3.1. Let  $\{\theta_t \mid t \geq 0\}$  be the trajectory of the parameter  $\theta$  of a GNN across different training epochs  $t \geq 0$ . Then, we have:  $p(\theta_t) = p(\Gamma_\pi(\theta_t))$  for all  $t \geq 0$ .*

**Proof:** For  $\text{iter} = 0$ , we have  $p(\theta_0) = p(\Gamma_\pi(\theta_0))$  by the i.i.d. initialization of parameters. For  $\text{iter} > 0$ , we use two key conditions: (1) The loss function is invariant under  $\Gamma_\pi$  (which holds, as our loss is permutation invariant in the GNN output). (2) The gradient and update steps are equivariant under  $\Gamma_\pi$ . We first note that:

$$p(\theta_t) = \int_{\underbrace{\mathcal{J} \times \dots \times \mathcal{J}}_{t \text{ times}}} \prod_{\text{iter}=1}^t p(\theta_{\text{iter}} \mid \theta_{<\text{iter}}) d\theta_{< t} \quad (41)$$

First, to build up intuition, consider a simpler setup which, instead of using an advanced optimizer like Adam/SGD, uses simple full batch gradient descent. Assuming the learning rate is 1, we will have:

$$\Theta_{\text{iter}}^{(\ell)} = \Theta_{\text{iter}-1}^{(\ell)} - \text{grad}^{(\ell)} \Big|_{\Theta=\Theta_{\text{iter}-1}^{(\ell)}} \quad (42)$$

Hence,  $p(\theta_{\text{iter}} \mid \theta_{<\text{iter}})$  is given by:

$$p(\theta_{\text{iter}} \mid \theta_{<\text{iter}}) = \delta(\theta_{\text{iter}} - \theta_{\text{iter}-1} + \text{grad}_{\text{iter}-1}) \quad (43)$$

Since  $\Gamma_\pi^{(\ell)}$  is a linear homeomorphism, we have

$$\Gamma_\pi^{(\ell)}(\Theta_{\text{iter}}^{(\ell)}) = \Gamma_\pi^{(\ell)}(\Theta_{\text{iter}-1}^{(\ell)}) - \Gamma_\pi^{(\ell)} \left( \text{grad}^{(\ell)} \Big|_{\Theta=\Theta_{\text{iter}-1}^{(\ell)}} \right) \quad (44)$$

$$= \Gamma_\pi^{(\ell)}(\Theta_{\text{iter}-1}^{(\ell)}) - \text{grad}^{(\ell)} \Big|_{\Theta=\Gamma_\pi^{(\ell)}(\Theta_{\text{iter}-1}^{(\ell)})} \quad (\text{Lemma 3}) \quad (45)$$

Given  $\Gamma_\pi(\theta) = \bigoplus_\ell \Gamma_\pi^{(\ell)}(\Theta^{(\ell)})$

$$\Gamma_\pi(\theta_{\text{iter}}) = \Gamma_\pi(\theta_{\text{iter}-1}) - \text{grad} \Big|_{\theta=\Gamma_\pi(\theta_{\text{iter}-1})} \quad (46)$$

This allows us to write:

$$p(\Gamma_\pi(\theta_{\text{iter}}) \mid \Gamma_\pi(\theta_{<\text{iter}})) = \delta(\Gamma_\pi(\theta_{\text{iter}}) - \Gamma_\pi(\theta_{\text{iter}-1}) + \Gamma_\pi(\text{grad}_{\text{iter}-1})) \quad (47)$$

Now, since Eq. (42) and Eq. (46) are equivalent, we have

$$p(\theta_{\text{iter}} | \theta_{<\text{iter}}) = p(\Gamma_{\boldsymbol{\pi}}(\theta_{\text{iter}}) | \Gamma_{\boldsymbol{\pi}}(\theta_{<\text{iter}})) \quad (48)$$

The above relationship suggests Eq. (41) is equivalent to

$$p(\theta_t) = \underbrace{\int_{\mathcal{J} \times \dots \times \mathcal{J}}}_{t \text{ times}} \prod_{\text{iter}=1}^t p(\Gamma_{\boldsymbol{\pi}}(\theta_{\text{iter}}) | \Gamma_{\boldsymbol{\pi}}(\theta_{<\text{iter}})) d\theta_{\text{iter}} \quad (49)$$

$$= \int_{(\Gamma_{\boldsymbol{\pi}} \circ \mathcal{J})^t} \prod_{\text{iter}=0}^t p(\Gamma_{\boldsymbol{\pi}}(\theta_{\text{iter}}) | \Gamma_{\boldsymbol{\pi}}(\theta_{<\text{iter}})) d(\Gamma_{\boldsymbol{\pi}}(\theta_{\text{iter}})) \left| \text{Det} \left( \frac{\partial \theta_{\text{iter}}}{\partial \Gamma_{\boldsymbol{\pi}}(\theta_{\text{iter}})} \right) \right|^{-1} \quad (50)$$

$$= p(\Gamma_{\boldsymbol{\pi}}(\theta_t)) \quad (51)$$

$\left| \text{Det} \left( \frac{\partial \theta_{\text{iter}}}{\partial \Gamma_{\boldsymbol{\pi}}(\theta_{\text{iter}})} \right) \right| = 1$  because  $\Gamma_{\boldsymbol{\pi}}$  consists only of permutation matrices. Here, we proved that Eq. (42) and Eq. (46) are equivalent for full batch gradient descent. This relationship also holds for other standard optimizers (such as listed in E.1.5), which is shown below. We may abstract the update step as follows –

$$\boldsymbol{\Theta}_{\text{iter}}^{(\ell)} = \text{Update}_{\ell, \text{iter}} \left( \left( \boldsymbol{\Theta}_b^{(\ell)} \mid b < \text{iter} \right), \left( \mathbf{grad}_b^{(\ell)} \mid b < \text{iter} \right) \right) \quad (52)$$

$$\text{This gives: } p(\theta_{\text{iter}} | \theta_{<\text{iter}}) = \prod_{\ell} \delta \left( \left[ \boldsymbol{\Theta}_{\text{iter}}^{(\ell)} - \text{Update}_{\ell, \text{iter}} \left( \left( \boldsymbol{\Theta}_b^{(\ell)} \mid b < \text{iter} \right), \left( \mathbf{grad}_b^{(\ell)} \mid b < \text{iter} \right) \right) \right] \right) \quad (53)$$

According to Lemma 10, Eq. (52) is equivalent to:

$$\Gamma_{\boldsymbol{\pi}}^{(\ell)}(\boldsymbol{\Theta}_{\text{iter}}^{(\ell)}) = \text{Update}_{\ell, \text{iter}} \left( \left( \Gamma_{\boldsymbol{\pi}}^{(\ell)}(\boldsymbol{\Theta}_b^{(\ell)}) \mid b < \text{iter} \right), \left( \Gamma_{\boldsymbol{\pi}}^{(\ell)}(\mathbf{grad}_b^{(\ell)}) \mid b < \text{iter} \right) \right) \quad (54)$$

as long as  $\Gamma_{\boldsymbol{\pi}}^{(\ell)}$  is a permutation matrix (which is the case according to Lemma 2). This implies that  $p(\theta_{\text{iter}} | \theta_{<\text{iter}})$  (53) is the same as:

$$p(\Gamma_{\boldsymbol{\pi}}(\theta_{\text{iter}}) | \Gamma_{\boldsymbol{\pi}}(\theta_{<\text{iter}})) = \prod_{\ell} \delta \left( \Gamma_{\boldsymbol{\pi}}^{(\ell)}(\boldsymbol{\Theta}_{\text{iter}}^{(\ell)}) - \text{Update}_{\ell, \text{iter}} \left( \left( \Gamma_{\boldsymbol{\pi}}^{(\ell)}(\boldsymbol{\Theta}_b^{(\ell)}) \mid b < \text{iter} \right), \left( \Gamma_{\boldsymbol{\pi}}^{(\ell)}(\mathbf{grad}_b^{(\ell)}) \mid b < \text{iter} \right) \right) \right) \quad (55)$$

#### E.1.4 PROOF OF THEOREM 5 AND PROPOSITION 6

We state both the results.

**Theorem 5.** *Given the setting described in Section 3.1. Then,  $\mathbf{X} = \text{GNN}_{\theta}(G)$  are exchangeable random variables, where the randomness is induced by the model initialization prior to training. That is,  $p(\mathbf{X}) = p(\mathbf{X}\boldsymbol{\pi})$ .*

**Proposition 6.** *Given two graphs  $G_q, G_c$ , let the settings in Section 3.1 hold true. Specifically, let us assume that the loss function be invariant to simultaneous permutations of the embeddings  $\mathbf{X}^{(q)} = \text{GNN}_{\theta}(G_q)$  and  $\mathbf{X}^{(c)} = \text{GNN}_{\theta}(G_c)$ . Then,  $\mathbf{Y} = [\mathbf{X}^{(q)}; \mathbf{X}^{(c)}] \in \mathbb{R}^{2n \times D}$  satisfies  $p(\mathbf{Y}) = p(\mathbf{Y}\boldsymbol{\pi})$ .*

We shall prove both of these in one go, as the latter implies the former.

**Proof:** Let  $\mathbf{Y}$  denote the concatenation of the query and corpus embeddings, i.e.,  $\mathbf{Y} = \begin{bmatrix} \mathbf{X}^{(q)} \\ \mathbf{X}^{(c)} \end{bmatrix}$ ,

where  $\mathbf{X}^{(\bullet)} \in \mathbb{R}^{m \times D}$ . We need to show that:

$$p(\mathbf{Y}) = p(\mathbf{Y}\boldsymbol{\pi}) \quad (56)$$

1350 This is precisely the condition for exchangeability as stated in Definition 1. We first observe that:  
 1351

$$1352 \quad p(\mathbf{Y}) = \int_{\mathcal{J}} p(\mathbf{Y} | \theta_t) p(\theta_t) d\theta_t \quad (\text{marginalization}) \quad (57)$$

$$1354 \quad = \int_{\mathcal{J}} p(\mathbf{Y}\boldsymbol{\pi} | \Gamma_{\boldsymbol{\pi}}(\theta_t)) p(\theta_t) d\theta_t \quad (\text{using } p(\mathbf{Y} | \theta_t) = p(\mathbf{Y}\boldsymbol{\pi} | \Gamma_{\boldsymbol{\pi}}(\theta_t))) \quad (58)$$

$$1356 \quad = \int_{\mathcal{J}} p(\mathbf{Y}\boldsymbol{\pi} | \Gamma_{\boldsymbol{\pi}}(\theta_t)) p(\Gamma_{\boldsymbol{\pi}}(\theta_t)) d\theta_t \quad (\text{using } p(\theta_t) = p(\Gamma_{\boldsymbol{\pi}}(\theta_t))) \quad (59)$$

$$1358 \quad = \int_{\Gamma_{\boldsymbol{\pi}} \circ \mathcal{J} = \mathcal{J}} p(\mathbf{Y}\boldsymbol{\pi} | \Gamma_{\boldsymbol{\pi}}(\theta_t)) p(\Gamma_{\boldsymbol{\pi}}(\theta_t)) d(\Gamma_{\boldsymbol{\pi}}(\theta_t)) \left| \frac{\partial \theta_t}{\partial \Gamma_{\boldsymbol{\pi}}(\theta_t)} \right| \\ 1361 \quad \quad \quad (\text{Random variable transform } \theta_t \mapsto \Gamma_{\boldsymbol{\pi}}\theta_t) \quad (60)$$

$$1362 \quad = \int_{\mathcal{J}} p(\mathbf{Y}\boldsymbol{\pi} | \Gamma_{\boldsymbol{\pi}}(\theta_t)) p(\Gamma_{\boldsymbol{\pi}}(\theta_t)) d(\Gamma_{\boldsymbol{\pi}}(\theta_t)) \cdot 1 = p(\mathbf{Y}\boldsymbol{\pi}) \quad (\text{marginalization}) \quad (61)$$

1364 Justifications of Eqs (57), (61) are trivial. We now provide justifications for the claims in Eq. (58)  
 1365 and Eq. (59) are as follows.

1366 **Justification for  $p(\mathbf{Y} | \theta_t) = p(\mathbf{Y}\boldsymbol{\pi} | \Gamma_{\boldsymbol{\pi}}(\theta_t))$  used in Eq. (58):** As the network output is determin-  
 1367 istic,  $p(\mathbf{Y} | \theta_t)$  can be written in terms of the network output  $\text{GNN}_{\theta}$  and the Dirac delta function as  
 1368 follows:

$$1369 \quad p(\mathbf{Y} | \theta_t) = \delta \left( \mathbf{Y} - \begin{bmatrix} \text{GNN}_{\theta_t}(G_q) \\ \text{GNN}_{\theta_t}(G_c) \end{bmatrix} \right) \quad (62)$$

1371 Here  $\delta(\bullet)$  is the Diract delta functional.  $\delta(\bullet) = \begin{cases} \infty & \text{if } \mathbf{Z} = \mathbf{0} \\ 0 & \text{otherwise} \end{cases}$  and  $\int_{\mathcal{J}} \delta(\mathbf{Z}) d\mathbf{Z} = 1$ .  
 1372

1373 Since the following relation holds:  $\mathbf{Y} = \begin{bmatrix} \text{GNN}_{\theta_t}(G_q) \\ \text{GNN}_{\theta_t}(G_c) \end{bmatrix}$  iff  $\mathbf{Y}\boldsymbol{\pi} = \begin{bmatrix} \text{GNN}_{\Gamma_{\boldsymbol{\pi}}(\theta_t)}(G_q) \\ \text{GNN}_{\Gamma_{\boldsymbol{\pi}}(\theta_t)}(G_c) \end{bmatrix}$ , we have  
 1374  $p(\mathbf{Y} | \theta_t) = p(\mathbf{Y}\boldsymbol{\pi} | \Gamma_{\boldsymbol{\pi}}(\theta_t))$ . Justification for  $p(\theta_t) = p(\Gamma_{\boldsymbol{\pi}}(\theta_t))$  in Eq. (59) occurs due to Lemma 4.  
 1375

1376 Here, we note that our result holds even in the presence of additional sources of randomness in the  
 1377 training process, such as data shuffling or batching. Since these sources are independent of parameter  
 1378 initialization, the proof extends by conditioning on the training randomness and then marginalizing,  
 1379 yielding the same conclusion.  
 1380

1381  
 1382  
 1383  
 1384  
 1385  
 1386  
 1387  
 1388  
 1389  
 1390  
 1391  
 1392  
 1393  
 1394  
 1395  
 1396  
 1397  
 1398  
 1399  
 1400  
 1401  
 1402  
 1403

1404 E.1.5 EQUIVARIANCE OF THE UPDATE STEP  
14051406 We shall present a general lemma that states the precise update step equivariance property. Later, we  
1407 will prove it for optimizers such as Adam, SGD, AdaGrad, RMSProp, followed by a more general  
1408 general formulation.  
14091410 **Lemma 10** (Equivariance of update step). *The update steps of the optimizer follow the functional  
1411 form and equivariance property. Specifically Eq. (63) holds true iff Eq. (64) holds true.*

1412 
$$\Theta_t^{(\ell)} \triangleq \text{Update}_{\ell,t} \left( \left( \Theta_{\text{iter}}^{(\ell)} \mid \text{iter} < t \right), \left( \text{grad}_{\text{iter}}^{(\ell)} \mid \text{iter} < t \right) \right) \quad (63)$$

1414 
$$\pi_1 \Theta_t^{(\ell)} \pi_2 = \text{Update}_{\ell,t} \left( \left( \pi_1 \Theta_{\text{iter}}^{(\ell)} \pi_2 \mid \text{iter} < t \right), \left( \pi_1 \text{grad}_{\text{iter}}^{(\ell)} \pi_2 \mid \text{iter} < t \right) \right) \quad (64)$$

1416 Note that this means that the update step is equivariant with respect to a transformation that permutes  
1417 the rows and columns of each parameter matrix. The transformation  $\pi_1$  permutes the rows of the  
1418 parameter matrix, while  $\pi_2$  permutes the columns.  
14191420 **Proof for Adam (Kingma et al., 2015)** We first describe the Adam update steps — For layer  
1421  $\ell$  at time  $t$ , we refer to the momentum of the gradients  $\mathbf{m}_t^{(\ell)}$ , and the squared gradients  $\mathbf{v}_t^{(\ell)}$ . The  
1422 corresponding bias-corrected terms which used by Adam are denoted by  $\widehat{\mathbf{m}}_t^{(\ell)}$  and  $\widehat{\mathbf{v}}_t^{(\ell)}$  respectively.1423 The hyperparameters for Adam are defined as follows:  $\beta_1$  and  $\beta_2$  are scalar coefficients that control  
1424 the exponential moving averages of the gradient and its square.  $\alpha$  denotes the learning rate.  $\epsilon$  is a  
1425 small positive constant added for numerical stability.  $\lambda$  is the weight decay parameter.  
14261427 The Adam optimizer (Kingma et al., 2014) updates each parameter as follows:  
1428

1429 
$$\Theta_t^{(\ell)} = \Theta_{t-1}^{(\ell)} - \alpha \frac{\widehat{\mathbf{m}}_t^{(\ell)}}{\sqrt{\widehat{\mathbf{v}}_t^{(\ell)}} + \epsilon} \quad (65)$$

1431 
$$\mathbf{g}_t^{(\ell)} = \text{grad}_t^{(\ell)} + \lambda \Theta_{t-1}^{(\ell)} \quad (66)$$

1432 
$$\widehat{\mathbf{m}}_t^{(\ell)} = \frac{\mathbf{m}_t^{(\ell)}}{1 - n^\top} \quad (67)$$

1434 
$$\mathbf{m}_t^{(\ell)} = \beta_1 \mathbf{m}_{t-1}^{(\ell)} + (1 - \beta_1) \mathbf{g}_t^{(\ell)} \quad (68)$$

1436 
$$\widehat{\mathbf{v}}_t^{(\ell)} = \frac{\mathbf{v}_t^{(\ell)}}{1 - \beta_2^\top} \quad (69)$$

1438 
$$\mathbf{v}_t^{(\ell)} = \beta_2 \mathbf{v}_{t-1}^{(\ell)} + (1 - \beta_2) (\mathbf{g}_t^{(\ell)} \odot \mathbf{g}_t^{(\ell)}) \quad (70)$$

1440 Where  $\mathbf{m}_0^{(\ell)} = \mathbf{v}_0^{(\ell)} = 0$ .  
1441Eq (63) can be represented by simply inductively writing out the update steps in terms of the previous  
1442 steps using  $\Theta_{<t}^{(\ell)}$  and  $\text{grad}_{<t}^{(\ell)}$ . Similarly for Eq. (64), we can show that each  $\mathbf{v}_{\text{iter}}^{(\ell)}$  and  $\mathbf{m}_{\text{iter}}^{(\ell)}$  are  
1443 permutation equivariant with respect to the gradients, and consequently even  $\widehat{\mathbf{m}}_{\text{iter}}^{(\ell)}$  and  $\widehat{\mathbf{v}}_{\text{iter}}^{(\ell)}$ . We  
1444 shall work this out here—  
14451446 Consider the transformation  $\Theta_{<t}^{(\ell)} \mapsto \pi_1^\top (\Theta_{<t}^{(\ell)}) \pi_2$ ,  
1447

1448 
$$\text{grad}_{<t}^{(\ell)} \mapsto \pi_1^\top \text{grad}_{<t}^{(\ell)} \pi_2 \quad (\text{assumption, shown in Lemma 3}) \quad (71)$$
  
1449

1450 We show equivariance for  $\mathbf{v}_t^{(\ell)}$  and  $\mathbf{m}_t^{(\ell)}$  by induction—  
1451

1452 
$$\mathbf{g}_t^{(\ell)} \mapsto \pi_1^\top (\mathbf{g}_t^{(\ell)}) \pi_2 \quad (72)$$

1453 
$$\mathbf{v}_0^{(\ell)} = (1 - \beta_2) (\mathbf{g}_0^{(\ell)} \odot \mathbf{g}_0^{(\ell)}) \mapsto (1 - \beta_2) (\pi_1^\top \mathbf{g}_0^{(\ell)} \pi_2 \odot \pi_1^\top \mathbf{g}_0^{(\ell)} \pi_2) \quad (73)$$

1454 
$$= \pi_1^\top (1 - \beta_2) (\mathbf{g}_0^{(\ell)} \odot \mathbf{g}_0^{(\ell)}) \pi_2 = \pi_1^\top \mathbf{v}_0^{(\ell)} \pi_2 \quad (74)$$

1456 
$$\mathbf{v}_t^{(\ell)} = \beta_2 \mathbf{v}_{t-1}^{(\ell)} + (1 - \beta_2) (\mathbf{g}_t^{(\ell)} \odot \mathbf{g}_t^{(\ell)}) \mapsto \beta_2 \pi_1^\top \mathbf{v}_{t-1}^{(\ell)} \pi_2 + \pi_1^\top (1 - \beta_2) (\mathbf{g}_t^{(\ell)} \odot \mathbf{g}_t^{(\ell)}) \pi_2 \quad (75)$$

1457 
$$= \pi_1^\top \mathbf{v}_t^{(\ell)} \pi_2 \quad (76)$$

1458

1459

$$\mathbf{m}_0^\ell = (1 - \beta_1)(\mathbf{g}_0^{(\ell)}) \mapsto (1 - \beta_1)(\boldsymbol{\pi}_1^\top \mathbf{g}_0^{(\ell)} \boldsymbol{\pi}_2) \quad (77)$$

1460

$$= \boldsymbol{\pi}_1^\top (1 - \beta_1)(\mathbf{g}_0^{(\ell)}) \boldsymbol{\pi}_2 = \boldsymbol{\pi}_1^\top \mathbf{m}_0^\ell \boldsymbol{\pi}_2 \quad (78)$$

1461

$$\mathbf{m}_t^\ell = \beta_1 \mathbf{m}_{t-1}^\ell + (1 - \beta_1)(\mathbf{g}_t^{(\ell)}) \mapsto \beta_1 \boldsymbol{\pi}_1^\top \mathbf{m}_{t-1}^\ell \boldsymbol{\pi}_2 + \boldsymbol{\pi}_1^\top (1 - \beta_1)(\mathbf{g}_t^{(\ell)}) \boldsymbol{\pi}_2 \quad (79)$$

1462

$$= \boldsymbol{\pi}_1^\top \mathbf{m}_t^\ell \boldsymbol{\pi}_2 \quad (80)$$

1463

1464

1465

1466

1467

$$\widehat{\mathbf{v}}_t^\ell = \frac{\mathbf{v}_t^\ell}{1 - \beta_2^\top} \mapsto \frac{\boldsymbol{\pi}_1^\top \mathbf{v}_t^\ell \boldsymbol{\pi}_2}{1 - \beta_2^\top} = \boldsymbol{\pi}_1^\top \widehat{\mathbf{v}}_t^\ell \boldsymbol{\pi}_2 \quad (81)$$

1468

1469

$$\widehat{\mathbf{m}}_t^\ell = \frac{\mathbf{m}_t^\ell}{1 - \beta_1^\top} \mapsto \frac{\boldsymbol{\pi}_1^\top \mathbf{m}_t^\ell \boldsymbol{\pi}_2}{1 - \beta_1^\top} = \boldsymbol{\pi}_1^\top \widehat{\mathbf{m}}_t^\ell \boldsymbol{\pi}_2 \quad (82)$$

1470

1471

1472

1473

1474

Finally, from (65),  $\Theta_t^{(\ell)}$  is permutation equivariant with respect to  $\Theta_{t-1}^{(\ell)}$  and the gradients.

1475

1476

$$\Theta_t^{(\ell)} = \Theta_{t-1}^{(\ell)} - \alpha \frac{\widehat{\mathbf{m}}_t^\ell}{\sqrt{\widehat{\mathbf{v}}_t^\ell + \epsilon}} \mapsto \boldsymbol{\pi}_1^\top \Theta_{t-1}^{(\ell)} \boldsymbol{\pi}_2 - \alpha \frac{\boldsymbol{\pi}_1^\top \widehat{\mathbf{m}}_t^\ell \boldsymbol{\pi}_2}{\sqrt{\boldsymbol{\pi}_1^\top \widehat{\mathbf{v}}_t^\ell \boldsymbol{\pi}_2 + \epsilon}} \quad (83)$$

1477

1478

$$= \boldsymbol{\pi}_1^\top \left( \Theta_{t-1}^{(\ell)} - \alpha \frac{\widehat{\mathbf{m}}_t^\ell}{\sqrt{\widehat{\mathbf{v}}_t^\ell + \epsilon}} \right) \boldsymbol{\pi}_2 = \boldsymbol{\pi}_1^\top \Theta_t^{(\ell)} \boldsymbol{\pi}_2 \quad (84)$$

1479

1480

1481

1482

1483

1484

1485

**Proof for SGD** SGD has hyperparameters for learning rate  $\alpha$ , and weight decay  $\lambda$ . For layer  $\ell$  at time  $t$ , the update step of SGD with weight decay is given by:

1486

$$\Theta_t^{(\ell)} = \Theta_{t-1}^{(\ell)} - \alpha \mathbf{g}_t^{(\ell)} \quad (85)$$

1487

1488

$$\mathbf{g}_t^{(\ell)} = \text{grad}_t^{(\ell)} + \lambda \Theta_{t-1}^{(\ell)} \quad (86)$$

1489

1490

Where  $\lambda$  is the weight decay term and  $\alpha$  is the learning rate.

1491

1492

1493

Here, the gradient is computed over a point/mini-batch of points sampled at time  $t$ . We can fix the randomness of the sampling by conditioning on the “trajectory” of sampled points(or mini-batches). Thus, we can treat  $\text{grad}_t^{(\ell)}$  as a deterministic function of  $\Theta_{<t}^{(\ell)}$ .

1494

1495

Furthermore, this gradient also follows the gradient equivariance property from Lemma 3.

1496

1497

Consider the transformation  $\Theta_{t-1}^{(\ell)} \mapsto \boldsymbol{\pi}_1^\top (\Theta_{t-1}^{(\ell)}) \boldsymbol{\pi}_2$  and  $\text{grad}_t^{(\ell)} \mapsto \boldsymbol{\pi}_1^\top (\text{grad}_t^{(\ell)}) \boldsymbol{\pi}_2$ . Then:

1498

1499

1500

1501

$$\mathbf{g}_t^{(\ell)} \mapsto \boldsymbol{\pi}_1^\top (\text{grad}_t^{(\ell)}) \boldsymbol{\pi}_2 + \lambda \boldsymbol{\pi}_1^\top (\Theta_{t-1}^{(\ell)}) \boldsymbol{\pi}_2 = \boldsymbol{\pi}_1^\top \mathbf{g}_t^{(\ell)} \boldsymbol{\pi}_2 \quad (87)$$

1502

1503

1504

$$\Theta_t^{(\ell)} \mapsto \boldsymbol{\pi}_1^\top \Theta_{t-1}^{(\ell)} \boldsymbol{\pi}_2 - \alpha \boldsymbol{\pi}_1^\top \mathbf{g}_t^{(\ell)} \boldsymbol{\pi}_2 \quad (88)$$

$$= \boldsymbol{\pi}_1^\top (\Theta_{t-1}^{(\ell)} - \alpha \mathbf{g}_t^{(\ell)}) \boldsymbol{\pi}_2 = \boldsymbol{\pi}_1^\top \Theta_t^{(\ell)} \boldsymbol{\pi}_2 \quad (89)$$

1505

1506

1507

1508

1509

Thus, the SGD update is equivariant with respect to the transformation. By conditioning on the trajectory, we actually show a stronger result for equivariance. We may show the equivariance without conditioning on the trajectory, by considering the expectation of the above result over the randomness of the sampling.  $\square$

1510

1511

**Proof for AdaGrad (Duchi et al., 2011)** AdaGrad has hyperparameters for (time dependent) learning rate  $\alpha_t$ , weight decay  $\lambda$ , and a small constant  $\epsilon$  for stability. For layer  $\ell$  at time  $t$ , we refer to the accumulated squared gradients as  $\mathbf{G}_t^{(\ell)}$  (which is defined below). The update steps for AdaGrad

1512 are given by:  
 1513

$$\Theta_t^{(\ell)} = \Theta_{t-1}^{(\ell)} - \frac{\alpha_t}{\sqrt{\mathbf{G}_t^{(\ell)}} + \epsilon} \odot \mathbf{g}_t^{(\ell)} \quad (90)$$

$$\mathbf{g}_t^{(\ell)} = \mathbf{grad}_t^{(\ell)} + \lambda \Theta_{t-1}^{(\ell)} \quad (91)$$

$$\mathbf{G}_t^{(\ell)} = \mathbf{G}_{t-1}^{(\ell)} + (\mathbf{g}_t^{(\ell)} \odot \mathbf{g}_t^{(\ell)}) \quad (92)$$

1519 Where  $\mathbf{G}_0^{(\ell)} = \mathbf{0}$ .  
 1520

1521 Consider the transformation  $\Theta_{<t}^{(\ell)} \mapsto \pi_1^\top(\Theta_{<t}^{(\ell)})\pi_2$  and  $\mathbf{grad}_{<t}^{(\ell)} \mapsto \pi_1^\top(\mathbf{grad}_{<t}^{(\ell)})\pi_2$ . We show that  
 1522  $\mathbf{G}_t^{(\ell)}$  is equivariant by induction:  
 1523

$$\mathbf{g}_t^{(\ell)} \mapsto \pi_1^\top(\mathbf{g}_t^{(\ell)})\pi_2 \quad (93)$$

$$\mathbf{G}_0^{(\ell)} = \mathbf{0} \mapsto \pi_1^\top \mathbf{0} \pi_2 = \mathbf{0} = \pi_1^\top \mathbf{G}_0^{(\ell)} \pi_2 \quad (94)$$

$$\mathbf{G}_t^{(\ell)} = \mathbf{G}_{t-1}^{(\ell)} + (\mathbf{g}_t^{(\ell)} \odot \mathbf{g}_t^{(\ell)}) \quad (95)$$

$$\mapsto \pi_1^\top \mathbf{G}_{t-1}^{(\ell)} \pi_2 + (\pi_1^\top \mathbf{g}_t^{(\ell)} \pi_2 \odot \pi_1^\top \mathbf{g}_t^{(\ell)} \pi_2) \quad (96)$$

$$= \pi_1^\top \mathbf{G}_{t-1}^{(\ell)} \pi_2 + \pi_1^\top (\mathbf{g}_t^{(\ell)} \odot \mathbf{g}_t^{(\ell)}) \pi_2 \quad (97)$$

$$= \pi_1^\top (\mathbf{G}_{t-1}^{(\ell)} + \mathbf{g}_t^{(\ell)} \odot \mathbf{g}_t^{(\ell)}) \pi_2 = \pi_1^\top \mathbf{G}_t^{(\ell)} \pi_2 \quad (98)$$

1533 Finally, for the weight update:  
 1534

$$\Theta_t^{(\ell)} = \Theta_{t-1}^{(\ell)} - \frac{\alpha_t}{\sqrt{\mathbf{G}_t^{(\ell)}} + \epsilon} \odot \mathbf{g}_t^{(\ell)} \quad (99)$$

$$\mapsto \pi_1^\top \Theta_{t-1}^{(\ell)} \pi_2 - \frac{\alpha_t}{\sqrt{\pi_1^\top \mathbf{G}_t^{(\ell)} \pi_2} + \epsilon} \odot \pi_1^\top \mathbf{g}_t^{(\ell)} \pi_2 \quad (100)$$

$$= \pi_1^\top \Theta_{t-1}^{(\ell)} \pi_2 - \pi_1^\top \left( \frac{\alpha_t}{\sqrt{\mathbf{G}_t^{(\ell)}} + \epsilon} \odot \mathbf{g}_t^{(\ell)} \right) \pi_2 \quad (101)$$

$$= \pi_1^\top \left( \Theta_{t-1}^{(\ell)} - \frac{\alpha_t}{\sqrt{\mathbf{G}_t^{(\ell)}} + \epsilon} \odot \mathbf{g}_t^{(\ell)} \right) \pi_2 = \pi_1^\top \Theta_t^{(\ell)} \pi_2 \quad (102)$$

1547 Thus, the AdaGrad update is equivariant with respect to the transformation.  $\square$   
 1548

1549 **Proof for RMSProp (Tieleman et al., 2012)** RMSProp has hyperparameters for learning rate  $\alpha$ ,  
 1550 weight decay  $\lambda$ , momentum  $\beta$ , and a small constant  $\epsilon$  for stability, and an additional mode if the  
 1551 square averages are centered. For layer  $\ell$  at time  $t$ , we refer to the moving average of squared gradients  
 1552 as  $\mathbf{v}_t^\ell$ , the “average” gradient as  $\mathbf{g}_t^{\text{ave}(\ell)}$  (which is required if the square averages are centered), and  
 1553 the buffer  $\mathbf{b}_t^{(\ell)}$ , which are all defined below. The update steps for RMSProp are given by:  
 1554

$$\Theta_t^{(\ell)} = \Theta_{t-1}^{(\ell)} - \alpha \mathbf{b}_t^\ell \quad (103)$$

$$\mathbf{b}_t^{(\ell)} = \mu \mathbf{b}_{t-1}^{(\ell)} + \frac{\mathbf{g}_t^{(\ell)}}{\sqrt{\mathbf{v}_t^\ell} + \epsilon} \quad (104)$$

$$\mathbf{g}_t^{(\ell)} = \mathbf{grad}_t^{(\ell)} + \lambda \Theta_{t-1}^{(\ell)} \quad (105)$$

$$\mathbf{v}_t^\ell = \beta \mathbf{v}_{t-1}^\ell + (1 - \beta)(\mathbf{g}_t^{(\ell)} \odot \mathbf{g}_t^{(\ell)}) \quad (\text{if not centered}) \quad (106)$$

$$\mathbf{v}_t^\ell = \beta \mathbf{v}_{t-1}^\ell + (1 - \beta)(\mathbf{g}_t^{(\ell)} \odot \mathbf{g}_t^{(\ell)}) - \mathbf{g}_t^{\text{ave}(\ell)} \odot \mathbf{g}_t^{\text{ave}(\ell)} \quad (\text{if centered}) \quad (107)$$

$$\mathbf{g}_t^{\text{ave}(\ell)} = \beta \mathbf{g}_{t-1}^{\text{ave}(\ell)} + (1 - \beta) \mathbf{g}_t^{(\ell)} \quad (\text{if centered}) \quad (108)$$

1564 Where  $\mathbf{g}_0^{\text{ave}(\ell)} = \mathbf{0}$ ,  $\mathbf{v}_0^\ell = \mathbf{0}$ ,  $\mathbf{b}_0^{(\ell)} = \mathbf{0}$ . Note that in the absense of momentum ( $\mu = 0$ ), the buffer  $\mathbf{b}_t^{(\ell)}$   
 1565 is not required, and the update step will simplify to  $\Theta_t^{(\ell)} = \Theta_{t-1}^{(\ell)} - \alpha \frac{\mathbf{g}_t^{(\ell)}}{\sqrt{\mathbf{v}_t^\ell} + \epsilon}$ .

1566 Consider the transformation  $\Theta_{<t}^{(\ell)} \mapsto \pi_1^\top(\Theta_{<t}^{(\ell)})\pi_2$  and  $\text{grad}_{<t}^{(\ell)} \mapsto \pi_1^\top(\text{grad}_{<t}^{(\ell)})\pi_2$ . We show that  
 1567 the other variables are equivariant by induction:  
 1568

$$g_t^{(\ell)} \mapsto \pi_1^\top(g_t^{(\ell)})\pi_2 \quad (109)$$

$$v_0^\ell = \mathbf{0} \mapsto \pi_1^\top \mathbf{0} \pi_2 = \mathbf{0} = \pi_1^\top v_0^\ell \pi_2 \quad (110)$$

$$v_t^\ell = \beta v_{t-1}^\ell + (1 - \beta)(g_t^{(\ell)} \odot g_t^{(\ell)}) \quad (111)$$

$$\mapsto \beta \pi_1^\top v_{t-1}^\ell \pi_2 + (1 - \beta)(\pi_1^\top g_t^{(\ell)} \pi_2 \odot \pi_1^\top g_t^{(\ell)} \pi_2) \quad (112)$$

$$= \beta \pi_1^\top v_{t-1}^\ell \pi_2 + (1 - \beta)\pi_1^\top(g_t^{(\ell)} \odot g_t^{(\ell)})\pi_2 \quad (113)$$

$$= \pi_1^\top(\beta v_{t-1}^\ell + (1 - \beta)(g_t^{(\ell)} \odot g_t^{(\ell)}))\pi_2 = \pi_1^\top v_t^\ell \pi_2 \quad (114)$$

$$g_0^{\text{ave}(\ell)} = \mathbf{0} \mapsto \pi_1^\top \mathbf{0} \pi_2 = \mathbf{0} = \pi_1^\top g_0^{\text{ave}(\ell)} \pi_2 \quad (115)$$

$$g_t^{\text{ave}(\ell)} = \beta g_{t-1}^{\text{ave}(\ell)} + (1 - \beta)g_t^{(\ell)} \quad (116)$$

$$\mapsto \beta \pi_1^\top g_{t-1}^{\text{ave}(\ell)} \pi_2 + (1 - \beta)\pi_1^\top g_t^{(\ell)} \pi_2 \quad (117)$$

$$= \pi_1^\top(\beta g_{t-1}^{\text{ave}(\ell)} + (1 - \beta)g_t^{(\ell)})\pi_2 = \pi_1^\top g_t^{\text{ave}(\ell)} \pi_2 \quad (118)$$

$$v_t^\ell = \beta v_{t-1}^\ell + (1 - \beta)(g_t^{(\ell)} \odot g_t^{(\ell)}) - g_t^{\text{ave}(\ell)} \odot g_t^{\text{ave}(\ell)} \quad (\text{if centered}) \quad (119)$$

$$\mapsto \beta \pi_1^\top v_{t-1}^\ell \pi_2 + (1 - \beta)(\pi_1^\top g_t^{(\ell)} \pi_2 \odot \pi_1^\top g_t^{(\ell)} \pi_2) - \pi_1^\top g_t^{\text{ave}(\ell)} \pi_2 \odot \pi_1^\top g_t^{\text{ave}(\ell)} \pi_2 \quad (120)$$

$$= \beta \pi_1^\top v_{t-1}^\ell \pi_2 + (1 - \beta)\pi_1^\top(g_t^{(\ell)} \odot g_t^{(\ell)})\pi_2 - \pi_1^\top(g_t^{\text{ave}(\ell)} \odot g_t^{\text{ave}(\ell)})\pi_2 \quad (121)$$

$$= \pi_1^\top(\beta v_{t-1}^\ell + (1 - \beta)(g_t^{(\ell)} \odot g_t^{(\ell)}) - g_t^{\text{ave}(\ell)} \odot g_t^{\text{ave}(\ell)})\pi_2 = \pi_1^\top v_t^\ell \pi_2 \quad (122)$$

$$b_0^{(\ell)} = \mathbf{0} \mapsto \pi_1^\top \mathbf{0} \pi_2 = \mathbf{0} = \pi_1^\top b_0^{(\ell)} \pi_2 \quad (123)$$

$$b_t^{(\ell)} = \mu b_{t-1}^{(\ell)} + \frac{g_t^{(\ell)}}{\sqrt{v_t^\ell + \epsilon}} \quad (124)$$

$$\mapsto \mu \pi_1^\top b_{t-1}^{(\ell)} \pi_2 + \frac{\pi_1^\top g_t^{(\ell)} \pi_2}{\sqrt{\pi_1^\top v_t^\ell \pi_2 + \epsilon}} \quad (125)$$

$$= \mu \pi_1^\top b_{t-1}^{(\ell)} \pi_2 + \pi_1^\top \left( \frac{g_t^{(\ell)}}{\sqrt{v_t^\ell + \epsilon}} \right) \pi_2 \quad (126)$$

$$= \pi_1^\top \left( \mu b_{t-1}^{(\ell)} + \frac{g_t^{(\ell)}}{\sqrt{v_t^\ell + \epsilon}} \right) \pi_2 = \pi_1^\top b_t^{(\ell)} \pi_2 \quad (127)$$

1603 Finally, for the weight update:  
 1604

$$\Theta_t^{(\ell)} = \Theta_{t-1}^{(\ell)} - \alpha \frac{g_t^{(\ell)}}{\sqrt{v_t^\ell + \epsilon}} \quad (128)$$

$$\mapsto \pi_1^\top \Theta_{t-1}^{(\ell)} \pi_2 - \alpha \frac{\pi_1^\top g_t^{(\ell)} \pi_2}{\sqrt{\pi_1^\top v_t^\ell \pi_2 + \epsilon}} \quad (129)$$

$$= \pi_1^\top \Theta_{t-1}^{(\ell)} \pi_2 - \pi_1^\top \left( \alpha \frac{g_t^{(\ell)}}{\sqrt{v_t^\ell + \epsilon}} \right) \pi_2 \quad (130)$$

$$= \pi_1^\top \left( \Theta_{t-1}^{(\ell)} - \alpha \frac{g_t^{(\ell)}}{\sqrt{v_t^\ell + \epsilon}} \right) \pi_2 = \pi_1^\top \Theta_t^{(\ell)} \pi_2 \quad (131)$$

1617 Thus, the RMSProp update is equivariant with respect to the transformation.  $\square$   
 1618

1619 **Proof for a general case** We can show that a general optimizer leads to equivariance under the  
 transformation if the update step can be separated for each scalar entry of the parameters.

1620 **Lemma 11** (Update Equivariance of a separable optimizer). *Let the parameters be updated by the  
1621 function  $f$ , such that for any step  $t$ ,*

$$\theta_{t+1} = f(\{\theta_{\text{iter}} : \text{iter} \leq t\}, \{g_{\text{iter}} : \text{iter} \leq t\}, \eta_t, Z_t) \quad (132)$$

1622 where,  $g_{\text{iter}}$  based on the optimizer may be the gradient (which may also be clipped and/or normalized  
1623 gradient) w.r.t. the parameters  $\theta_{\text{iter}}$  which is equivariant under  $\Gamma_\pi$ .

1624 *Let  $\eta_t$  be the set of hyperparameters of the optimizer (this may include learning rate, momentum, etc.)  
1625 at update step  $t$ , and  $Z_t$  be a latent random variable representing any stochasticity in the update step  
1626 (such as data selection for SGD/mini-batch).*

1627 *We call  $f$  to be separable over each scalar, if we can write for any parameter  $\Theta^{(\ell)}$ , for all of its  
1628 entries entries  $i, j$ ,*

$$\Theta_{t+1}^{(\ell)}[i, j] = f^{(\ell)}(\{\Theta_{\text{iter}}^{(\ell)}[i, j] : \text{iter} \leq t\}, \{g_{\text{iter}}^{(\ell)}[i, j] : \text{iter} \leq t\}, \eta_t, Z_t) \quad (133)$$

1629 where  $f^{(\ell)}$  is an appropriate function which may be different for each layer  $\ell \in d$ .

1630 *Then, the update step is equivariant (conditioned on  $(Z_i : i \leq t)$ ) to any transformation  $\Gamma_\pi$  applied  
1631 jointly to each of  $\{\theta_{\text{iter}}, g_{\text{iter}}\}$  for  $\text{iter} \leq t$ .*

1632 Note that this functional form is quite general despite the separability condition, as it subsumes  
1633 commonly used optimizers - GD, SGD, Momentum, RMSProp, Adam, AdamW, Adagrad, etc. The  
1634 conditioning on the latent random variables implies that the equivariance also holds in expectation  
1635 over the randomness.

1636 *Proof:*

1637 The proof follows from the fact that the transformation  $\Gamma_\pi$  is composed of permutations in each of  
1638 the weights. Consider a layer  $\ell$  with parameters  $\theta^{(\ell)}$ , of size  $d_1 \times d_2$ . We may find a permutation  
1639  $\hat{\pi} : [d_1] \times [d_2] \mapsto [d_1] \times [d_2]$  such that for any entry  $(i, j)$  of a matrix  $\mathbf{A}$ ,  $\Gamma_\pi^{(\ell)}(\mathbf{A})[i, j] = \mathbf{A}[\hat{\pi}(i, j)]$ .  
1640 To reiterate, under the transformation  $\Gamma_\pi$ ,  $\forall t \forall (i, j) \in [d_1] \times [d_2]$ ,  $\Theta^{(\ell)}[i, j] \mapsto \Theta^{(\ell)}[\hat{\pi}(i, j)]$  and  
1641  $\mathbf{g}^{(\ell)}[i, j] \mapsto \mathbf{g}^{(\ell)}[\hat{\pi}(i, j)]$ .

1642 Then, for any step  $t$ , under the action of  $\Gamma_\pi$  on  $\{\theta_{\text{iter}}, g_{\text{iter}}\}$  for  $\text{iter} \leq t$ ,

$$\begin{aligned} 1643 f^{(\ell)}(\{\Theta_{\text{iter}}^{(\ell)}[i, j] : \text{iter} \leq t\}, \{g_{\text{iter}}^{(\ell)}[i, j] : \text{iter} \leq t\}, \eta_t, Z_t) \\ 1644 \mapsto f^{(\ell)}(\{\Theta_{\text{iter}}^{(\ell)}[\hat{\pi}(i, j)] : \text{iter} \leq t\}, \{g_{\text{iter}}^{(\ell)}[\hat{\pi}(i, j)] : \text{iter} \leq t\}, \eta_t, Z_t) \\ 1645 \end{aligned} \quad (134)$$

$$1646 = \Theta_{t+1}^{(\ell)}[\hat{\pi}(i, j)] = \Gamma_\pi^{(\ell)}(\Theta_{t+1}^{(\ell)})[i, j] \quad (135)$$

1647 Thus  $\Theta_{t+1}^{(\ell)}[i, j] \mapsto \Gamma_\pi^{(\ell)}(\Theta_{t+1}^{(\ell)})[i, j]$ . Since this holds for all entries  $(i, j)$ , we have  $\Theta_{t+1}^{(\ell)} \mapsto$   
1648  $\Gamma_\pi^{(\ell)}(\Theta_{t+1}^{(\ell)})$ . Finally, since this holds for all layers  $\ell$ , we have  $\theta_{t+1} \mapsto \Gamma_\pi(\theta_{t+1})$ . ■

### 1649 E.1.6 ADDITIONAL RESULTS ON EXCHANGEABILITY

1650 **Loss functions without permutation equivariance** In this paper, we take the loss to be a direct  
1651 function of the embeddings, which necessitates that the loss function be permutation invariant.

1652 When we consider settings where the loss is not permutation invariant, for example a classification  
1653 task, the 'representations' exist within the middle of the network rather than at the end. Moreover,  
1654 such representations can be shown to be exchangeable.

1655 For this analysis, we may partition the network into two, which could be referred to as the 'embedding'  
1656 network and the 'classifier head'. We may write  $\mathbf{X} = \text{NN}(G)$  where we refer to  $\mathbf{X}$  as the embeddings  
1657 and  $\hat{\mathbf{y}} = \text{Clf}(\mathbf{X})$  where  $\hat{\mathbf{y}}$  is the prediction label vector across nodes. We can characterize and prove  
1658 the exchangeability of  $\mathbf{X}$  for this setting.

1659 Let the parameters of the entire network at  $t$  timesteps be represented by  $\theta = (\theta_{\text{NN}}, \theta_{\text{Clf}})$ , corresponding  
1660 to the parameters of either network. Let us also define the permutation inducing transformation  
1661 as  $\Gamma_\pi = \Gamma_{\text{NN}, \pi} \otimes \Gamma_{\text{Clf}, \pi}$ , i.e.  $\Gamma_\pi(\theta) = (\Gamma_{\text{NN}, \pi}(\theta_{\text{NN}}), \Gamma_{\text{Clf}, \pi}(\theta_{\text{Clf}}))$ .

1662 Given the dataset, we may reparameterise the loss function as  $\mathcal{L}(\mathbf{X}, \text{Clf})$ , or equivalently,  $\mathcal{L}(\mathbf{X}, \theta_{\text{Clf}})$ .

1674 The new condition for the transformation boils down to  
 1675

- $\mathbf{X} \mapsto \mathbf{X}\pi$  under  $\Gamma_{\text{NN},\pi}$
- the loss is invariant under  $(\pi, \Gamma_{\text{Clf},\pi})$ , i.e.

$$\mathcal{L}(\mathbf{X}, \theta_{\text{Clf}}) = \mathcal{L}(\mathbf{X}\pi, \Gamma_{\text{Clf},\pi}(\theta_{\text{Clf}})) \quad (136)$$

1679 Under these conditions, exchangeability follows with the same steps - exchangeability at initialisation,  
 1680 equivariance of gradient, equivariance of update step.

1681 To illustrate this, consider a three class classification task with a single layer for both NN and  
 1682 Clf. Let the input feature be **feat**. Let us focus on one channel/node of  $\mathbf{X}$  denoted as  $\mathbf{x} =$   
 1683  $\mathbf{X}[:, \bullet]$  and  $\hat{y}[\bullet] = y$ . We have:  $\mathbf{x} = \text{NN}(\mathbf{feat}) = \sigma(\mathbf{feat}\Theta_{\text{NN}})$ . Hence, we will have:  $\hat{y} =$   
 1684  $\text{Softmax}([(x \cdot w_1), (x \cdot w_2), (x \cdot w_3)])$ .

1685 The transformation  $\Gamma_{\text{NN},\pi}$  can then be represented as,  $\Theta_{\text{NN}} \mapsto \Theta_{\text{NN}}\pi$  and  $[w_1, w_2, w_3] \mapsto$   
 1686  $[\pi^\top w_1, \pi^\top w_2, \pi^\top w_3]$ . Under this transformation  $\mathbf{x} \mapsto \mathbf{x}\pi$  but  $\hat{y}$  remains invariant—therefore,  
 1687 the loss is invariant.

1688 **Effect of normalization** Batch norm, layer norm, etc. do not break exchangeability condition. If  
 1689 the network without the norm layers can be shown to give exchangeable embeddings, the same will  
 1690 hold for the embeddings for the network with batch norm or layer norm.

1691 We denote a normalization layer as  $NL_{\gamma, \beta}$ , where  $\gamma$  and  $\beta$  are parameters. Such layers allow us to  
 1692 extend permutation inducing transformation  $\gamma_\pi$  to  $\gamma'_\pi$ . For simplicity, assume that the normalization  
 1693 layer  $NL_{\gamma, \beta}$  is applied on one layer  $\ell$ . Suppose,  $\theta \rightarrow \gamma_\pi(\theta)$  gives  $\mathbf{Z} \rightarrow \mathbf{Z}\pi$  in that  $\ell$  layer (where  
 1694  $\mathbf{Z} \in \mathbb{R}^{n \times \text{dim}_z}$ ). Then we can obtain a transformation  $\gamma'_\pi$  such that  $\theta \cup \{\gamma, \beta\} \rightarrow \gamma'_\pi(\theta \cup \{\gamma, \beta\})$   
 1695 will also give  $\mathbf{Z} \rightarrow \mathbf{Z}\pi$ .

1696 Let the batch of inputs be  $G_1, G_2, \dots, G_B$  and a single batch norm layer, with the cor-  
 1697 responding inputs  $\mathbf{Y}_1, \mathbf{Y}_2, \dots, \mathbf{Y}_B$  to the layer. Then, we have:  $\mathbf{Z}_1, \mathbf{Z}_2, \dots, \mathbf{Z}_B =$   
 1698  $\text{BatchNorm}(\mathbf{Y}_1, \mathbf{Y}_2, \dots, \mathbf{Y}_B; \gamma, \beta)$ . Suppose:  $\hat{\mathbf{Y}} = \frac{[\mathbf{Y}_1, \mathbf{Y}_2, \dots, \mathbf{Y}_B] - \bar{\mathbf{Y}}}{\sqrt{\text{Var}(\mathbf{Y}_1, \mathbf{Y}_2, \dots, \mathbf{Y}_B) + \epsilon}}$  where  $\bar{\mathbf{Y}}$  is the batch  
 1699 mean. Then, we have:  $\mathbf{Z}_1, \mathbf{Z}_2, \dots, \mathbf{Z}_B = \hat{\mathbf{Y}} \odot \gamma + \beta$ . Now, suppose  $\theta \rightarrow \gamma_\pi(\theta)$  gives  $\mathbf{Y} \rightarrow \mathbf{Y}\pi$ .  
 1700 This would give  $\hat{\mathbf{Y}} \rightarrow \hat{\mathbf{Y}}\pi$ . Suppose, we now transform  $\gamma \rightarrow \gamma\pi$  and  $\beta \rightarrow \beta\pi$ . Then,  
 1701  $\mathbf{Z}_1, \mathbf{Z}_2, \dots, \mathbf{Z}_B \rightarrow \hat{\mathbf{Y}}\pi \odot (\gamma\pi) + \beta\pi = (\hat{\mathbf{Y}} \odot \gamma + \beta)\pi = \mathbf{Z}_1\pi, \mathbf{Z}_2\pi, \dots, \mathbf{Z}_B\pi$ .

1702 Consider layer norm. Assume the corresponding input is  $\mathbf{y}$  and output in one channel is  $\mathbf{z} =$   
 1703  $\text{LayerNorm}(\mathbf{y}; \gamma, \beta)$ . Suppose:  $\hat{\mathbf{y}} = \frac{\mathbf{y} - y_1}{\sqrt{\text{Var}(\mathbf{y}) + \epsilon}}$  where  $y$  is the feature mean. Then, we have:  
 1704  $\mathbf{z} = \hat{\mathbf{y}} \odot \gamma + \beta$ . Now, suppose  $\theta \rightarrow \gamma_\pi(\theta)$  gives  $\mathbf{y} \rightarrow \mathbf{y}\pi$ . This would give  $\hat{\mathbf{y}} \rightarrow \hat{\mathbf{y}}\pi$ . Suppose, we  
 1705 now transform  $\gamma \rightarrow \gamma\pi$  and  $\beta \rightarrow \beta\pi$ . Then,  $\mathbf{z} \rightarrow \hat{\mathbf{y}} \odot (\gamma\pi) + \beta\pi = \mathbf{z}\pi$ .

1706 Hence,  $\gamma'_\pi(\theta \cup \{\gamma, \beta\}) = (\gamma_\pi(\theta), \gamma\pi, \beta\pi)$ . Therefore, Lemma 2 holds true even when we apply  
 1707 Batch norm or Layer norm on each layer/feature. Since Lemma 2 is used to prove Lemma 3, 4 and  
 1708 these lemmas are used to prove the final result in Theorem 5, our results of exchangeability remain  
 1709 the same, regardless of normalization layer.

1710  
 1711  
 1712  
 1713  
 1714  
 1715  
 1716  
 1717  
 1718  
 1719  
 1720  
 1721  
 1722  
 1723  
 1724  
 1725  
 1726  
 1727

1728 E.2 PROOFS OF THE TECHNICAL RESULTS IN SECTION 4  
17291730 Here, we first prove Proposition 7, and then derive the equivalence of Eqs. (3) and (4).  
17311732 E.2.1 PROOF OF PROPOSITION 7  
17331734 **Proposition 7.** For any  $\epsilon > 0, \delta > 0$ , setting  $D > \frac{1}{\epsilon^2 \delta}$  ensures that, for some  $\beta_0 = O_D(1)$ , we have:  
1735

1736 
$$\Pr \left( \left| \frac{1}{D} \text{sim}(G_c, G_q) - \text{sim}_d(G_c, G_q) \right| \leq \epsilon \right) \geq 1 - \beta_0 \delta \quad (137)$$
  
1737

1738 **Proof:** For the purposes of the proof, we introduce a new similarity measure  $\overline{\text{sim}}(G_c, G_q)$ ,  
1739

1740 
$$\overline{\text{sim}}(G_c, G_q) = \max_{\mathbf{P} \in \mathcal{P}_n} \sum_{u, u' \in [n] \times [n]} \mathbb{E}[\mathbf{s}(\mathbf{x}^{(q)}(u)[d] - \mathbf{x}^{(c)}(u')[d]) \mathbf{P}[u, u']]. \quad (138)$$
  
1741

We use the above to prove two results:  
1742

1743 
$$\Pr \left( \left| \frac{1}{D} \text{sim}(G_c, G_q) - \overline{\text{sim}}(G_c, G_q) \right| \leq \epsilon \right) \geq 1 - \beta \delta \quad (139)$$
  
1744

1745 
$$\Pr \left( \left| \text{sim}_d(G_c, G_q) - \overline{\text{sim}}(G_c, G_q) \right| \leq \epsilon \right) \geq 1 - \beta \delta \quad (140)$$
  
1746

1747 where  $\beta = O_D(1)$ . Finally, we will use the union bound to get the desired result. In addition to  
1748  $\overline{\text{sim}}(G_c, G_q)$ , we also introduce additional notation to facilitate the proofs:  
17491750 (1)  $\mathbf{Z}$  is a matrix indexed by the pair of nodes, and the embedding dimension. In particular,  
1751

1752 
$$\mathbf{Z}[(u, u'), d] \triangleq \mathbf{s}(\mathbf{x}^{(q)}(u)[d] - \mathbf{x}^{(c)}(u')[d]) \quad (141)$$
  
1753

1754 (2) We define the vector  $\mathbf{Z}_d$  by fixing the value at dimension  $d$ .  
1755

1756 
$$\mathbf{Z} \triangleq [\mathbf{Z}[(u, u'), d]]_{(u, u'), d} \quad (142)$$
  
1757

1758 
$$\mathbf{Z}_d \triangleq [\mathbf{Z}[(u, u'), d]]_{(u, u')} \quad (143)$$
  
1759

1760 (3)  $\overline{\mathbf{Z}}$  is the expectation value of  $\mathbf{Z}_d$  with respect to the initialization of the embedding model. As it  
1761 follows from the exchangeability of the dimensions in Theorem 15, we have:  $\mathbb{E}[\mathbf{Z}_1] = \mathbb{E}[\mathbf{Z}_2] =$   
1762  $\dots = \mathbb{E}[\mathbf{Z}_D]$ .  
1763

1764 
$$\overline{\mathbf{Z}} = \mathbb{E}[\mathbf{Z}_d] \quad (144)$$
  
1765

1766 (4) Our estimator is denoted by the vector  $\widehat{\mathbf{Z}}$ .  
1767

1768 
$$\widehat{\mathbf{Z}} \triangleq \frac{1}{D} \sum_{i=1}^D \mathbf{Z}_d \quad (145)$$
  
1769

1770 Thus, our similarity can be written as  
1771

1772 
$$\frac{1}{D} \text{sim}(G_c, G_q) = \max_{\mathbf{P} \in \mathcal{P}_n} \sum_{u, u' \in [n] \times [n]} \widehat{\mathbf{Z}}[(u, u')] \mathbf{P}[u, u'] \quad (146)$$
  
1773

1774 Suppose  $\mathbf{R}$  is any matrix in  $\mathbb{R}^{n \times n}$ . Then, we define the following quantities:  
1775

1776 
$$\Lambda(\mathbf{R}, \mathbf{P}) \triangleq \sum_{u, u' \in [n] \times [n]} \mathbf{R}[(u, u')] \mathbf{P}[u, u'] \quad (147)$$
  
1777

1778 
$$\mathbf{P}^*(\mathbf{R}) \triangleq \arg \max_{\mathbf{P} \in \mathcal{P}_n} \Lambda(\mathbf{R}, \mathbf{P}) \quad (148)$$
  
1779

1780 
$$\Lambda^*(\mathbf{R}) \triangleq \max_{\mathbf{P} \in \mathcal{P}_n} \Lambda(\mathbf{R}, \mathbf{P}) = \Lambda(\mathbf{R}, \mathbf{P}^*(\mathbf{Z})) \quad (149)$$
  
1781

1782 Thus we have:  $\frac{1}{D} \text{sim}(G_c, G_q) = \Lambda^*(\widehat{\mathbf{Z}})$  and  $\text{sim}_d(G_c, G_q) = \Lambda^*(\mathbf{Z}_d)$ . Therefore, we first establish  
1783 that if  $D > \frac{1}{\epsilon^2 \delta}$ , then  
1784

1785 
$$\Pr \left( \left| \Lambda^*(\widehat{\mathbf{Z}}) - \Lambda^*(\overline{\mathbf{Z}}) \right| \geq \epsilon \right) \leq \beta \delta. \quad (150)$$
  
1786

1787 We begin by showing that  $\Lambda^*$  is  $\sqrt{n}$ -Lipschitz. Convexity of  $\Lambda^*$  follows from the convexity of  $\Lambda(\cdot, \mathbf{P})$   
1788 and Danskin's Theorem (Theorem 13). By Danskin's theorem, the semi-derivative of  $\Lambda^*$  with respect  
1789 to  $\mathbf{R}$  is given by  
1790

1791 
$$\partial_{\mathbf{R}} \Lambda^*(\mathbf{R}) = \nabla_{\mathbf{R}} \Lambda(\mathbf{R}, \mathbf{P}) \Big|_{\mathbf{P}=\mathbf{P}^*(\mathbf{R})} \quad (151)$$
  
1792

1782 From Eq. (147), we have:  $|\partial_{\mathbf{R}} \Lambda^*(\mathbf{R})| \leq \|\text{vec}(\mathbf{P})\|_2 = \sqrt{n}$ . This gives us:

$$1783 \quad |\Lambda^*(\mathbf{R}_1) - \Lambda^*(\mathbf{R}_2)| \leq \sqrt{n} \|\text{vec}(\mathbf{R}_1) - \text{vec}(\mathbf{R}_2)\|_2 \quad (152)$$

$$1784 \quad \leq \sqrt{n} \|\mathbf{R}_1 - \mathbf{R}_2\|_F \quad (153)$$

1785 This proves that  $\Lambda^*$  is Lipschitz, from which it follows that for any  $\epsilon$ ,  $|\Lambda^*(\mathbf{R}_1) - \Lambda^*(\mathbf{R}_2)| \geq \epsilon \implies \sqrt{n} \|\mathbf{R}_1 - \mathbf{R}_2\|_2 \geq \epsilon$ . This gives us: We now use this fact in proving Eq. (139).

$$1786 \quad \Pr \left( |\Lambda^*(\widehat{\mathbf{Z}}) - \Lambda^*(\overline{\mathbf{Z}})| \geq \epsilon \right) \leq \Pr \left( \|\widehat{\mathbf{Z}} - \overline{\mathbf{Z}}\|_2 \geq \frac{1}{\sqrt{n}} \epsilon \right) \quad (\text{Eq. (153)}) \quad (154)$$

$$1787 \quad \leq \frac{\sum_{u,u' \in [n] \times [n]} \text{Var}(\widehat{\mathbf{Z}}[(u, u')])}{\left(\frac{\epsilon}{\sqrt{n}}\right)^2} \quad (\text{Chebyshev's Inequality})$$

$$1788 \quad = \frac{n}{D^2 \epsilon^2} \sum_{u,u' \in [n] \times [n]} \text{Var} \left( \sum_{d \in [D]} \mathbf{Z}_d[(u, u')] \right) \quad (155)$$

$$1789 \quad = \frac{\beta}{D \epsilon^2} \quad (156)$$

1790 Here,  $\beta$  is computed using the variance bound computed by Lemma 16:  $\beta = n \cdot 4L_s^2 B^2 \cdot n^2$ . To  
1791 prove Eq. (140), we directly invoke the Lipschitz condition for  $\Lambda^*$  from Eq. (153).

$$1792 \quad \Pr \left( |\Lambda^*(\mathbf{Z}_i) - \Lambda^*(\overline{\mathbf{Z}})| \geq \epsilon \right) \leq \Pr \left( \|\mathbf{Z}_i - \overline{\mathbf{Z}}\|_2 \geq \frac{\epsilon}{\sqrt{n}} \right) \quad (\text{Eq. (153)}) \quad (157)$$

$$1793 \quad \leq \frac{\sum_{u,u' \in [n] \times [n]} \text{Var}(\mathbf{Z}_i[(u, u')])}{\left(\frac{\epsilon}{\sqrt{n}}\right)^2} \quad (\text{Chebyshev's Inequality})$$

$$1794 \quad \leq \sum_{u,u' \in [n] \times [n]} \frac{n}{\epsilon^2} \cdot \frac{4L_s^2 B^2}{D} \quad (\text{From variance bound, Lemma 17}) \quad (158)$$

$$1795 \quad = \frac{\beta}{D \epsilon^2}, \quad \text{where } \beta = n \cdot 4L_s^2 B^2 \cdot n^2. \quad (159)$$

1800 Using the results in Eqs. (139) and (140), we now prove the main result (5), using the union bound

$$1801 \quad \Pr(|\text{sim}(G_c, G_q) - \text{sim}_d(G_c, G_q)| \geq \epsilon)$$

$$1802 \quad \leq \Pr(|\text{sim}(G_c, G_q) - \overline{\text{sim}}(G_c, G_q)| \geq \frac{\epsilon}{2}) \\ 1803 \quad + \Pr(|\text{sim}_d(G_c, G_q) - \overline{\text{sim}}(G_c, G_q)| \geq \frac{\epsilon}{2}) \quad (160)$$

$$1804 \quad \leq \frac{4\beta}{D \epsilon^2} + \frac{4\beta}{D \epsilon^2} = \frac{8\beta}{D \epsilon^2}$$

$$1805 \quad =: \frac{\beta_0}{D \epsilon^2} \quad (161)$$

■

## E.2.2 PROOF OF THE FACT THAT EQ. (3) AND EQ. (4) ARE EQUIVALENT

Here, we will show that if we have:

$$\text{sim}_d(G_c, G_q) = \max_{P \in \mathcal{P}_n} \sum_{u, u'} s(\mathbf{x}^{(q)}(u)[d] - \mathbf{x}^{(c)}(u')[d]) \mathbf{P}[u, u'], \quad (162)$$

then  $\text{sim}_d$  can also be written as:

$$\text{sim}_d(G_c, G_q) = s(\text{SORT}(\mathbf{X}^{(q)}[:, d]) - \text{SORT}(\mathbf{X}^{(c)}[:, d])) \quad (163)$$

In the following, we provide this result, in terms of any two vectors  $\mathbf{x}$  and  $\mathbf{y}$ .

**Theorem 12** (Rearrangement for  $s$ ). *Given a convex function  $\rho : \mathbb{R}^D \rightarrow [0, \infty)$ , which is not necessarily symmetric and satisfies  $\rho(\mathbf{x}) = \sum_i \rho(\mathbf{x}[i])$ , and a score function  $s$  that is of the form  $s(\cdot) = \rho_{\max} - \rho(\cdot)$ <sup>1</sup>, for all  $\mathbf{x}, \mathbf{y}$  with  $\|\mathbf{x}\|_\infty, \|\mathbf{y}\|_\infty \leq x_{\max}$ , we have:*

$$\max_{P \in \mathcal{P}_n} \sum_{u, u'} s(\mathbf{x}[u] - \mathbf{y}[u']) \mathbf{P}[u, u'] = s(\text{SORT}(\mathbf{x}) - \text{SORT}(\mathbf{y})) \quad (164)$$

**Proof** This is a well known result for  $L_p$  metric. For optimal transport between distributions, such result exists for convex distances (Santambrogio, 2015, Proposition 2.17). We still provide the proof for self containment. Here, we will apply Lemma 14. But that requires some conditions on  $s(\bullet - \bullet)$  (stated as  $\mu(\bullet, \bullet)$  therein). We will prove that as long as  $\rho$  is convex,  $s$  satisfies those conditions required to apply Lemma 14.

Those conditions requires us to show the following: For  $a_1, a_2, b_1, b_2 \in \mathbb{R}$  with  $a_1 \geq a_2, b_1 \geq b_2$ ,

$$\rho(a_1 - b_2) + \rho(a_2 - b_1) \geq \rho(a_1 - b_1) + \rho(a_2 - b_2) \quad (165)$$

To show this, we invoke the convexity of  $\rho(\cdot)$ . For any  $x, y, z \in \mathbb{R}$  with  $x \geq y$  and  $z \geq 0$ , consider the case  $x \geq y$ , then  $x + z \geq x \geq y, x + z \geq y + z \geq y$ . Convexity of  $\rho$  gives us:

$$\frac{(x - y)\rho(x + z) + z\rho(y)}{x + z - y} \geq \rho(x) \quad (166)$$

$$\frac{z\rho(x + z) + (x - y)\rho(y)}{x + z - y} \geq \rho(y + z) \quad (167)$$

Summing both inequalities, we have:  $\rho(x + z) + \rho(y) \geq \rho(x) + \rho(y + z)$ . W.l.o.g. consider  $a_1, a_2, b_1, b_2 \in \mathbb{R}$  with  $a_1 \geq a_2, b_1 \geq b_2$ , of the following form:

$$a_1 = b_1 + x$$

$$a_2 = b_1 + y$$

$$b_2 = b_1 - z$$

This gives us Eq. (165).

To finish proving the theorem, we notice that: due to  $\max_{P \in \mathcal{P}_n} \sum_{u, u'} s(\mathbf{x}[u] - \mathbf{y}[u']) \mathbf{P}[u, u'] = \max_{P \in \mathcal{P}_n} \sum_{u, u'} s((\mathbf{P}' \mathbf{x})[u] - \mathbf{y}[u']) \mathbf{P}[u, u']$  for any permutation  $\mathbf{P}'$ , we have:

$$\max_{P \in \mathcal{P}_n} \sum_{u, u'} s(\mathbf{x}[u] - \mathbf{y}[u']) \mathbf{P}[u, u'] = \max_{P \in \mathcal{P}_n} \sum_{u, u'} s(\text{SORT}(\mathbf{x})[u] - \mathbf{y}[u']) \mathbf{P}[u, u'] \quad (168)$$

Now, thanks to Eq. (165),  $s(\bullet)$  satisfies the conditions in Lemma 14 with  $\mu(x, y)$  in that Lemma satisfies  $\mu(x, y) = s(x - y)$ . This gives us:  $\max_{P \in \mathcal{P}_n} \sum_{u, u'} s(\mathbf{x}[u] - \mathbf{y}[u']) \mathbf{P}[u, u'] = s(\text{SORT}(\mathbf{x}) - \text{SORT}(\mathbf{y}))$ .  $\blacksquare$

1877

1878

1879

1880

1881

1882

1883

1884

1885

1886

1887

1888

1889

<sup>1</sup>as designed before introducing Eq. 2.

1890 E.2.3 AUXILIARY RESULTS USED TO PROVE LEMMAS IN APPENDIX E.2  
18911892 **Lemma 13** (Danskin's Theorem (Danskin, 1967)). *Let  $g : \mathbb{R}^m \times Z \rightarrow \mathbb{R}$  be a continuous function of  
1893 two arguments where  $Z \subset \mathbb{R}^l$  is a compact set. Let  $f(x) = \max_{z \in Z} g(x, z)$ , then*1894 

- $f$  is convex if  $g(\cdot, z)$  is convex for any  $z \in Z$ .
- $f$  is differentiable at  $x$  if the  $\arg \max_z$  is a single possible element.
- The semi-differential of  $f$  in the direction of  $\mathbf{v}$  is given by

1898 
$$\partial_{\mathbf{v}} f(x) = \max_{z \in Z^*} g'(x, z | \mathbf{v}) \quad (169)$$

1899 where  $g'(x, z | \mathbf{v})$  is the derivative of  $g$  in the direction  $\mathbf{v}$ , and  $Z^*$  is the set of maximising  
1900 points of  $g(\cdot, z)$ 1901 

- If  $f$  is differentiable at  $x$ , then the gradient of  $f$  is given by  $\nabla_{\mathbf{x}} f(\mathbf{x}) = \nabla_{\mathbf{x}} g(\mathbf{x}, z^*) =$   
1902  $\nabla_1 g(\mathbf{x}, z^*)$  (gradient in the first argument).

1903 **Lemma 14** (Rearrangement Inequality). (Wu, 2020, Theorem 7) *Let  $\mu$  be a real-valued function of 2  
1904 variables defined on  $I_a \times I_b$ . If*

1906 
$$\mu(x_2, y_2) - \mu(x_2, y_1) - \mu(x_1, y_2) + \mu(x_1, y_1) \geq 0$$

1907 for all  $x_1 \leq x_2$  in  $I_a$  and  $y_1 \leq y_2$  in  $I_b$ , then

1909 
$$\sum_{i \in [n]} \mu(a_i, b_{n-i+1}) \leq \sum_{i \in [n]} \mu(a_i, b_{\pi(i)}) \leq \sum_{i \in [n]} \mu(a_i, b_i) \quad (170)$$

1911 for all sequences  $a_1 \leq a_2 \leq \dots \leq a_n$  in  $I_a$ ,  $b_1 \leq b_2 \leq \dots \leq b_n$  in  $I_b$ , and all permutations  $\pi$  of  $[n]$ .1913 **Theorem 15.** *If the columns of  $\mathbf{X}$  are distributed exchangeably, then for any  $d, d' \in [D]$  and  
1914  $u, v \in [n]$* 

1915 
$$\mathbb{E}_{\mathbf{x}_u[d], \mathbf{x}_v[d]} s(\mathbf{x}_u[d] - \mathbf{x}_v[d]) = \mathbb{E}_{\mathbf{x}_u[d'], \mathbf{x}_v[d']} s(\mathbf{x}_u[d'] - \mathbf{x}_v[d']) \quad (171)$$

1917 **Proof** As columns of  $\mathbf{X}$  are distributed exchangeably, the joint distribution of  $(\mathbf{x}_u, \mathbf{x}_v)$  is also  
1918 exchangeable. Thus the marginals are also the same,  $p_{\mathbf{x}_u[d], \mathbf{x}_v[d]} = p_{\mathbf{x}_u[d'], \mathbf{x}_v[d']}$ . Therefore,

1920 
$$\mathbb{E}_{\mathbf{x}_u[d], \mathbf{x}_v[d]} s(\mathbf{x}_u[d] - \mathbf{x}_v[d]) = \int_{\mathbb{R}^2} s(x, y) p_{\mathbf{x}_u[d], \mathbf{x}_v[d]}(x, y) dx dy \quad (172)$$

1922 
$$= \int_{\mathbb{R}^2} s(x, y) p_{\mathbf{x}_u[d'], \mathbf{x}_v[d']}(x, y) dx dy \quad (173)$$

1924 
$$= \mathbb{E}_{\mathbf{x}_u[d'], \mathbf{x}_v[d']} s(\mathbf{x}_u[d'] - \mathbf{x}_v[d']). \quad (174)$$

1925  $\blacksquare$ 1926 **Lemma 16** (Variance Bound for  $\sum_{d \in [D]} \mathbf{Z}_d$ ). *Let  $\mathbf{Z}_d$  be defined as in Eq. (143). Given that  
1927  $\|\mathbf{x}^{(c)}(u')\|_2, \|\mathbf{x}^{(q)}(u)\|_2 \leq B$ , then we can bound*

1930 
$$\text{Var} \left( \sum_{d \in [D]} \mathbf{Z}_d[(u, u')] \right) \leq 4L_s^2 DB^2. \quad (175)$$

1933 **Proof** We write the variance as follows:

1935 
$$\text{Var} \left( \sum_{d \in [D]} \mathbf{Z}_d[(u, u')] \right) \quad (176)$$
  
1936 
$$= \sum_{d, d' \in [D] \times [D]} \text{Cov}(\mathbf{Z}_d[(u, u')], \mathbf{Z}_{d'}[(u, u')])$$
  
1937

1940 
$$= \sum_{d, d' \in [D] \times [D]} \mathbb{E} \left[ \left( s(\mathbf{x}^{(q)}(u)[i] - \mathbf{x}^{(c)}(u')[i]) - \mathbb{E}[s(\mathbf{x}^{(q)}(u)[i] - \mathbf{x}^{(c)}(u')[i])] \right) \right. \\ 1941 \left. \cdot \left( s(\mathbf{x}^{(q)}(u)[j] - \mathbf{x}^{(c)}(u')[j]) - \mathbb{E}[s(\mathbf{x}^{(q)}(u)[j] - \mathbf{x}^{(c)}(u')[j])] \right) \right] \quad (177)$$
  
1942

1943

1944 We refer to  $\mathbf{x}^{(q)}(u)[i] - \mathbf{x}^{(c)}(u')[i]$  as  $\delta_d$  so that Eq. (177) can be rewritten as  
 1945

$$1946 = \sum_{d, d' \in [D] \times [D]} \mathbb{E}[(s(\delta_d) - \mathbb{E}[s(\delta_d)])(s(\delta_{d'}) - \mathbb{E}[s(\delta_{d'})])] \quad (178)$$

$$1948 = \sum_{d, d' \in [D] \times [D]} \mathbb{E}[(s(\delta_d) - s(0) - \mathbb{E}[s(\delta_d) - s(0)])(s(\delta_{d'}) - s(0) - \mathbb{E}[s(\delta_{d'}) - s(0)])] \quad (179)$$

$$1950 = \sum_{d, d' \in [D] \times [D]} \mathbb{E}[(s(\delta_d) - s(0))(s(\delta_{d'}) - s(0))] - \mathbb{E}[(s(\delta_d) - s(0))]\mathbb{E}[(s(\delta_{d'}) - s(0))] \quad (180)$$

$$1953 = \sum_{d, d' \in [D] \times [D]} \mathbb{E}[(s(\delta_d) - s(0))(s(\delta_{d'}) - s(0))] - \left( \sum_{d \in [D]} \mathbb{E}[(s(\delta_d) - s(0))] \right)^2. \quad (181)$$

1956 We can write  $|s(\delta_d) - s(0)| \leq \left| \frac{\partial s}{\partial \delta} \right|_{\max(-2B, 2B)} |\delta_d| = L_s |\delta_d|$ . Thus Eq. (181) can be reduced to  
 1957

$$1958 \sum_{d, d' \in [D] \times [D]} \mathbb{E}[(s(\delta_d) - s(0))(s(\delta_{d'}) - s(0))] - \left( \sum_{d \in [D]} \mathbb{E}[(s(\delta_d) - s(0))] \right)^2 \\ 1959 \leq \sum_{d, d' \in [D] \times [D]} \mathbb{E}[(s(\delta_d) - s(0))(s(\delta_{d'}) - s(0))] \quad (182)$$

$$1964 \leq L_s^2 \sum_{d, d' \in [D] \times [D]} \mathbb{E}[|\delta_d| |\delta_{d'}|] = L_s^2 \mathbb{E}[\|\delta\|_1^2] \quad (183)$$

$$1966 \leq L_s^2 \cdot \mathbb{E}[D \|\delta\|_2^2] \leq 4L_s^2 \cdot D \cdot B^2 \quad (184)$$

1967 Where the final bound in Eq. (184) uses the bound on  $\mathbf{x}^{(\bullet)}(u)$ .  $\blacksquare$   
 1968

1969 **Lemma 17** (Variance Bound for  $Z_d$ ). Let  $Z_d$  be defined as in Eq. (143). Given that  
 1970  $\|\mathbf{x}^{(c)}(u')\|_2, \|\mathbf{x}^{(q)}(u)\|_2 \leq B$ , then we can bound

$$1971 \text{Var}(Z_d[(u, u')]) \leq \frac{4L_s^2 B^2}{D} \quad (185)$$

1973 *Proof for the Variance Bound* We follow similar steps as the proof for Lemma 16.

$$1974 \text{Var}(Z_d[(u, u')]) \leq \mathbb{E}[(s(\delta_d) - \mathbb{E}[s(\delta_d)])(s(\delta_d) - \mathbb{E}[s(\delta_d)])] \quad (186)$$

$$1975 \leq \mathbb{E}[(s(\delta_d) - s(0))^2] - \mathbb{E}[s(\delta_d) - s(0)]^2 \quad (187)$$

$$1977 \leq \mathbb{E}[(s(\delta_d) - s(0))^2] \quad (188)$$

$$1979 \leq L_s^2 \mathbb{E}[\delta_d^2] = L_s^2 \left( \frac{1}{D} \sum_{d \in [D]} \mathbb{E}[\delta_d^2] \right) \quad \text{as } \mathbb{E}[\delta_1^2] = \mathbb{E}[\delta_2^2] = \dots = \mathbb{E}[\delta_D^2] \quad (189)$$

$$1982 = L_s^2 \left( \frac{1}{D} \mathbb{E}[\|\delta\|_2^2] \right) \leq \frac{L_s^2}{D} \cdot 4B^2. \quad (190)$$

1984 Here, the final bound in Eq. (190) uses the bound on  $\mathbf{x}^{(\bullet)}(u)$ .  $\blacksquare$   
 1985

1986  
 1987  
 1988  
 1989  
 1990  
 1991  
 1992  
 1993  
 1994  
 1995  
 1996  
 1997

1998  
1999

## E.2.4 PROOFS OF LSH RESULTS

2000  
2001  
2002  
2003

We show that our random hyperplane hashing on  $\widehat{\mathbf{T}}_{q,d}$  and  $\widehat{\mathbf{T}}_{c,d}$  used in Eq. (9) gives us produce a valid LSH for the similarity measure  $\text{sim}_d(G_c, G_q)$  and  $\text{sim}(G_c, G_q)$ . We first establish some key details of our procedure.

2004  
2005  
2006  
2007  
2008  
2009

**Augmentation of Low Pass Filter with scoring function  $s(\cdot)$**  Since  $s(\cdot)$  is bounded and absolutely convergent, its Fourier transform  $S(\iota\omega) = \frac{1}{2\pi} \int_{x \in \mathbb{R}} s(x) \exp(-\iota\omega x) dx$  is finite. This allows us to write  $s(x) = \int_{\omega \in \mathbb{R}} S(\iota\omega) \exp(\iota\omega x) d\omega$ . However, for simple scoring functions,  $S(\iota\omega)$  imparts significant amount of high frequency signals, which leads to divergence of the integral of  $|S(\iota\omega)|$ . To tackle this problem, we multiply a smooth low pass filter  $\text{LPF}_\lambda(\omega) = \frac{1}{2\pi} \frac{\lambda}{\lambda + \omega}$  with  $S(\iota\omega)$  to obtain  $S_\lambda(\omega) = \text{LPF}_\lambda(\omega)S(\iota\omega)$  which is absolutely integrable, i.e.,  $\int_{\omega \in \mathbb{R}} |S_\lambda(\iota\omega)| d\omega < \infty$ .

2010  
2011  
2012  
2013

We first demonstrate that the integral  $\int_{\omega \in \mathbb{R}} |\text{Re}(S(\iota\omega))| + |\text{Im}(S(\iota\omega))| d\omega$  may diverge in the absence of smoothing. Consider  $\rho$  as the hinge function,  $\rho(x) = [x]_+$ . Applying the construction, we obtain  $s(\bullet)$  and  $S(\bullet)$  similar to the formulation in (Roy et al., 2023).

2014  
2015  
2016

$$s(x) = \begin{cases} x_{\max} & -x_{\max} \leq x \leq 0 \\ x_{\max} - x & 0 < x \leq x_{\max} \\ 0 & \text{otherwise} \end{cases} \quad (191)$$

2017  
2018  
2019

$$S(\iota\omega) = \left[ x_{\max} \frac{\sin \omega x_{\max}}{2\pi\omega} + 2 \frac{\sin^2(\frac{\omega x_{\max}}{2})}{2\pi\omega^2} \right] + \iota \left[ \frac{\sin \omega x_{\max}}{2\pi\omega^2} - \frac{x_{\max} \cos \omega x_{\max}}{2\pi\omega} \right] \quad (192)$$

2020  
2021

In order to show that the integral diverges, it suffices to show that the +ve tail diverges—

2022  
2023  
2024

$$\int_{\omega_0}^{\infty} |\text{Re}(S(\iota\omega))| + |\text{Im}(S(\iota\omega))| d\omega \geq \int_{\omega_0}^{\infty} |\text{Re}(S(\iota\omega)) + \text{Im}(S(\iota\omega))| d\omega \quad \text{using } |a + b| \leq |a| + |b| \quad (193)$$

2025

$$= \int_{\omega_0}^{\infty} \left| x_{\max} \frac{\sin \omega x_{\max}}{2\pi\omega} + 2 \frac{\sin^2(\frac{\omega x_{\max}}{2})}{2\pi\omega^2} + \frac{\sin \omega x_{\max}}{2\pi\omega^2} - \frac{x_{\max} \cos \omega x_{\max}}{2\pi\omega} \right| d\omega \quad (194)$$

2026  
2027  
2028  
2029  
2030

$$= \int_{\omega_0}^{\infty} \left| \left( x_{\max} \frac{\sin \omega x_{\max}}{2\pi\omega} - \frac{x_{\max} \cos \omega x_{\max}}{2\pi\omega} \right) + \left( 2 \frac{\sin^2(\frac{\omega x_{\max}}{2})}{2\pi\omega^2} + \frac{\sin \omega x_{\max}}{2\pi\omega^2} \right) \right| d\omega \quad (195)$$

2031  
2032  
2033

$$\geq \int_{\omega_0}^{\infty} \left| x_{\max} \frac{\sin \omega x_{\max}}{2\pi\omega} - \frac{x_{\max} \cos \omega x_{\max}}{2\pi\omega} \right| d\omega - \int_{\omega_0}^{\infty} \left| 2 \frac{\sin^2(\frac{\omega x_{\max}}{2})}{2\pi\omega^2} + \frac{\sin \omega x_{\max}}{2\pi\omega^2} \right| d\omega \quad (196)$$

2034  
2035

The second term is finite; hence we focus on the first term. Choose  $\omega_0 x_{\max} = 2\pi n_0 + \frac{\pi}{4}$  for a natural number  $n_0$ . This allows us to write

2036  
2037  
2038

$$\int_{\omega_0}^{\infty} \left| x_{\max} \frac{\sin \omega x_{\max}}{2\pi\omega} - \frac{x_{\max} \cos \omega x_{\max}}{2\pi\omega} \right| d\omega = \int_{\omega_0}^{\infty} \frac{x_{\max} \sqrt{2}}{2\pi\omega} |\sin(\omega x_{\max} - \frac{\pi}{4})| d\omega \quad (197)$$

2039  
2040

$$= \int_{2\pi n_0 + \frac{\pi}{4}}^{\infty} \frac{\sqrt{2}}{2\pi\omega} |\sin(t - \frac{\pi}{4})| dt \quad \text{substituting } t = \omega x_{\max}. \quad (198)$$

2041  
2042  
2043

$$= \sum_{n=2n_0}^{\infty} \int_{\pi n + \frac{\pi}{4}}^{\pi(n+1) + \frac{\pi}{4}} \frac{\sqrt{2}}{2\pi\omega} |\sin(t - \frac{\pi}{4})| dt \quad (199)$$

2044  
2045  
2046

$$\geq \sum_{n=2n_0}^{\infty} \frac{\sqrt{2}}{2\pi(\pi(n+1) + \frac{\pi}{4})} \int_{\pi n + \frac{\pi}{4}}^{\pi(n+1) + \frac{\pi}{4}} |\sin(t - \frac{\pi}{4})| dt \quad (200)$$

2047  
2048  
2049

$$= \sum_{n=2n_0}^{\infty} \frac{\sqrt{2}}{2\pi(\pi(n+1) + \frac{\pi}{4})} \cdot 2 > \sum_{n=2n_0}^{\infty} \frac{\sqrt{2}}{\pi^2(n+2)} = \infty \quad (201)$$

2050  
2051

Finally, we show that that after the low pass filter is applied, the resultant integral is  $\int_{\omega \in \mathbb{R}} |\text{Re}(S_\lambda(\iota\omega))| + |\text{Im}(S_\lambda(\iota\omega))| d\omega < \infty$  integrable for the general  $s$  function considered in

2052 this paper.

2053  $|\text{Re}(S_\lambda(\iota\omega))| + |\text{Im}(S_\lambda(\iota\omega))| \leq \sqrt{2}|S_\lambda(\iota\omega)|$  Modulus of the complex number (202)

2054  $= \sqrt{2}|S(\iota\omega)| \cdot |\text{LPF}_\lambda(\omega)|$  (203)

2055 As  $s(\bullet)$  is a measurable, bounded, absolutely integrable function, we know that  $\lim_{\omega \rightarrow \pm\infty} |S(\iota\omega)| = 0$  by the Riemann-Lebesgue Lemma (Bochner et al., 1949).

2056 Thus,  $|S(\iota\omega)|$  is  $o(1)$ .  $|\text{LPF}_\lambda(\omega)| = \frac{1}{2\pi} \frac{\lambda}{\sqrt{\lambda^2 + \omega^2}} \sim \frac{1}{|\omega|}$ . Thus,  $|S_\lambda(\iota\omega)| = o(\frac{1}{|\omega|})$ , and thus,

2057  $\int_{-\infty}^{\infty} |S_\lambda(\iota\omega)| d\omega < \infty$ .

2058 
$$\int_{\omega \in \mathbb{R}} |\text{Re}(S_\lambda(\iota\omega))| + |\text{Im}(S_\lambda(\iota\omega))| d\omega \leq \int_{\omega \in \mathbb{R}} \sqrt{2}|S_\lambda(\iota\omega)| d\omega < \infty \quad (204)$$

2061

2062

2063

2064

2065

2066

2067

2068

2069

2070

2071

2072

2073

2074

2075

2076

2077

2078

2079

2080

2081

2082

2083

2084

2085

2086

2087

2088

2089

2090

2091

2092

2093

2094

2095

2096

2097

2098

2099

2100

2101

2102

2103

2104

2105

2106 **Proof that RH on the approximate Fourier vectors  $\widehat{\mathbf{T}}_{q,d}$  and  $\widehat{\mathbf{T}}_{c,d}$  give LSH** Finally, we show  
 2107 our results which shows that the above Algorithms result in valid LSH.  
 2108

2109 **Theorem 18.** Let  $\text{sim}(\bullet, \bullet)$  and  $\text{sim}_d(\bullet, \bullet)$  be defined as in Eq. (2) and Eq. (3) respectively. We  
 2110 compute  $h^{(d)}(G_c) = \text{sign}(\mathbf{w}^\top \widehat{\mathbf{T}}_{q,d})$  with  $\mathbf{w} \in \mathcal{N}(0, \mathbb{I})$ . Then we have the following results:  
 2111

- 2112 1. (LSH for  $\text{sim}_d(\bullet, \bullet)$ ) For  $\epsilon > 0$ , there exist  $p, p', \lambda_{\min}(\epsilon) > 0$  and  $M_{\min}(\epsilon) > 0$  such that  
 2113 the above random hyperplane hashing will give a  $(S_0, \gamma S_0, p, p')$ -ALSH for  $\text{sim}_d(\bullet, \bullet)$  when  
 2114  $\lambda > \lambda_{\min}(\epsilon)$ ,  $M > M_{\min}(\epsilon)$ .
- 2115 2. (LSH for  $\text{sim}(\bullet, \bullet)$ ) For  $\epsilon, \epsilon' > 0$ , there exists  $\widehat{p}, \widehat{p}', \lambda_{\min}(\epsilon, \epsilon') > 0$  and  $M_{\min}(\epsilon, \epsilon') > 0$   
 2116 such that the above random hyperplane hashing will give a  $(S_1, \gamma S_1, \widehat{p}, \widehat{p}')$ -ALSH for  
 2117  $\text{sim}(\bullet, \bullet)$  when  $\lambda > \lambda_{\min}(\epsilon, \epsilon')$ ,  $M > M_{\min}(\epsilon, \epsilon')$  and  $D > 1/\epsilon^2 \epsilon'$ .

2119 **Proof of (1)** Assume  $L_s$  is the Lipschitz constant for  $s(\bullet)$  and  $L_{\cos}$  is Lipschitz constant for  $\cos^{-1}$ ;  
 2120  $\delta_{\max} \triangleq \max_{c,q} \|\text{SORT}(\mathbf{x}^{(q)}) - \text{SORT}(\mathbf{x}^{(c)})\|_{\infty}$  and  $x_{\max} = \max\{\|\mathbf{X}^{(q)}\|_{\infty, \infty}, \|\mathbf{X}^{(c)}\|_{\infty, \infty}\}$ . Our  
 2121 random projection hashing is finally based on the similarity measure  $\widehat{\text{sim}}_d$  from Section 4, which is  
 2122 the Monte Carlo estimate of  $\text{sim}_d$ :

$$2124 \quad \widehat{\text{sim}}_d(G_c, G_q) \triangleq \frac{1}{M} \widehat{\mathbf{T}}_{q,d}^\top \widehat{\mathbf{T}}_{c,d} \quad (205)$$

2127 In the following proofs, we shall trace back the approximations from  $\text{sim}$  leading up to  $\widehat{\text{sim}}_d$ , and  
 2128 appropriately bound the differences. Let  $I_{\lambda} \triangleq \int_{\mathbb{R}} |\text{Re}(S_{\lambda}(\iota\omega))| + |\text{Im}(S_{\lambda}(\iota\omega))| d\omega$ . Then,

$$2131 \quad \|\mathbf{T}_{\bullet,d}(\omega)\|_2^2 = \frac{|\text{Re}(S_{\lambda}(\iota\omega))| + |\text{Im}(S_{\lambda}(\iota\omega))|}{\frac{|\text{Re}(S_{\lambda}(\iota\omega))| + |\text{Im}(S_{\lambda}(\iota\omega))|}{I_{\lambda}}} = I_{\lambda} \quad (206)$$

2134 We also observe that  $\|\mathbf{T}_{\bullet,d}(\omega)\|_2^2 = nI_{\lambda}$  and  $\|\widehat{\mathbf{T}}_{\bullet,d}\|_2^2 = MnI_{\lambda}$ . From now on we drop  $d$  from  
 2135  $f^{(d)}(G_q)$  and  $h^{(d)}(G_c)$ .

$$2138 \quad \Pr_{f,h} (f(G_q) = h(G_c) | \omega) = 1 - \frac{1}{\pi} \cos^{-1} \left( \frac{\widehat{\mathbf{T}}_{q,d}^\top \widehat{\mathbf{T}}_{c,d}}{\|\widehat{\mathbf{T}}_{q,d}\|_2 \cdot \|\widehat{\mathbf{T}}_{c,d}\|_2} \right) \quad (207)$$

$$2140 \quad = 1 - \frac{1}{\pi} \cos^{-1} \left( \frac{\widehat{\mathbf{T}}_{q,d}^\top \widehat{\mathbf{T}}_{c,d}}{\|\widehat{\mathbf{T}}_{q,d}\|_2 \cdot \|\widehat{\mathbf{T}}_{c,d}\|_2} \right) \\ 2141 \quad + \frac{1}{\pi} \cos^{-1} \left( \frac{\text{sim}_d(G_c, G_q)}{\int_{\mathbb{R}} \|\mathbf{T}_{q,d}(\omega)\|_2 \cdot \|\mathbf{T}_{c,d}(\omega)\|_2 p_{\lambda}(\omega) d\omega} \right) \quad (208)$$

$$2143 \quad - \frac{1}{\pi} \cos^{-1} \left( \frac{\text{sim}_d(G_c, G_q)}{\int_{\mathbb{R}} \|\mathbf{T}_{q,d}(\omega)\|_2 \cdot \|\mathbf{T}_{c,d}(\omega)\|_2 p_{\lambda}(\omega) d\omega} \right) \quad (209)$$

$$2145 \quad = 1 - \underbrace{\frac{1}{\pi} \cos^{-1} \left( \frac{\widehat{\text{sim}}_d(G_c, G_q)}{nI_{\lambda}} \right)}_{\mathcal{I}_1} + \frac{1}{\pi} \cos^{-1} \left( \frac{\text{sim}_d(G_c, G_q)}{nI_{\lambda}} \right) \\ 2146 \quad - \underbrace{\frac{1}{\pi} \cos^{-1} \left( \frac{\text{sim}_d(G_c, G_q)}{nI_{\lambda}} \right)}_{\mathcal{I}_2} + \frac{1}{\pi} \cos^{-1} \left( \frac{\text{sim}_d(G_c, G_q)}{nI_{\lambda}} \right) \\ 2147 \quad - \frac{1}{\pi} \cos^{-1} \left( \frac{\text{sim}_d(G_c, G_q)}{nI_{\lambda}} \right) \quad (210)$$

2158 Note that the argument  $\text{sim}_d(G_c, G_q)/nI_{\lambda}$  in the final term must reside within the domain of  $\cos^{-1}$ .  
 2159 Since  $I_{\lambda}$  is monotonically increasing in  $\lambda$ , it suffices to require  $\lambda > \inf_{\lambda} \{\lambda : I_{\lambda} > s_{\max}/n\}$ .

We shall now bound each of the terms in Eq. (210)

$$|\mathcal{I}_1| \leq \frac{1}{\pi} L_{\cos} \frac{1}{nI_{\lambda}} \left| \widehat{\text{sim}}_d(G_c, G_q) - \text{sim}_d(G_c, G_q) \right| \quad (211)$$

$$\mathbb{E}_{\omega}[|\mathcal{I}_1|] \leq \frac{L_{\cos}}{\pi n I_{\lambda}} \mathbb{E} \left| \widehat{\text{sim}}_d(G_c, G_q) - \text{sim}_d(G_c, G_q) \right| \quad (212)$$

$$\leq \frac{L_{\cos}}{\pi n I_{\lambda}} \sqrt{\frac{n}{M} \mathbb{E} (\|\mathbf{T}_{q,d}(\omega_u)\|_2^2 \|\mathbf{T}_{c,d}(\omega_u)\|_2^2)} \quad (\text{Lemma 19}) \quad (213)$$

$$= \frac{L_{\cos}}{\pi n I_{\lambda}} \sqrt{\frac{n I_{\lambda}^2}{M}} = \frac{L_{\cos}}{\pi \sqrt{Mn}} \quad (214)$$

As  $\cos^{-1}$  is monotonically decreasing, and Lipschitz in our context, we can use the bound in Lemma 20, *i.e.*,

$$-\frac{L_{\cos}}{\pi I_{\lambda}} \left( \frac{L_s}{\lambda} + \frac{s_{\max}}{\lambda} \frac{e^{-1}}{x_{\max} - \delta_{\max}} \right) \leq \mathcal{I}_2 \leq \frac{L_{\cos} L_s}{\pi I_{\lambda} \lambda} \quad (215)$$

Thus,

$$\Pr_{f,h}(f(G_q) = h(G_c)) \leq 1 - \frac{1}{\pi} \cos^{-1} \left( \frac{\text{sim}_d(G_c, G_q)}{nI_{\lambda}} \right) + \frac{L_{\cos}}{\pi \sqrt{Mn}} + \frac{L_{\cos} L_s}{\pi I_{\lambda} \lambda} \quad (216)$$

$$\Pr_{f,h}(f(G_q) = h(G_c)) \geq 1 - \frac{1}{\pi} \cos^{-1} \left( \frac{\text{sim}_d(G_c, G_q)}{nI_{\lambda}} \right) - \frac{L_{\cos}}{\pi \sqrt{Mn}} \quad (217)$$

$$- \frac{L_{\cos}}{\pi \lambda I_{\lambda}} \left( L_s + s_{\max} \frac{e^{-1}}{x_{\max} - \delta_{\max}} \right) \quad (218)$$

Using Lagrange's mean value theorem, we have:

$$\frac{1}{\pi} \left[ \cos^{-1} \left( \frac{\gamma S_0}{nI_{\lambda}} \right) - \cos^{-1} \left( \frac{S_0}{nI_{\lambda}} \right) \right] = \frac{1}{\pi} \left( \frac{(\gamma - 1) S_0}{nI_{\lambda}} \right) [(\cos^{-1})'(t)] \quad t \in \left( \frac{\gamma S_0}{nI_{\lambda}}, \frac{S_0}{nI_{\lambda}} \right) \quad (219)$$

$$\geq \frac{(1 - \gamma) S_0}{\pi n I_{\lambda}} \quad \text{as } (\cos^{-1})'(t) \leq -1 \quad (220)$$

Using Eq. (220) on the bounds obtained in Eq. (216) and Eq. (218), we have

$$p' = 1 - \frac{1}{\pi} \cos^{-1} \left( \frac{\gamma S_0}{nI_{\lambda}} \right) + \frac{L_{\cos}}{\pi \sqrt{Mn}} + \frac{L_{\cos} L_s}{\pi I_{\lambda} \lambda} \quad (221)$$

$$p = 1 - \frac{1}{\pi} \cos^{-1} \left( \frac{S_0}{nI_{\lambda}} \right) - \frac{L_{\cos}}{\pi \sqrt{Mn}} - \frac{L_{\cos}}{\pi \lambda I_{\lambda}} \left( L_s + s_{\max} \frac{e^{-1}}{x_{\max} - \delta_{\max}} \right) \quad (222)$$

We have  $p > p'$  if

$$\frac{1}{\pi} \left[ \cos^{-1} \left( \frac{\gamma S_0}{nI_{\lambda}} \right) - \cos^{-1} \left( \frac{S_0}{nI_{\lambda}} \right) \right] > \frac{2L_{\cos}}{\pi \sqrt{Mn}} + \frac{L_{\cos}}{\pi \lambda I_{\lambda}} \left( 2L_s + s_{\max} \frac{e^{-1}}{x_{\max} - \delta_{\max}} \right) \quad (223)$$

The sufficient conditions for the above equation is:

$$\frac{(1 - \gamma) S_0}{2\pi n I_{\lambda}} > \frac{2L_{\cos}}{\pi \sqrt{Mn}} \quad (224)$$

This gives us:

$$\frac{(1 - \gamma) S_0}{2\pi n I_{\lambda}} > \frac{L_{\cos}}{\pi \lambda I_{\lambda}} \left( 2L_s + s_{\max} \frac{e^{-1}}{x_{\max} - \delta_{\max}} \right) \quad (225)$$

We obtain

$$\lambda > \frac{2L_{\cos} n \left( 2L_s + s_{\max} \frac{e^{-1}}{x_{\max} - \delta_{\max}} \right)}{(1 - \gamma) S_0} \quad M > \frac{8L_{\cos}^2 n I_{\lambda}^2}{(1 - \gamma)^2 S_0^2} \quad (226)$$

This is a sufficient condition for the LSH to hold that denotes the existence of appropriate  $n_{\min}, \lambda_{\min}$  such that the LSH holds. We can also choose other bounds on  $M$  and  $\lambda$  such that the above conditions are satisfied, and the LSH is valid. We now show the second part of the theorem.

**Proof for (2)** Now that we have shown that we have a  $(S_0, \gamma S_0, p, p')$ -ALSH for  $\text{sim}_d$ , we show that it is a hash for  $\text{sim}$ . We shall use the concentration result in Proposition 7. Given  $|\frac{1}{D} \text{sim}(G_c, G_q) -$

2214  $\text{sim}_d(G_c, G_q) | \leq \epsilon$  with probability  $1 - \beta_0\delta$ , we can express this as:

$$2215 \quad -\epsilon \leq \frac{1}{D} \text{sim}(G_c, G_q) - \text{sim}_d(G_c, G_q) \leq \epsilon \quad (227)$$

2216 with probability  $1 - \beta_0\delta$ . Here, the randomness arises from  $\text{sim}_d$ . This can be rewritten as:

$$2217 \quad -\epsilon \leq \frac{1}{D} \text{sim}(G_c, G_q) - \text{sim}_d(G_c, G_q) \leq \epsilon \quad (228)$$

$$2218 \quad \Rightarrow \begin{cases} \text{sim}_d(G_c, G_q) \leq \frac{1}{D} \text{sim}(G_c, G_q) + \epsilon & \text{(condition 1),} \\ \text{sim}_d(G_c, G_q) \geq \frac{1}{D} \text{sim}(G_c, G_q) - \epsilon & \text{(condition 2).} \end{cases} \quad (229)$$

2219 Both condition 1 and condition 2 have probability  $\geq 1 - \beta_0\delta$ . Here,  $p$  and  $p'$  are computed in the proof of (1).

2220 1. Condition 1 implies that if  $\frac{1}{D} \text{sim}(G_c, G_q) \leq \gamma S_0 - \epsilon$ , then  $\text{sim}_d(G_c, G_q) \leq \gamma S_0$  with probability  $\geq 1 - \beta_0\delta$ . Therefore, when  $\frac{1}{D} \text{sim}(G_c, G_q) \leq \gamma S_0 - \epsilon$

$$2221 \quad \begin{aligned} \Pr_{f,h}(f(G_q) = h(G_c)) \\ = \Pr(f(G_q) = h(G_c) | \text{sim}_d(G_c, G_q) \leq \gamma S_0) \cdot \Pr(\text{sim}_d(G_c, G_q) \leq \gamma S_0) \\ + \Pr(f(G_q) = h(G_c) | \text{sim}_d(G_c, G_q) > \gamma S_0) \cdot \Pr(\text{sim}_d(G_c, G_q) > \gamma S_0) \end{aligned} \quad (230)$$

$$2222 \quad \leq p'(1 - \beta_0\delta) + 1 \cdot \beta_0\delta \quad (231)$$

2223 2. Condition 2 implies that if  $\frac{1}{D} \text{sim}(G_c, G_q) \geq S_0 + \epsilon$ , then  $\text{sim}_d(G_c, G_q) \geq S_0$  with probability  $\geq 1 - \beta_0\delta$ . Therefore, when  $\frac{1}{D} \text{sim}(G_c, G_q) \geq S_0 + \epsilon$

$$2224 \quad \begin{aligned} \Pr_{f,h}(f(G_q) = h(G_c)) \\ = \Pr(f(G_q) = h(G_c) | \text{sim}_d(G_c, G_q) \geq S_0) \cdot \Pr(\text{sim}_d(G_c, G_q) \geq S_0) \\ + \Pr(f(G_q) = h(G_c) | \text{sim}_d(G_c, G_q) < S_0) \cdot \Pr(\text{sim}_d(G_c, G_q) < S_0) \end{aligned} \quad (232)$$

$$2225 \quad \geq \Pr(f(G_q) = h(G_c) | \text{sim}_d(G_c, G_q) \geq S_0) \Pr(\text{sim}_d(G_c, G_q) \geq S_0) \quad (233)$$

$$2226 \quad \geq p(1 - \beta_0\delta) \quad (234)$$

2227 Then, we have a  $(D(S_0 + \epsilon), D(\gamma S_0 - \epsilon), p(1 - \beta_0\delta), p'(1 - \beta_0\delta) + \beta_0\delta)$ -ALSH if

$$2228 \quad p(1 - \beta_0\delta) > p'(1 - \beta_0\delta) + \beta_0\delta \quad (235)$$

$$2229 \quad p > p' + \frac{\beta_0\delta}{1 - \beta_0\delta} \quad (236)$$

2230 We shall find a sufficient condition for Eq. (236) to hold. We use the expressions in the previous results. Finally, we reparameterize the problem with  $S_1 \triangleq D(S_0 + \epsilon)$ ,  $\gamma_1 S_1 \triangleq D(\gamma S_0 - \epsilon)$  with  $\gamma_1 = \gamma - \frac{\epsilon}{S_0} < \gamma < 1$ ,  $\hat{p} = p(1 - \beta_0\delta)$  and  $\hat{p}' = p'(1 - \beta_0\delta) + \beta_0\delta$

2231 For  $p_\lambda(\omega) \propto |\text{Re}(S_\lambda(\omega))| + |\text{Im}(S_\lambda(\omega))|$ , the above criteria are achieved by taking

$$2232 \quad M > n \left( \frac{2L_{\cos}}{\frac{(1-\gamma)S_0}{2I_\lambda} + \frac{n\pi\beta_0\delta}{1-\beta_0\delta}} \right)^2 \quad (237)$$

2233 for the same  $\lambda$ . Reparameterizing with  $S_1, \gamma_1$ , we obtain

$$2234 \quad M > n \left( \frac{2L_{\cos}}{\frac{(1-\gamma_1)S_1/D - 2\epsilon}{2I_\lambda} + \frac{n\pi\beta_0\delta}{1-\beta_0\delta}} \right)^2, D > \frac{1}{\delta\epsilon^2}, \lambda > \frac{2L_{\cos}n \left( 2L_s + s_{\max} \frac{e^{-1}}{x_{\max} - \delta_{\max}} \right)}{(1 - \gamma_1)S_1/D - 2\epsilon} \quad (238)$$

2235 As before, we pick  $M_{\min}, \lambda_{\min}$  such that the above conditions are satisfied. We can also choose other

2236 bounds on  $M$  and  $\lambda$  such that the above conditions are satisfied, and the LSH is valid.  $\blacksquare$

2237 Note that here we have considered the randomness of model initialization to be part of the randomness of the hashing routine.

2238  
2239  
2240  
2241  
2242  
2243  
2244  
2245  
2246  
2247  
2248  
2249  
2250  
2251  
2252  
2253  
2254  
2255  
2256  
2257  
2258  
2259  
2260  
2261  
2262  
2263  
2264  
2265  
2266  
2267

2268 E.2.5 AUXILIARY RESULTS USED TO PROVE RESULTS IN THIS SUBSECTION E.2.4  
22692270 **Lemma 19.** Suppose  $\text{sim}_d$  is defined as Eq. (7) and  $\widehat{\text{sim}}_d$  is defined as Eq. (9). Then, we have the  
2271 following concentration bound:  
2272

2273 
$$\mathbb{E} \left| \widehat{\text{sim}}_d(G_c, G_q) - \text{sim}_d(G_c, G_q) \right| \leq \sqrt{\frac{n}{M} \mathbb{E} \left[ \left( \mathbf{T}_{q,d}(\omega_u)^\top \mathbf{T}_{c,d}(\omega_u) \right)^2 \right]} \quad (239)$$
  
2274

2275 **Proof** We observe that:  
2276

2277 
$$\mathbb{E} \left| \widehat{\text{sim}}_d(G_c, G_q) - \text{sim}_d(G_c, G_q) \right| \leq \sqrt{\mathbb{E} \left| \widehat{\text{sim}}_d(G_c, G_q) - \text{sim}_d(G_c, G_q) \right|^2} = \sqrt{\text{Var} \left( \widehat{\text{sim}}_d(G_c, G_q) \right)} \quad (240)$$
  
2278

2279 
$$= \sqrt{\text{Var} \left( \frac{1}{M} \sum_{m \in [M]} \sum_{u \in [n]} \mathbf{T}_{q,d}(\omega_u)^\top \mathbf{T}_{c,d}(\omega_u) \right)} \quad (241)$$
  
2280

2281 
$$= \sqrt{\frac{n}{M} \text{Var} \left( \mathbf{T}_{q,d}(\omega_u)^\top \mathbf{T}_{c,d}(\omega_u) \right)} = \sqrt{\frac{n}{M} \mathbb{E} \left[ \left( \mathbf{T}_{q,d}(\omega_u)^\top \mathbf{T}_{c,d}(\omega_u) \right)^2 \right]} \quad (242)$$
  
2282

2283 Here, Eq. (242) follows from the i.i.d sampling of  $\omega_u$ .  
22842285 **Lemma 20.** Suppose  $\text{sim}_d$  is defined as Eq. (7) and  $\widehat{\text{sim}}_d$  is defined as Eq. (3). Then, we have the  
2286 following concentration bound:  
2287

2288 
$$- \left( \frac{nL_s}{\lambda} + \frac{ns_{\max}}{\lambda} \frac{e^{-1}}{x_{\max} - \delta_{\max}} \right) \leq \text{sim}_d(G_c, G_q) - \text{sim}_d(G_c, G_q) \leq \frac{nL_s}{\lambda} \quad (243)$$
  
2289

2290 where  $L_s$  is the Lipschitz constant for  $s$ ;  $\delta_{\max} \triangleq \max_{c,q} \|\text{SORT}(\mathbf{x}^{(q)}) - \text{SORT}(\mathbf{x}^{(c)})\|_\infty$ ; and  
2291  $\max\{\|\mathbf{X}^{(q)}\|_{\infty,\infty}, \|\mathbf{X}^{(c)}\|_{\infty,\infty}\} < x_{\max}$   
22922293 *Proof.* Let  $s_\lambda$  denote the fourier inverse of  $S_\lambda$ .  
2294

2295 
$$\text{sim}_d(G_c, G_q) = \sum_{u \in [n]} \int_{\mathbb{R}} S_\lambda(\iota\omega) e^{\iota\omega(\mathbf{x}^{(q)}(u)[d] - \mathbf{x}^{(q)}(u)[d])} d\omega \quad (244)$$
  
2296

2297 
$$= \sum_{u \in [n]} s_\lambda(\mathbf{x}^{(q)}(u)[d] - \mathbf{x}^{(q)}(u)[d]) \quad (245)$$
  
2298

2299 We shall bound the deviation of the smoothed score function  $s_\lambda$  from the original score function  
2300

2301 
$$s_\lambda(x) = \int_{\mathbb{R}} s(x-t) \mathcal{F}^{-1}[\text{LPF}_\lambda](t) dt \quad \text{using } \mathcal{F}^{-1}[fg] = \mathcal{F}^{-1}[f] * \mathcal{F}^{-1}[g] \quad (246)$$
  
2302

2303 
$$= \int_{\mathbb{R}} s(x-t) \lambda e^{\lambda t} H(-t) dt = \int_{-\infty}^0 s(x-t) \lambda e^{\lambda t} dt \quad (247)$$
  
2304

2305 (where  $H(\cdot)$  is the Heaviside step function)  
2306

2307 
$$= \int_0^\infty s(x + \frac{t}{\lambda}) e^{-t} dt \quad \text{substitution with } t \mapsto -\lambda t \quad (248)$$
  
2308

2309 
$$= \int_0^\infty s(x) e^{-t} dt + \int_0^\infty (s(x + \frac{t}{\lambda}) - s(x)) e^{-t} dt \quad (249)$$
  
2310

2311 
$$= s(x) + \underbrace{\int_0^\infty (s(x + \frac{t}{\lambda}) - s(x)) e^{-t} dt}_{\mathcal{I}_1} \quad (250)$$
  
2312

2313 We shall use the fact that  $s$  is clipped within  $[-x_{\max}, x_{\max}]$ . We have the following possible cases:  
23142315 Case 1  $x + \frac{t}{\lambda} > x_{\max} \implies t > \lambda(x_{\max} - x)$   
23162317 Case 2  $x_{\max} \geq x + \frac{t}{\lambda} \geq -x_{\max} \implies \lambda(x_{\max} - x) \geq t > 0 > \lambda(-x_{\max} - x)$   
2318

2322 This lets us split the integral in  $\mathcal{I}_1$  into two in order to bound the term.  
 2323

$$\begin{aligned} 2324 \int_0^\infty (s(x + \frac{t}{\lambda}) - s(x))e^{-t} dt &= \int_0^{\lambda(x_{\max} - x)} (s(x + \frac{t}{\lambda}) - s(x))e^{-t} dt \\ 2325 &\quad + \int_{\lambda(x_{\max} - x)}^\infty (0 - s(x))e^{-t} dt \end{aligned} \quad (251)$$

$$2328 = \underbrace{\left[ \int_0^{\lambda(x_{\max} - x)} (s(x + \frac{t}{\lambda}) - s(x))e^{-t} dt \right]}_{\mathcal{I}_2} - s(x)e^{-\lambda(x_{\max} - x)} \quad (252)$$

2333 We now bound  $|\mathcal{I}_2|$  as follows:  
 2334

$$2335 |\mathcal{I}_2| \leq \int_0^{\lambda(x_{\max} - x)} L_s \frac{t}{\lambda} e^{-t} dt \quad (s \text{ is Lipschitz with constant } L_s) \quad (253)$$

$$2337 = \frac{L_s}{\lambda} [-(t+1)e^{-t}]_{t=0}^{\lambda(x_{\max} - x)} \leq \frac{L_s}{\lambda} [-(t+1)e^{-t}]_{t=0}^{\lambda(x_{\max} + \max\|x\|_\infty)} \quad (254)$$

$$2339 = \frac{L_s}{\lambda} \left( 1 - e^{-\lambda(x_{\max} + \delta_{\max})} - \lambda(x_{\max} + \delta_{\max})e^{-\lambda(x_{\max} + \delta_{\max})} \right) \quad (255)$$

$$2341 \leq \frac{L_s}{\lambda} [-(t+1)e^{-t}]_{t=0}^\infty = \frac{L_s}{\lambda} \cdot 1 \quad (256)$$

2342 The bound in (254) relies on integrating over a larger domain. This yields the bound Eq. (255).  
 2343 However, for purposes of this proof, we use the looser bound Eq. (256) by integrating over  $(0, \infty)$ .  
 2344

2345 Using the fact that  $0 \leq s(\cdot) \leq s_{\max}$  in Eq (252)

$$2346 -|\mathcal{I}_2| - s_{\max}e^{-\lambda(x_{\max} - x)} \leq \mathcal{I}_1 \leq |\mathcal{I}_2| \quad (257)$$

$$2347 -\frac{L_s}{\lambda} - \frac{s_{\max}e^{-1}}{\lambda(x_{\max} - x)} \leq \mathcal{I}_1 \leq \frac{L_s}{\lambda} \quad (258)$$

$$2350 -\frac{L_s}{\lambda} - \frac{s_{\max}e^{-1}}{\lambda(x_{\max} - \delta_{\max})} \leq \mathcal{I}_1 \leq \frac{L_s}{\lambda} \quad (259)$$

2352 ■

2353  
 2354  
 2355  
 2356  
 2357  
 2358  
 2359  
 2360  
 2361  
 2362  
 2363  
 2364  
 2365  
 2366  
 2367  
 2368  
 2369  
 2370  
 2371  
 2372  
 2373  
 2374  
 2375

2376 **F LIST OF GNNs**  
 2377

2378 We collect the following list from Pytorch Geometric.  
 2379

2380 **1. GNN**  
 2381

- (1) Gated GNN (Li et al., 2016; Gilmer et al., 2017) (Already showed)
- (2) GCN (Kipf et al., 2017)
- (3) ChebConv (Defferrard et al., 2016)
- (4) SAGE (Hamilton et al., 2017)
- (5) ResGatedGraphConv (Bresson et al., 2017)
- (6) GAT (Veličković et al., 2018)
- (7) AGNNConv (Thekumparampil et al., 2018)
- (8) GIN (Xu et al., 2019)
- (9) SGConv (Wu et al., 2019)
- (10) TAGConv (Du et al., 2017)
- (11) APPNP (Gasteiger et al., 2018)
- (12) SSGConv (Zhu et al., 2021)
- (13) MFConv (Duvenaud et al., 2015)

2382 **2. Graph Transformers**  
 2383

- (1) Graph Transformer (GraphGPS-style) (Rampášek et al., 2022)
- (2) Graphomer (Ying et al., 2021)
- (3) Spectral Attention Network (SAN) (Kreuzer et al., 2021)
- (4) Exphomer (Shirzad et al., 2023)
- (5) NodeFormer (Wu et al., 2023)

2384 Here, we will take node embeddings  $\mathbf{x}$  to be column vectors, but the graph embedding  $\mathbf{X}$  to have  $\mathbf{x}$   
 2385 along rows. As such we will use  $\Theta$  for the parameters right multiplied and  $\mathbf{W}$  for left multiplied.  
 2386  $D, A, L$  refer to the degree, adjacency and Laplacian matrices respectively. Similarly,  $\hat{D}, \hat{A}, \hat{L}$  refer  
 2387 to the normalized degree, adjacency and Laplacian matrices respectively.  
 2388

2389 We demonstrate transformations for various graph layers that can be used to maintain/induce permuta-  
 2390 tions in the output, which would be required for showing exchangeability at a certain layer. Where  
 2391 applicable, we may take arbitrary permutation  $\pi_2$  on the input and a corresponding  $\pi_1$  in the output.  
 2392 For some cases the permutations are more restrictive (such as  $\pi_1 = \pi_2$ ).  
 2393

2394 These transformations can then be composed to generate the permutation inducing transformation for  
 2395 the entire network.  
 2396

2397 We have shown transformation for architectures such as the MLP (FF) and GRU (GRU). For a given  
 2398 permutation (where it is clear from context), we define the transformed versions as follows:  
 2399

$$\begin{aligned} \text{GRU}^*(\mathbf{X}\pi, \mathbf{H}\pi) &= \text{GRU}(\mathbf{X}, \mathbf{H})\pi \\ \text{FF}^*(\mathbf{X}\pi) &= \text{FF}(\mathbf{X})\pi \end{aligned}$$

2400 or if the input and output permutations are different:  
 2401

$$\text{FF}^*(\mathbf{X}\pi_2) = \text{FF}(\mathbf{X})\pi_1$$

2402 **F.1 GRAPH NEURAL NETWORK**  
 2403

2404 Based on the original formulation,  $\mathbf{x}$  can be row or column vector and therefore  $\pi$  is pre-multiplied  
 2405 or post-multiplied.  
 2406

2407 **(1) GCN (Kipf et al., 2017):**  
 2408

$$\mathbf{X}' = \hat{\mathbf{D}}^{-1/2} \hat{\mathbf{A}} \hat{\mathbf{D}}^{-1/2} \mathbf{X} \Theta \quad (260)$$

$$\mathbf{X}'\pi = \hat{\mathbf{D}}^{-1/2} \hat{\mathbf{A}} \hat{\mathbf{D}}^{-1/2} \mathbf{X} (\Theta\pi) \quad (261)$$

$$\mathbf{X}'\pi_1 = \hat{\mathbf{D}}^{-1/2} \hat{\mathbf{A}} \hat{\mathbf{D}}^{-1/2} (\mathbf{X}\pi_2)(\pi_2^\top \Theta\pi_1) \quad (262)$$

2409 **(2) ChebConv (Defferrard et al., 2016):** It uses Chebyshev polynomial filters on the rescaled  
 2410 Laplacian. The Chebyshev polynomials are defined as  $T_0(x) = 1$ ,  $T_1(x) = x$  and  $T_k(x) =$   
 2411  $2xT_{k-1}(x) - T_{k-2}(x)$  for  $k \geq 2$ .  
 2412

2430

2431

2432

2433

2434

2435

2436

$$\mathbf{X}^{(k)} = \sum_{\ell=0}^K T_\ell(\tilde{L}) \mathbf{X}^{(k-1)} \Theta_\ell \quad (263)$$

$$\mathbf{X}^{(k)} \boldsymbol{\pi}_1 = \sum_{\ell=0}^K T_\ell(\tilde{L}) (\mathbf{X}^{(k-1)} \boldsymbol{\pi}_2) (\boldsymbol{\pi}_2^\top \Theta_\ell \boldsymbol{\pi}_1) \quad (264)$$

(3) **SAGEConv** (Hamilton et al., 2017): We take the aggregate function to be permutation equivariant (eg. mean/sum).

$$\mathbf{x}_i^{(k)} = \sigma(\mathbf{W}_1 \mathbf{x}_i^{(k-1)} + \mathbf{W}_2 \cdot \text{AGGREGATE}(\{\mathbf{x}_j^{(k-1)}\})) \quad (265)$$

$$\boldsymbol{\pi} \mathbf{x}_i^{(k)} = \sigma((\boldsymbol{\pi} \mathbf{W}_1 \boldsymbol{\pi}^\top) \boldsymbol{\pi} \mathbf{x}_i^{(k-1)} + (\boldsymbol{\pi} \mathbf{W}_2 \boldsymbol{\pi}^\top) \cdot \text{AGGREGATE}(\{\boldsymbol{\pi} \mathbf{x}_j^{(k-1)}\})) \quad (266)$$

or, there may be a layer before the aggregation (allowing for more flexibility in the transformation):

$$\mathbf{x}_i^{(k)} = \sigma(\mathbf{W}_1 \mathbf{x}_i^{(k-1)} + \mathbf{W}_2 \cdot \text{AGGREGATE}(\{\text{FF}(\mathbf{x}_j^{(k-1)})\})) \quad (267)$$

$$\boldsymbol{\pi}_1 \mathbf{x}_i^{(k)} = \sigma((\boldsymbol{\pi}_1 \mathbf{W}_1 \boldsymbol{\pi}_2^\top) \boldsymbol{\pi}_2 \mathbf{x}_i^{(k-1)} + (\boldsymbol{\pi}_1 \mathbf{W}_2 \boldsymbol{\pi}_2^\top) \cdot \text{AGGREGATE}(\{\text{FF}^*(\boldsymbol{\pi}_2 \mathbf{x}_j^{(k-1)})\})) \quad (268)$$

(4) **ResGatedGraphConv** (Bresson et al., 2017): Adds a residual connection over a gated convolution mechanism.

$$\mathbf{x}_i^{(k)} = \mathbf{W}_1 \mathbf{x}_i^{(k-1)} + \sum_{j \in \mathcal{N}(i)} \mathbf{W}_2 \mathbf{x}_j^{(k-1)} \odot \sigma(\mathbf{W}_3 \mathbf{x}_i^{(k-1)} + \mathbf{W}_4 \mathbf{x}_j^{(k-1)}) \quad (269)$$

$$\begin{aligned} \boldsymbol{\pi}_1 \mathbf{x}_i^{(k)} &= (\boldsymbol{\pi}_1 \mathbf{W}_1 \boldsymbol{\pi}_2^\top) (\boldsymbol{\pi}_2 \mathbf{x}_i^{(k-1)}) \\ &+ \sum_{j \in \mathcal{N}(i)} (\boldsymbol{\pi}_1 \mathbf{W}_2 \boldsymbol{\pi}_2^\top) (\boldsymbol{\pi}_2 \mathbf{x}_j^{(k-1)}) \odot \sigma((\boldsymbol{\pi}_1 \mathbf{W}_3 \boldsymbol{\pi}_2^\top) (\boldsymbol{\pi}_2 \mathbf{x}_i^{(k-1)})) \\ &+ (\boldsymbol{\pi}_1 \mathbf{W}_4 \boldsymbol{\pi}_2^\top) (\boldsymbol{\pi}_2 \mathbf{x}_j^{(k-1)}) \end{aligned} \quad (270)$$

(5) **GAT** (Veličković et al., 2018): The attention score  $\alpha$  can be made invariant.

$$\mathbf{x}_i^{(k)} = \sum_{j \in \mathcal{N}(i)} \alpha_{ij}^{(h)} W^{(h)} \mathbf{x}_j^{(k-1)} \quad (271)$$

$$\boldsymbol{\pi} \mathbf{x}_i^{(k)} = \sum_{j \in \mathcal{N}(i)} \alpha_{ij}^{(h)} (\boldsymbol{\pi}_h W^{(h)} \boldsymbol{\pi}^\top) \boldsymbol{\pi} \mathbf{x}_j^{(k-1)} \quad (272)$$

$$\alpha_{ij} = \frac{\exp(\text{LeakyReLU}(\mathbf{a}^T [\mathbf{W} \mathbf{x}_i \| \mathbf{W} \mathbf{x}_j]))}{\sum_{k \in \mathcal{N}(i) \cup \{i\}} \exp(\text{LeakyReLU}(\mathbf{a}^T [\mathbf{W} \mathbf{x}_i \| \mathbf{W} \mathbf{x}_k]))} \quad (273)$$

$$\alpha_{ij} = \frac{\exp(\text{LeakyReLU}(\mathbf{a}^T [\mathbf{W} \boldsymbol{\pi}^\top \boldsymbol{\pi} \mathbf{x}_i \| \mathbf{W} \boldsymbol{\pi}^\top \boldsymbol{\pi} \mathbf{x}_j]))}{\sum_{k \in \mathcal{N}(i) \cup \{i\}} \exp(\text{LeakyReLU}(\mathbf{a}^T [\mathbf{W} \boldsymbol{\pi}^\top \boldsymbol{\pi} \mathbf{x}_i \| \mathbf{W} \boldsymbol{\pi}^\top \boldsymbol{\pi} \mathbf{x}_k]))} \quad (274)$$

If the aggregation is concatenation instead of sum, the output will not be exchangeable for all dimensions. rather, each block of dimensions corresponding to a head will be exchangeable.

(6) **AGNNConv** (Thekumparampil et al., 2018):

$$\mathbf{X}' = \mathbf{P} \mathbf{X} \quad (275)$$

Where,

$$\mathbf{P}_{i,j} = \frac{\exp(\beta \cdot \cos(\mathbf{x}_i, \mathbf{x}_j))}{\sum_{k \in \mathcal{N}(i) \cup \{i\}} \exp(\beta \cdot \cos(\mathbf{x}_i, \mathbf{x}_k))} = \frac{\exp\left(\beta \cdot \frac{(\boldsymbol{\pi} \mathbf{x}_i)^\top \boldsymbol{\pi} \mathbf{x}_j}{\|\boldsymbol{\pi} \mathbf{x}_i\| \|\boldsymbol{\pi} \mathbf{x}_j\|}\right)}{\sum_{k \in \mathcal{N}(i) \cup \{i\}} \exp\left(\beta \cdot \frac{(\boldsymbol{\pi} \mathbf{x}_i)^\top \boldsymbol{\pi} \mathbf{x}_k}{\|\boldsymbol{\pi} \mathbf{x}_i\| \|\boldsymbol{\pi} \mathbf{x}_k\|}\right)} \quad (276)$$

So this layer is equivariant to any permutation  $\boldsymbol{\pi}$ .

(7) **GIN** (Xu et al., 2019):

$$\mathbf{X}' = \text{FF}((1 + \epsilon) \cdot \mathbf{X} + \mathbf{A} \mathbf{X}) \quad (277)$$

$$\mathbf{X}' \boldsymbol{\pi}_1 = \text{FF}^*((1 + \epsilon) \cdot (\mathbf{X} \boldsymbol{\pi}_2) + \mathbf{A}(\mathbf{X} \boldsymbol{\pi}_2)) \quad (278)$$

A powerful injective update via MLP which combines self-feature (with learnable epsilon) plus neighbor sum.

2484 (8) **SGConv** (Wu et al., 2019): A K-step precomputed propagation that simplifies convolution.  
 2485

$$2486 \quad \mathbf{X}' = \left( \mathbf{D}^{-1/2} \hat{\mathbf{A}} \mathbf{D}^{-1/2} \right)^K \mathbf{X} \Theta, \quad \hat{\mathbf{A}} = \mathbf{A} + \mathbf{I} \quad (279)$$

$$2488 \quad \mathbf{X}' \pi_1 = \left( \mathbf{D}^{-1/2} \hat{\mathbf{A}} \mathbf{D}^{-1/2} \right)^K (\mathbf{X} \pi_2) (\pi_2^\top \Theta \pi_1) \quad (280)$$

2489 (281)

2490 (9) **TAGConv** (Du et al., 2017):  
 2491

$$2492 \quad \mathbf{X}' = \sum_{k=0}^K \left( \mathbf{D}^{-1/2} \mathbf{A} \mathbf{D}^{-1/2} \right)^k \mathbf{X} \Theta_k \quad (282)$$

$$2495 \quad \mathbf{X}' \pi_1 = \sum_{k=0}^K \left( \mathbf{D}^{-1/2} \mathbf{A} \mathbf{D}^{-1/2} \right)^k (\mathbf{X} \pi_2) (\pi_2^\top \Theta_k \pi_1) \quad (283)$$

2497 (10) **APPNP** (Gasteiger et al., 2018):  
 2498

$$2499 \quad \mathbf{X}^{(0)} = \mathbf{X} \quad (284)$$

$$2500 \quad \mathbf{X}^{(k)} = (1 - \alpha) \hat{D}^{-1/2} \hat{A} \hat{D}^{-1/2} \mathbf{X}^{(k-1)} + \alpha \mathbf{X}^{(0)} \quad (285)$$

$$2501 \quad \mathbf{X}' = \mathbf{X}^{(K)} \quad (286)$$

2502 This layer is equivariant to any permutation  $\pi$ .  
 2503

$$2504 \quad \mathbf{X}^{(0)} \pi = \mathbf{X} \pi \quad (287)$$

$$2505 \quad \mathbf{X}^{(k)} \pi = (1 - \alpha) \hat{D}^{-1/2} \hat{A} \hat{D}^{-1/2} \mathbf{X}^{(k-1)} \pi + \alpha \mathbf{X}^{(0)} \pi \quad (288)$$

$$2506 \quad \mathbf{X}' \pi = \mathbf{X}^{(K)} \pi \quad (289)$$

2507 (11) **SSGConv** (Zhu et al., 2021):  
 2508

$$2509 \quad \mathbf{X}' = (1 - \alpha) \left( \mathbf{D}^{-1/2} \hat{\mathbf{A}} \mathbf{D}^{-1/2} \right)^K \mathbf{X} \Theta_1 + \alpha \mathbf{X} \Theta_2 \quad (290)$$

$$2511 \quad \mathbf{X}' \pi_1 = (1 - \alpha) \left( \mathbf{D}^{-1/2} \hat{\mathbf{A}} \mathbf{D}^{-1/2} \right)^K \mathbf{X} \pi_2 \pi_2^\top \Theta_1 \pi_1 + \alpha \mathbf{X} \pi_2 \pi_2^\top \Theta_2 \pi_1 \quad (291)$$

2512 Skip-connection version of SGConv with initial-feature mixing via  $\alpha$ .  
 2513

2514 (12) **MFConv** (Duvenaud et al., 2015): This has a distinct weight matrix for nodes of each degree.  
 2515

$$2515 \quad \mathbf{x}'_i = \mathbf{W}_{\deg(i)} \mathbf{x}_i + \sum_{j \in \mathcal{N}(i)} \frac{1}{\sqrt{d_i d_j}} \hat{\mathbf{W}}_{\deg(i)} \mathbf{x}_j \quad (292)$$

$$2517 \quad \pi_1 \mathbf{x}'_i = (\pi_1 \mathbf{W}_{\deg(i)} \pi_2^\top) (\pi_2 \mathbf{x}_1) + \sum_{j \in \mathcal{N}(1)} \frac{1}{\sqrt{\pi_2 d_1 \pi_2 d_j}} (\pi_1 \hat{\mathbf{W}}_{\deg(i)} \pi_2^\top) (\pi_2 \mathbf{x}_j) \quad (293)$$

## F.2 GRAPH TRANSFORMERS

2522 **Multi-Head Attention (MHA)** Before examining specific Graph Transformer architectures, we  
 2523 first establish the standard Multi-Head Attention (MHA) mechanism that forms the foundation of  
 2524 most transformer-based models. The MHA operation transforms input representations  $\mathbf{H}^{(\ell)} \in \mathbb{R}^{n \times d}$   
 2525 through learned query ( $\mathbf{Q}$ ), key ( $\mathbf{K}$ ), and value ( $\mathbf{V}$ ) projections:

$$2527 \quad \mathbf{Q}^{(h)} = \mathbf{H}^{(\ell)} \mathbf{W}_Q^{(h)}, \quad \mathbf{K}^{(h)} = \mathbf{H}^{(\ell)} \mathbf{W}_K^{(h)}, \quad \mathbf{V}^{(h)} = \mathbf{H}^{(\ell)} \mathbf{W}_V^{(h)} \quad (294)$$

$$2529 \quad \alpha_{ij}^{(h)} = \text{softmax}_j \left( \frac{\mathbf{Q}_i^{(h)} (\mathbf{K}_j^{(h)})^\top}{\sqrt{d_k}} + B_{ij} \right) \quad (295)$$

$$2531 \quad \mathbf{Z}^{(h)} = \alpha^{(h)} \mathbf{V}^{(h)} \quad (296)$$

$$2533 \quad \text{MHA}_B(\mathbf{H}^{(\ell)}) = \text{Concat}(\mathbf{Z}^{(1)}, \dots, \mathbf{Z}^{(\ell)}) \mathbf{W}_O \quad (297)$$

2534 where each attention head  $h \in \{1, \dots, \ell\}$  computes scaled dot-product attention independently, and  
 2535  $\mathbf{W}_O$  projects the concatenated multi-head output. Given the input  $\mathbf{H} \mapsto \mathbf{H} \pi_2$ , we can transform  
 2536  $\mathbf{W}_Q^{(h)}$ ,  $\mathbf{W}_K^{(h)}$ , and  $\mathbf{W}_V^{(h)}$  as  $\mathbf{W}^{(h)} \mapsto \pi_2^\top \mathbf{W}^{(h)}$ . And the output of MHA can be transformed by  $\pi_1$   
 2537 by  $\mathbf{W}_O \mapsto \mathbf{W}_O \pi_1$ .

2538 Using the above, we define  $\text{MHA}_B^*$  such that  $\text{MHA}_B^*(\mathbf{X}\boldsymbol{\pi}) = \text{MHA}_B(\mathbf{X})\boldsymbol{\pi}$ .  
 2539

2540 Note that in general, different attention mechanisms are dealt with similarly - the attention parameters  
 2541 can be used to undo the effect of a preceding permutation, hence the attention score computation  
 2542 remains unchanged.

2543 Transformer layers also typically include Layer Normalization, that we will largely omit here, as it is  
 2544 straightforward to see that it is permutation equivariant.

2545 **(1) Graph Transformer (Rampášek et al., 2022):**

$$2546 \quad \mathbf{Q}^{(h)} = \mathbf{H}^{(\ell)} \mathbf{W}_Q^{(h)}, \quad \mathbf{K}^{(h)} = \mathbf{H}^{(\ell)} \mathbf{W}_K^{(h)}, \quad \mathbf{V}^{(h)} = \mathbf{H}^{(\ell)} \mathbf{W}_V^{(h)} \quad (298)$$

$$2548 \quad \alpha_{ij}^{(h)} = \text{softmax}_j \left( \frac{\mathbf{Q}_i^{(h)} (\mathbf{K}_j^{(h)})^\top}{\sqrt{d_k}} + B_{ij} \right) \quad (299)$$

$$2551 \quad \mathbf{Z}^{(h)} = \alpha^{(h)} \mathbf{V}^{(h)} \quad (300)$$

$$2552 \quad \tilde{\mathbf{H}}^{(\ell+1)} = \mathbf{H}^{(\ell)} + \text{MHA}_B(\mathbf{H}^{(\ell)}) \quad (301)$$

$$2554 \quad \mathbf{H}^{(\ell+1)} = \tilde{\mathbf{H}}^{(\ell+1)} + \text{FF}(\tilde{\mathbf{H}}^{(\ell+1)}) \quad (302)$$

2555 We observe the transformations,

$$2556 \quad \tilde{\mathbf{H}}^{(\ell+1)}\boldsymbol{\pi} = \mathbf{H}^{(\ell)}\boldsymbol{\pi} + \text{MHA}_B^*(\mathbf{H}^{(\ell)}\boldsymbol{\pi}) \quad (303)$$

$$2557 \quad \mathbf{H}^{(\ell+1)}\boldsymbol{\pi} = \tilde{\mathbf{H}}^{(\ell+1)}\boldsymbol{\pi} + \text{FF}^*(\tilde{\mathbf{H}}^{(\ell+1)}\boldsymbol{\pi}) \quad (304)$$

2558 **(2) Graphomer (Ying et al., 2021):** Firstly, the graphomer adds centrality encodings to the node  
 2559 embedding  $\mathbf{x}^{(0)}$ . Hence these encoding require the same permutation as that of the input node  
 2560 features. The graphomer adds spatial and edge encodings as attention biases  $B_{ij}$ . As our  
 2561 transformation does not affect the Q-K dot product, it does not affect the attention scores.

$$2562 \quad \mathbf{Q}^{(h)} = \mathbf{H}^{(\ell)} \mathbf{W}_Q^{(h)}, \quad \mathbf{K}^{(h)} = \mathbf{H}^{(\ell)} \mathbf{W}_K^{(h)}, \quad \mathbf{V}^{(h)} = \mathbf{H}^{(\ell)} \mathbf{W}_V^{(h)} \quad (305)$$

$$2564 \quad \alpha_{ij}^{(h)} = \text{softmax}_j \left( \frac{\mathbf{Q}_i^{(h)} (\mathbf{K}_j^{(h)})^\top}{\sqrt{d_k}} + b_{\text{enc}}^{\text{SPD}}(\text{SPD}(i, j)) + b_{\text{enc}}^{\text{edge}}(\text{edge-path}(i, j)) \right) \quad (306)$$

$$2566 \quad \mathbf{Z}^{(h)} = \alpha^{(h)} \mathbf{V}^{(h)} \quad (307)$$

$$2568 \quad \mathbf{H}^{(\ell+1)} = \text{FF}(\mathbf{H}^{(\ell)} + \text{MHA}(\mathbf{H}^{(\ell)})) \quad (308)$$

2569 Hence, the same transformations as the graph transformer follow, as  $\alpha_{i,j}^{(h)}$  remains unchanged.

2570 **(3) Spectral Attention Network (SAN) (Kreuzer et al., 2021):**

$$2571 \quad \tilde{\mathbf{H}}^{(\ell)} = \mathbf{H}^{(\ell)} + \mathbf{S} \quad (309)$$

$$2573 \quad \mathbf{Q}^{(h)} = \tilde{\mathbf{H}}^{(\ell)} \mathbf{W}_Q^{(h)}, \quad \mathbf{K}^{(h)} = \tilde{\mathbf{H}}^{(\ell)} \mathbf{W}_K^{(h)}, \quad \mathbf{V}^{(h)} = \tilde{\mathbf{H}}^{(\ell)} \mathbf{W}_V^{(h)} \quad (310)$$

$$2575 \quad \alpha_{ij}^{(h)} = \text{softmax}_j \left( \frac{\mathbf{Q}_i^{(h)} (\mathbf{K}_j^{(h)})^\top}{\sqrt{d_k}} \right) \quad (311)$$

$$2577 \quad \mathbf{Z}^{(h)} = \alpha^{(h)} \mathbf{V}^{(h)} \quad (312)$$

$$2578 \quad \mathbf{H}^{(\ell+1)} = \text{FF}(\mathbf{H}^{(\ell)} + \text{MHA}(\tilde{\mathbf{H}}^{(\ell)})) \quad (313)$$

2579 Graph Transformer variant using learned Laplacian spectral positional encodings (LPE) added  
 2580 to node features.

2581 If  $\mathbf{H}$  is permuted, the transformation of the Laplacian spectral positioning architecture to induce  
 2582 a permutation of the input features that is consistent with the learned encoding.

$$2583 \quad \tilde{\mathbf{H}}^{(\ell)}\boldsymbol{\pi} = \mathbf{H}^{(\ell)}\boldsymbol{\pi} + \mathbf{S}\boldsymbol{\pi} \quad (314)$$

2584 **(4) Exphormer (Shirzad et al., 2023):** The changes here pertain to the expander graph and the  
 2585 global virtual nodes. As these can be regarded as structural changes to the graph before applying  
 2586 the graph transformer, we can take the same transformations as the graph transformer.

2587 **(5) NodeFormer (Wu et al., 2023):** Notably, the modification over the base graph transformer is  
 2588 related to the computation of the attention. As the above outlined transformation ensures that  
 2589 the QK  $\mathbf{W}\mathbf{x} \mapsto \mathbf{W}\boldsymbol{\pi}_2^\top \boldsymbol{\pi}_2 \mathbf{x} = \mathbf{W}\mathbf{x}$  is invariant, the same transformation also holds for the  
 2590 NodeFormer.

2591 **(6) Gophormer (Zhao et al., 2021):** The proximity score term in the attention can be seen as a  
 2592 structural bias that is not affected by the permutations along the embedding dimension. Once

again, by transforming the  $\mathbf{W}_Q, \mathbf{W}_K, \mathbf{W}_V$  matrices accordingly, we ensure that the same transformations as the graph transformer follow.

$$\mathbf{Q}^{(h)} = \mathbf{H}^{(\ell)} \mathbf{W}_Q^{(h)}, \quad \mathbf{K}^{(h)} = \mathbf{H}^{(\ell)} \mathbf{W}_K^{(h)}, \quad \mathbf{V}^{(h)} = \mathbf{H}^{(\ell)} \mathbf{W}_V^{(h)} \quad (315)$$

$$\alpha_{uv}^{(h)} = \text{softmax}_{v \in \mathcal{S}_i} \left( \frac{\mathbf{Q}_u^{(h)} (\mathbf{K}_v^{(h)})^\top}{\sqrt{d_k}} + b^{\text{prox}}(u, v) \right) \quad (316)$$

$$Z_u^{(h)} = \sum_{v \in \mathcal{S}_i} \alpha_{uv}^{(h)} V_v^{(h)} \quad (317)$$

$$\mathbf{H}_{\mathcal{S}_i}^{(\ell+1)} = \text{FF}(\mathbf{H}_{\mathcal{S}_i}^{(\ell)} + \text{MHA}(\mathbf{H}_{\mathcal{S}_i}^{(\ell)})) \quad (318)$$

(7) **SpecFormer** (Bo et al., 2023): This extracts spectral information from the attention. Once again, by transforming the  $\mathbf{W}_Q, \mathbf{W}_K, \mathbf{W}_V$  matrices accordingly, we ensure that the same attention scores. A permutation can also be induced in the MLP FF. Then by additionally permuting  $\mathbf{W}_x$  accordingly, we can ensure that the output is permuted by  $\pi_1$ .

### F.3 SET-BASED NEURAL NETWORK

**DeepSets** (Zaheer et al., 2017):

$$\mathbf{y} = \rho \left( \sum_{i=1}^n \phi(\mathbf{x}_i) \right) \quad (319)$$

$\phi$  encodes elements,  $\rho$  decodes aggregated representation.

It is sufficient that (1) a permutation can be induced in  $\rho$ , such as if  $\rho$  is an MLP or any other admissible architecture. (2) if  $\rho$  is permutation equivariant (such as a sum) and  $\phi$  admits a permutation inducing transformation.

**Set Transformer** (Lee et al., 2019):

$$\mathbf{Y} = \text{ISAB}(\mathbf{X}) = \text{MAB}(\mathbf{X}, \text{MAB}(\mathbf{I}, \mathbf{X})) \quad (320)$$

where

$$\text{MAB}(\mathbf{Q}, \mathbf{K}) = \text{LayerNorm}(\mathbf{H} + \text{FF}(\mathbf{H})) \quad (321)$$

$$\mathbf{H} = \text{LayerNorm}(\mathbf{Q} + \text{MHA}(\mathbf{Q}, \mathbf{K}, \mathbf{K})) \quad (322)$$

The Set Transformer uses Multihead Attention Blocks (MAB), Set Attention Blocks (SAB), Induced Set Attention Blocks (ISAB), and Pooling by Multihead Attention (PMA) blocks. The encoder consists of two ISAB blocks, and the decoder consists of an SAB block followed by a PMA block.

$$\text{Enc}(\mathbf{X}) = \text{ISAB}_m(\text{ISAB}_m(\mathbf{X})) \quad (323)$$

$$\text{Decoder}(\mathbf{Z}) = \text{FF}(\text{SAB}(\text{PMA}_k(\mathbf{Z}))) \quad (324)$$

**$\pi$ -inducing transformation** For the final output:  $\Gamma_\pi^{(\text{FF})}(\Theta^{(\text{FF})}) = \Theta^{(\text{FF})}\pi$ .

For intermediate layers:

$$\Gamma_\pi^{(0, \text{PMA})}(\Theta) = \Theta\pi \quad \Gamma_\pi^{(2, \text{PMA})}(\Theta) = \pi^\top \Theta\pi \quad (325)$$

$$\Gamma_\pi^{((Q, i), \text{PMA})}(\Theta) = \pi^\top \Theta \quad \Gamma_\pi^{(4, \text{PMA})}(\Theta) = \Theta\pi \quad (326)$$

$$\Gamma_\pi^{(1, \text{SAB})}(\Theta) = \pi^\top \Theta\pi \quad \Gamma_\pi^{(3, \text{SAB})}(\Theta) = \Theta\pi \quad (327)$$

$$\Gamma_\pi^{((Q, i), \text{SAB})}(\Theta) = \pi^\top \Theta \quad \Gamma_\pi^{((K, i), \text{SAB})}(\Theta) = \pi^\top \Theta \quad \Gamma_\pi^{((V, i), \text{SAB})}(\Theta) = \pi^\top \Theta \quad (328)$$

It uses Induced Set Attention Blocks (ISAB) with learnable inducing points  $\mathbf{I}$  for efficient  $O(nm)$  complexity vs  $O(n^2)$ .

2646 **G ADDITIONAL DETAILS ABOUT EXPERIMENTS**  
26472648 **G.1 DATASETS**  
2649

2650 We build retrieval datasets from four benchmarks in the TU Graph Dataset collection (Morris et al.,  
2651 2020): ptc-fr, ptc-fm, cox2, and ptc-mr. Each dataset contains 500 queries and a corpus of  
2652 100,000 graphs, following the setup in (Roy et al., 2022; Lou et al., 2020). To sample graphs, we  
2653 adopt the BFS-based extraction strategy introduced in (Lou et al., 2020): starting from a randomly  
2654 chosen node, a BFS traversal is performed until the induced subgraph spans between 5 and 25 nodes.  
2655 This method is applied independently to construct both query and corpus graphs.

2656 For **subgraph matching (SM)**, binary relevance labels are generated using the VF2 subgraph  
2657 isomorphism algorithm (Hagberg et al., 2020). A corpus graph  $G_c$  is marked relevant to a query  $G_q$   
2658 if  $G_q$  is a subgraph of  $G_c$ , i.e.,  $\text{rel}(G_c, G_q) = \llbracket G_q \subset G_c \rrbracket$ , where  $\llbracket \cdot \rrbracket$  denotes the indicator function.

2659 For **graph edit distance (GED)**, we use the GEDLIB solver (Blumenthal et al., 2019), setting  
2660 insertion cost  $e_{\oplus} = 1$  and deletion cost  $e_{\ominus} = 2$ . Relevance is determined by thresholding the  
2661 computed GED:  $\text{rel}(G_c, G_q) = \llbracket \text{GED}(G_c, G_q) \leq \text{Thrs} \rrbracket$ , for a fixed threshold Thrs. Results under  
2662 a symmetric cost setting (Eq. cost GED) with  $e_{\oplus} = e_{\ominus} = 1$  are also reported in Appendix.

2663 For all datasets, we partition the 500 queries into 60% train, 20% validation, and 20% test splits.  
2664 Dataset statistics for the subgraph matching and GED tasks are summarized in Table 6 and Table 7,  
2665 respectively.

2666 Table 6: Graph statistics for each dataset generated for Subgraph Matching (SM).  
2667

Dataset	Query Graphs		Corpus Graphs		$E[\frac{ y=1 }{ y=0 }]$
	Nodes (min / max / avg)	Edges (min / max / avg)	Nodes (min / max / avg)	Edges (min / max / avg)	
<b>PTC-FR</b>	(6 / 15 / 12.65)	(6 / 15 / 12.41)	(16 / 25 / 18.68)	(15 / 28 / 20.17)	0.13
<b>PTC-FM</b>	(7 / 15 / 12.58)	(7 / 15 / 12.35)	(16 / 25 / 18.70)	(15 / 28 / 20.14)	0.12
<b>COX2</b>	(6 / 15 / 13.21)	(6 / 16 / 12.82)	(16 / 25 / 19.65)	(15 / 26 / 20.24)	0.12
<b>PTC-MR</b>	(6 / 15 / 12.66)	(7 / 15 / 12.41)	(16 / 25 / 18.72)	(15 / 28 / 20.18)	0.12

2668 Table 7: Graph statistics for each dataset generated for GED.  
2669

Dataset	Query Graphs		Corpus Graphs		$E[\frac{ y=1 }{ y=0 }]$
	Nodes (min / max / avg)	Edges (min / max / avg)	Nodes (min / max / avg)	Edges (min / max / avg)	
<b>PTC-FR</b>	(9 / 14 / 11.14)	(8 / 16 / 12.25)	(6 / 20 / 14.66)	(5 / 24 / 15.77)	0.07
<b>PTC-FM</b>	(9 / 14 / 11.09)	(8 / 15 / 12.08)	(6 / 20 / 14.64)	(5 / 24 / 15.73)	0.07
<b>COX2</b>	(9 / 15 / 11.61)	(8 / 17 / 12.90)	(7 / 20 / 15.48)	(6 / 20 / 15.79)	0.04
<b>PTC-MR</b>	(9 / 14 / 10.90)	(8 / 15 / 11.71)	(6 / 20 / 14.67)	(5 / 24 / 15.80)	0.08

2687 **G.2 EMBEDDING MODEL ARCHITECTURE**  
2688

2689 To supervise retrieval with transport-based distances, we train a neural scoring model composed of  
2690 a GNN encoder and a Gumbel-Sinkhorn aligner, optimized using pairwise ranking loss (Roy et al.,  
2691 2022; Jain et al., 2024). Here,  $\text{init}_{\theta}$  is an LRL implemented as a single-layer MLP that maps node  
2692 features to a 10-dimensional embedding space.  $\text{msg}_{\theta}$  is a message passing block consisting of two  
2693 linear message functions (forward and reverse), each mapping concatenated node-edge features to a  
2694 20-dimensional hidden state, followed by a GRU with hidden size 10 to aggregate incoming messages.  
2695  $\text{upd}_{\theta}$  is a two-layer aggregation MLP: the first layer expands the node embedding to 20 dimensions,  
2696 and the second reduces it back to 10 dimensions to produce the final node representation. To compute  
2697 the permutation matrix  $P$ , we solve a linear assignment problem via 10 Sinkhorn iterations at a  
2698 temperature of 0.1.

2699 Separate models are trained for each supervision type—Subgraph Matching (SM) and Graph Edit  
2700 Distance (GED)—based on their respective distance formulations using Eq. (1). The model is trained

2700 to assign lower distance scores to relevant corpus graphs compared to irrelevant ones, using the  
 2701 following hinge-based loss:

$$2702 \quad \sum_q \sum_{\substack{c: \text{rel}(G_c, G_q) = 1 \\ c': \text{rel}(G_{c'}, G_q) = 0}} [\Delta(G_c, G_q) - \Delta(G_{c'}, G_q) + \gamma]_+,$$

2703 where  $\gamma \in \{0.1, 0.5\}$  is a fixed margin, and  $\Delta(\cdot, \cdot)$  is the transport-based distance (Eq. (1)). We set  
 2704 the node embedding dimensionality to  $D = 10$  in all experiments.

### 2705 G.3 FOURIER-MAP AND HASHCODE TRAINING

2706 We adopt the training framework proposed by Roy et al. (2023) to improve the quality of Fourier-  
 2707 based representations and optimize the hashcodes derived from them. Specifically, we apply two  
 2708 neural networks  $\Psi_q$  and  $\Psi_c$  that take as input the Fourier representations  $\widehat{\mathbf{T}}_{q,d}$  and  $\widehat{\mathbf{T}}_{c,d}$  of query and  
 2709 corpus graphs respectively, and output transformed feature vectors:

$$2710 \quad \mathbf{z}_q = \Psi_q(\widehat{\mathbf{T}}_{q,d}), \quad \mathbf{z}_c = \Psi_c(\widehat{\mathbf{T}}_{c,d}). \quad (329)$$

2711 These transformed vectors are trained using a binary cross-entropy loss that promotes high cosine  
 2712 similarity between relevant query-corpus pairs:

$$2713 \quad \min_{\phi_q, \phi_c} \sum_{(G_q, G_c)} -\text{rel}(G_c, G_q) \log(1 + \cos(\mathbf{z}_q, \mathbf{z}_c)) - (1 - \text{rel}(G_c, G_q)) \log(1 - \cos(\mathbf{z}_q, \mathbf{z}_c)). \quad (330)$$

2714 To generate binary hashcodes from the transformed fourier feature vectors, we use a learned projection  
 2715 matrix  $\mathbf{W} \in \mathbb{R}^{\text{dim}_h \times \text{dim}_T}$  and apply the random hyperplane method:

$$2716 \quad f^{(d)}(G_q) = \text{sign}(\mathbf{W}\mathbf{z}_q), \quad h^{(d)}(G_c) = \text{sign}(\mathbf{W}\mathbf{z}_c). \quad (331)$$

2717 for each  $d \in [D] = [10]$ . In practice  $\text{dim}_T = 10$ ,  $\text{dim}_h = 64$ . We set the number of  $\omega$  samples  
 2718  $M = 10$ . We use the frequency cutoff  $\lambda$  in the low pass filter as 100. During training, we use  
 2719  $\tanh(\mathbf{W}\mathbf{z})$  as a differentiable approximation to  $\text{sign}(\mathbf{W}\mathbf{z})$ , and optimize  $\mathbf{W}$  using the following  
 2720 composite loss:

$$2721 \quad \mathcal{L}_{\text{hash}} = \lambda_1 \Delta_1 + \lambda_2 \mu_2 + \lambda_3 \mu_3, \quad (332)$$

2722 where:

- 2723 • **Collision Minimizer** — Encourages higher hashcode overlap between  $G_q$  and its most  
 2724 relevant corpus graphs compared to irrelevant ones.
- 2725 • **Fence-Sitting Penalty** — Penalizes intermediate values of  $\tanh(\mathbf{W}\mathbf{z})$  to enforce hash  
 2726 bits near  $\pm 1$ .
- 2727 • **Bit Balance** — Promotes equal usage of  $+1$  and  $-1$  bits across all corpus hashcodes.

2728 We use the default hyperparameters and network configurations proposed in FourierHashNet (Roy  
 2729 et al., 2023) for  $\Psi_q$ ,  $\Psi_c$ , and the loss weights  $\mu_i$ .

2730 This training process improves both retrieval relevance and the discriminability of learned hashcodes.  
 2731 Algorithm 1 and 2 summarize the index construction and query retrieval procedures based on these  
 2732 learned hashcodes.

### 2733 G.4 BASELINES

2734 We compare GRAPHHASH against a range of methods that fall into three broad categories: LSH-based  
 2735 methods operating on single-vector graph embeddings, inverted index-based multi-vector retrieval  
 2736 using FAISS, and graph-based ANN using DiskANN. We also include a naive random sampling  
 2737 baseline for reference.

2738 **Hyperplane based hashing** These methods rely on locality-sensitive hashing (LSH) applied to a  
 2739 single-vector embedding for each graph, typically obtained via mean pooling over node representa-  
 2740 tions.

- 2741 • **FourierHashNet** (Roy et al., 2023): A learned LSH scheme that approximates hinge-based  
 2742 dominance distances through Fourier transformation. It encodes asymmetric containment-style  
 2743 similarities in a form suitable for efficient hash-based retrieval using random hyperplanes in the  
 2744 frequency domain. We use the default hyperparameters and network configurations proposed  
 2745 in FourierHashNet (Roy et al., 2023). Specifically, we use  $\omega = 10$  samples for the Fourier  
 2746 features, a trainable Fourier map optimized using the BCE loss with embedding dimension 10, and

2754 hashcodes of length 64. We train using the loss function defined in Eq. (332), sweeping across  
 2755 all combinations of  $\lambda$  and other hyperparameters as described in their original paper. To evaluate  
 2756 efficiency–effectiveness tradeoffs, we vary the number of hash table buckets from  $2^1$  to  $2^{60}$  during  
 2757 retrieval.

2758 • **Random Hyperplane (RH) Hashing:** A classical LSH method that applies cosine similarity  
 2759 hashing to mean-pooled graph vectors. Since it uses symmetric cosine distance, it does not capture  
 2760 subgraph asymmetry or node-level structure. We train the baseline using the same loss function as  
 2761 in FourierHashNet (Eq. (332)), sweeping over all hyperparameter combinations reported in their  
 2762 work. The hashcode dimension is set to 64, and we vary the number of selected hyperplanes (i.e.,  
 2763 the subset size) from  $2^1$  to  $2^{60}$  to generate the tradeoff curves.

2764 **Inverted Index (IVF)** We implement the inverted file index from FAISS (Douze et al., 2024) in  
 2765 a multi-vector setup, where each corpus graph is decomposed into its node embeddings. These are  
 2766 indexed independently, and during retrieval, each query node probes the index. Retrieved nodes are  
 2767 then aggregated by graph ID to form the candidate set. This simulates node-level matching using  
 2768 learned dense vectors.

2769 For the FAISS baseline, we use the IVF-Flat indexing scheme with `nlist` = 128 clusters. The index  
 2770 is built over node-level embeddings extracted from the corpus graphs. Depending on the specified  
 2771 distance metric (`cosine` or `l2`), we use either inner product similarity or Euclidean distance. For  
 2772 cosine similarity, all corpus embeddings are L2-normalized prior to indexing.

2773 **Graph-Based ANN (DiskANN)** DiskANN (Simhadri et al., 2023) builds compact HNSW-style  
 2774 proximity graphs for approximate nearest neighbor retrieval at scale. In our setting, each node  
 2775 embedding from the corpus is indexed independently, and the query node embeddings probe this  
 2776 graph. Retrieved node hits are aggregated to rank corpus graphs. DiskANN offers scalability and  
 2777 fast retrieval, but operates with symmetric distances (e.g.,  $L_2$ , cosine) which may not align well with  
 2778 asymmetric retrieval objectives.

2779 We employ the `StaticMemoryIndex` implementation with cosine or Euclidean distance as the retrieval  
 2780 metric. The memory-based index is built using a graph degree of 16, build-time complexity of 32, and  
 2781 a search-time initial complexity of  $2^{21}$ . We disable product quantization (PQ) and OPQ refinements  
 2782 by setting `use_pq_build=False` and `use_opq=False`, respectively, opting for full-precision vectors.  
 2783 During index construction, we set `alpha=1.2` and `filter_complexity=32`, with multi-threading enabled  
 2784 using 16 threads. We vary the top- $K$  parameter during querying to generate the efficiency–accuracy  
 2785 tradeoff plots.

2786 **Random Sampling** This baseline selects a fixed number of graphs uniformly at random from the  
 2787 corpus, without using any learned embeddings or indexing structure. It serves as a lower-bound  
 2788 reference to contextualize retrieval performance. Here, we simulate retrieval by uniformly sampling a  
 2789 fixed number of corpus items for each query. We sweep over the number of retrieved items using  
 2790 the set:  $\{10, 100, 1000, 2000\} \cup \{5000, 10000, \dots, 95000\}$ , to generate efficiency–accuracy tradeoff  
 2791 curves.

## 2792 G.5 EVALUATION METRICS

2793 **MAP** To assess the trade-off between retrieval accuracy and candidate set size, we compute the  
 2794 Mean Average Precision (MAP). For a query graph  $G_q \in \mathcal{Q}$ , let  $\mathcal{C}_{q\oplus} \subseteq \mathcal{C}$  denote the set of relevant  
 2795 corpus graphs. Given a retrieved ranking  $\Pi_q$  over retrieved candidate set  $\mathcal{R}_q$ , the average precision  
 2796 (AP) is computed as:

$$2797 \text{AP}(G_q) = \frac{1}{|\mathcal{C}_{q\oplus}|} \sum_{r=1}^{|\Pi_q|} \text{Prec}@r \cdot \mathbb{I}[\Pi_q(r) \in \mathcal{C}_{q\oplus}],$$

2800 where  $\text{Prec}@r$  is the precision at rank  $r$ , and  $\mathbb{I}[\cdot]$  is the indicator function. We compute MAP by  
 2801 averaging AP across all test queries in  $\mathcal{Q}_{\text{test}}$ :

$$2802 \text{MAP} = \frac{1}{|\mathcal{Q}_{\text{test}}|} \sum_{G_q \in \mathcal{Q}_{\text{test}}} \text{AP}(G_q).$$

2803 This formulation penalizes high precision with low recall, ensuring models are rewarded only when  
 2804 most number of relevant items are retrieved with high retrieval accuracy.

2805 **AUC** To summarize the trade-off between accuracy and candidate set size, we convert the MAP  
 2806 vs. candidate set size curve into a single scalar metric by computing the area under the trade-curve.

2808 We normalize the candidate set size by the total corpus size  $|\mathcal{C}|$ , and numerically integrate the MAP  
 2809 values over the normalized x-axis.

2810 **Normalized Discounted Cumulative Gain (NDCG)** We also report NDCG to evaluate the quality  
 2811 of ranked lists. For each query  $G_q$ , let  $\text{rel}_q(r) \in \{0, 1\}$  denote the relevance label of the item ranked  
 2812 at position  $r$  in  $\Pi_q$ . The DCG at rank  $k$  is given by:

$$2813 \quad \text{DCG}@k = \sum_{r=1}^k \frac{2^{\text{rel}_q(r)} - 1}{\log_2(r + 1)},$$

2814 and the corresponding ideal DCG (IDCG) is computed from a perfect ranking. The NDCG is then:

$$2815 \quad \text{NDCG}@k = \frac{\text{DCG}@k}{\text{IDCG}@k}.$$

2816 We average NDCG over all test queries to obtain a corpus-level evaluation. This metric does not  
 2817 penalize high precision with low recall. We set  $k = 1000$ .

## 2818 G.6 HARDWARE AND LICENSES

2819 All experiments were run on a local NAS server configured with seven NVIDIA RTX A6000 GPUs  
 2820 (48GB each), a 96-core processor, and 20TB of storage, operating under Debian 6.1. All model  
 2821 components, including GNN encoders and hash function training, were executed on GPU memory  
 2822 without resource bottlenecks.

2823 Regarding licensing, GMN (Li et al., 2019) is distributed under the MIT license. The implementations  
 2824 of Isonet (Roy et al., 2022) and FourierHashNet (Roy et al., 2023) are open source and have been  
 2825 cited appropriately in our work. Our full codebase and datasets will be released for public use upon  
 2826 publication.

2827  
 2828  
 2829  
 2830  
 2831  
 2832  
 2833  
 2834  
 2835  
 2836  
 2837  
 2838  
 2839  
 2840  
 2841  
 2842  
 2843  
 2844  
 2845  
 2846  
 2847  
 2848  
 2849  
 2850  
 2851  
 2852  
 2853  
 2854  
 2855  
 2856  
 2857  
 2858  
 2859  
 2860  
 2861

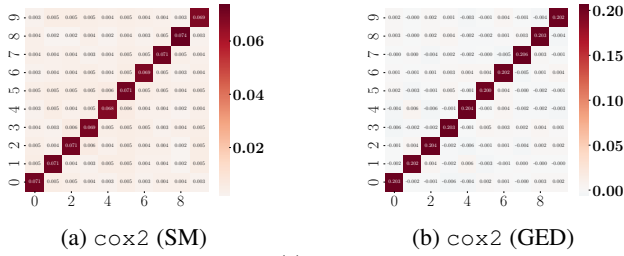
## 2862 H ADDITIONAL EXPERIMENTS

2863  
 2864 We present supplementary experimental results to support the findings in the main paper. These  
 2865 include validations of embedding exchangeability on additional datasets and evaluation of retrieval  
 2866 performance under alternate metrics and supervision settings. Our goal is to assess whether the trends  
 2867 observed in the main experiments persist across diverse configurations.

### 2868 H.1 ADDITIONAL EXCHANGEABILITY RESULTS

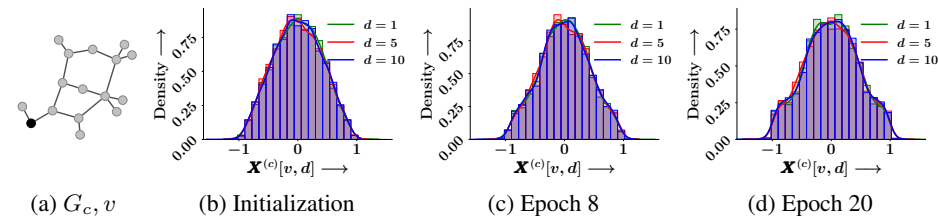
2869 The following experiments reuse the same setup as before: 5,000 GNNs are trained independently on  
 2870 a subset of 1,024 query-corpus graph pairs, each with  $D = 10$  embedding dimensions, and trained  
 2871 for 20 epochs using a pairwise ranking loss. For a fixed node in one corpus graph, we collect the  
 2872 scalar embedding values across dimensions  $d \in [D]$  from all models.

2873 **Covariance of Node embeddings** Another consequence of exchangeability is the symmetry of  
 2874 higher order moments of the embedding. Specifically, we expect the covariance between two  
 2875 dimensions to remain constant across all pairs of dimensions, which is a stronger demonstration of  
 2876 symmetry in the joint distribution.



2877  
 2878 Figure 8: Sample covariance matrix for the  $\mathbf{X}^{(c)}[v, d]$  for the highlighted nodes in Figures 1, 9. The  
 2879 figure shows that the off-diagonal covariances are roughly, which strongly indicates that the coupling  
 2880 between dimensions is symmetric.

2881 Figure 8 shows the covariance matrices for two nodes from different graphs. The  $[i, j]^{th}$  entry of  
 2882 each matrix matrix represents the estimate for  $\text{Cov}(\mathbf{X}^{(c)}[v, i], \mathbf{X}^{(c)}[v, j])$ . We observe that all the  
 2883 off diagonal elements are close to one another, and similarly, all diagonal elements too are close to  
 2884 one another, which indicates that there is symmetry in the coupling between dimensions.



2885  
 2886 Figure 9: Empirical probability density of  $\mathbf{X}^{(c)}[v, d]$  for the highlighted node  $v$  in the example  
 2887 corpus graph  $G_c$  in ptc-fr, obtained using 5,000 independently trained instances of the GNN  
 2888 model under GED-based supervision. Panels (b)–(d) show the density of  $\mathbf{X}^{(c)}[v, d]$  at initialization  
 2889 and at intermediate stages of training. The observed similarity of distributions across embedding  
 2890 dimensions reaffirms the exchangeability result (Theorem 5) in a different dataset and task setting.

2891 **Marginal distributions on a different dataset** In Section 5.1, we validated the exchangeability  
 2892 of embedding dimensions by examining the marginal distributions of node embeddings across  
 2893 dimensions, under repeated training runs. Here, we present an additional experiment on a different  
 2894 dataset (PTC-FR) and a different supervision signal (GED with asymmetric costs), to confirm the  
 2895 generality of our claims. Figure 9 shows the distribution of  $\mathbf{X}^{(c)}[v, d]$  for three representative  
 2896 dimensions ( $d = 1, 5, 10$ ) at three points during training. Similar to the findings on cox2 (main  
 2897 paper), the distributions remain near-identical across dimensions and throughout training. This  
 2898 supports the robustness of Theorem 5, even under varied datasets and training objectives.

2899 **Remark.** For the distribution plots of node embeddings (Figure 1 and Figure 9), we use histograms  
 2900 with 25 bins and apply kernel density estimation for smoothing. These visualizations are generated  
 2901 using the built-in functionality of the seaborn library.

2916  
2917

## H.2 FURTHER EVALUATION OF GRAPHHASH'S RETRIEVAL PERFORMANCE

2918  
2919  
2920

In the main paper (Section 5.2), we evaluated GRAPHHASH under two supervision signals—Subgraph Matching (SM) and asymmetric GED—using conservative MAP as the primary evaluation metric. Here, we extend that analysis along two axes.

2921  
2922  
2923

First, we report additional results on a more commonly used GED variant, where both insertion and deletion costs are set to  $e_{\oplus} = e_{\ominus} = 1$ . This equal-cost GED setting alters the notion of relevance and allows us to assess the generality of our approach under a different supervision signal.

2924  
2925  
2926  
2927

Second, we evaluate retrieval performance using NDCG, a position-sensitive ranking metric that complements MAP. These additional results evaluate whether the trends observed in the main paper persist under both metric and supervision signal variations.

2928  
2929

## H.2.1 MAP ON EQUAL-COST GED

2930  
2931  
2932

In the main paper, we evaluated retrieval performance under asymmetric GED costs ( $e_{\oplus} = 1, e_{\ominus} = 2$ ). Here, we assess whether the key trends persist under the equal-cost variant where  $e_{\oplus} = e_{\ominus} = 1$ , a widely used formulation in the literature.

2933  
2934

Figure 10 shows the MAP vs. retrieved graphs trade-off curves for all baselines under equal-cost GED supervision. We summarize our observations below:

2935  
2936  
2937

1. **GRAPHHASH and FourierHashNet remain the strongest performers across all datasets.** Even under equal-cost supervision, both methods consistently outperform other baselines in MAP across retrieval budgets.

2938  
2939  
2940  
2941  
2942

2. **FourierHashNet shows marginal improvement in this regime**, particularly on `ptc-fm`, where it slightly surpasses GRAPHHASH, and on `cox2` and `ptc-mr`, where its MAP approaches that of GRAPHHASH at lower candidate counts. However, FourierHashNet often fails to span the full selectivity spectrum, unlike GRAPHHASH, which yields a smoother and more complete accuracy-efficiency trade-off.

2943  
2944  
2945  
2946  
2947

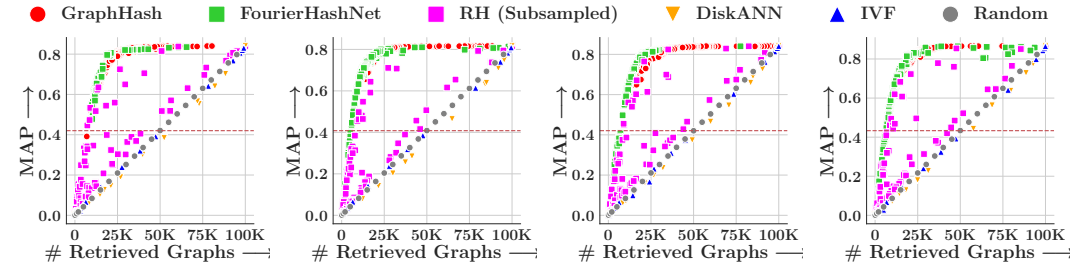
3. **RH Hashing remains unstable.** While it occasionally matches GRAPHHASH on `cox2` and `ptc-mr`, its high variance limits its practical utility.

4. **DiskANN, IVF, and Random sampling continue to underperform.** As in the asymmetric setting, these methods yield substantially lower MAP, highlighting the advantage of trainable indexing strategies like GRAPHHASH and FourierHashNet.

2948  
2949

These trends are consistent with our findings from the main paper and further validate the generality of GRAPHHASH across different supervision regimes.

2950

2951  
2952  
2953  
2954  
2955  
2956  
2957  
2958

(a) `ptc-fm` (Eq. cost GED) (b) `cox2` (Eq. cost GED) (c) `ptc-fm` (Eq. cost GED) (d) `ptc-mr` (Eq. cost GED)

2959  
2960  
2961  
2962  
2963  
2964  
2965  
2966  
2967  
2968  
2969

Figure 10: Trade-off between mean average precision (MAP) and number of retrieved graphs, for all the methods, *viz.*, GRAPHHASH, FourierHashNet (Roy et al., 2023), Random Hyperplane (RH) (Charikar, 2002; Indyk et al., 1997), IVF (Douze et al., 2024), DiskANN (Simhadri et al., 2023) and Random, across all datasets. Retrieval based on Equal cost GED ( $e_{\bullet} = 1$ ). Horizontal red line denotes 50% of exhaustive MAP. Our method shows a better trade-off than others in majority of the cases.

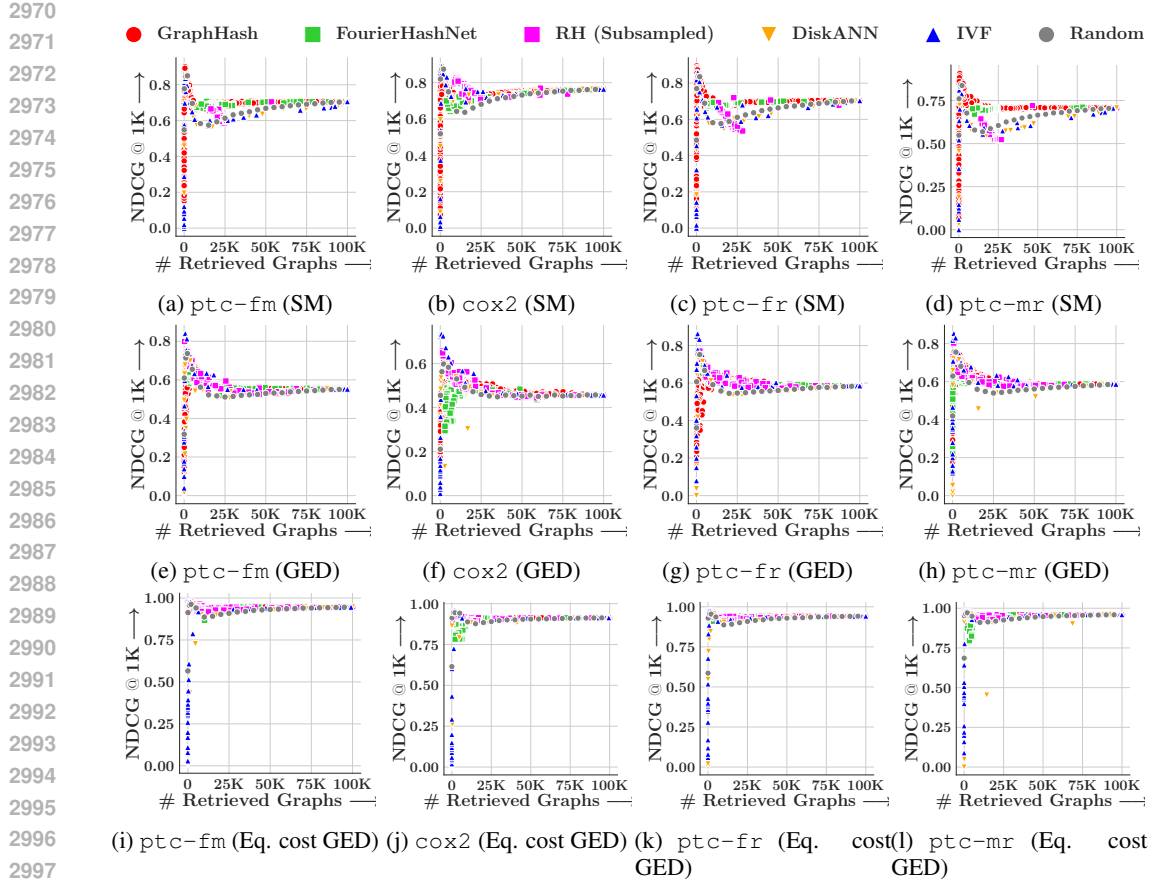


Figure 11: Trade-off between NDCG at top 1000 and number of retrieved graphs, for all the methods, *viz.*, GRAPHHASH, FourierHashNet (Roy et al., 2023), Random Hyperplane (RH) (Charikar, 2002; Indyk et al., 1997), IVF (Douze et al., 2024), DiskANN (Simhadri et al., 2023) and Random, across all datasets. Top row: Retrieval based on Subgraph Matching (SM); Middle row: Retrieval based on GED; Bottom row: Retrieval based on Equal cost GED ( $e_{\bullet} = 1$ ). Our method shows a better trade-off than others in majority of the cases.

## H.2.2 EVALUATION USING NDCG

To complement our MAP-based evaluation, we assess ranking quality using NDCG across all datasets and relevance definitions. Figure 11 reports results for Subgraph Matching, unequal-cost GED, and equal-cost GED.

1. **GRAPHHASH consistently achieves the highest or near-highest NDCG across all datasets and relevance settings.** This confirms that GRAPHHASH not only retrieves more relevant graphs overall, but also ranks them effectively near the top of the candidate list.
2. **Relative gains over baselines are smaller compared to MAP.** While GRAPHHASH leads in most cases, RH hashing performs competitively under unequal-cost GED, and nearly all baselines exhibit similar performance under equal-cost GED. This suggests that some methods manage to prioritize a few relevant graphs early, even if overall recall is limited.
3. **DiskANN and IVF show competitive NDCG despite low MAP.** These methods often retrieve a handful of highly relevant graphs early in the ranking, which boosts NDCG but fails to capture the full relevant set.
4. **Random sampling yields flat and significantly lower NDCG.** This reinforces the importance of structured indexing and learning-based methods for meaningful ranked retrieval.

Overall, NDCG results validate our MAP findings and demonstrate that GRAPHHASH excels at not just retrieving relevant graphs but also ranking them effectively within large candidate pools.

3024 H.2.3 CLARIFICATION ON RH (SUBSAMPLED)  
3025

3026 In Figure 4 of the main paper and Figures 10 and 11 in the appendix, we display retrieval performance  
 3027 as scatter plots, as described in Section 5.2. The label “RH (Subsampled)” in these figures refers to a  
 3028 subsampling of the full set of trade-off points obtained for the Random Hyperplane (RH) method.  
 3029 This subsampling was performed solely to prevent visual clutter and improve readability of the main  
 3030 figures.

3031 To ensure full transparency, Figures 12 and 13 present the complete set of RH performance points  
 3032 generated via a comprehensive hyperparameter sweep. Specifically, we vary the hash table size and  
 3033 the loss weights in Eq. (332), following the experimental protocol recommended in the FourierHash-  
 3034 Net (Roy et al., 2023). These figures show retrieval performance for all datasets across all three  
 3035 supervision signals (Subgraph Matching, GED, and Equal-cost GED), evaluated using both MAP  
 3036 and NDCG at top 1000.

3037 We make the following observations:

1. **Consistency with main trends:** Even with the full set of hyperparameter configurations, the qualitative findings from the earlier results remain consistent—GRAPHHASH outperforms RH on both MAP and NDCG for Subgraph Matching (SM), and also on MAP for GED. RH achieves comparable performance only on NDCG for GED, but remains less reliable overall.
2. **Pronounced variability:** With more points shown, the performance of RH appears highly scattered, especially at fixed retrieval sizes. This reinforces its sensitivity to hyperparameter selection.
3. **Practical tuning challenge:** The high variance observed for RH across sweeps suggests that achieving consistently strong performance would require extensive tuning, which may not be practical in real-world deployments.

3048

3049

3050

3051

3052

3053

3054

3055

3056

3057

3058

3059

3060

3061

3062

3063

3064

3065

3066

3067

3068

3069

3070

3071

3072

3073

3074

3075

3076

3077

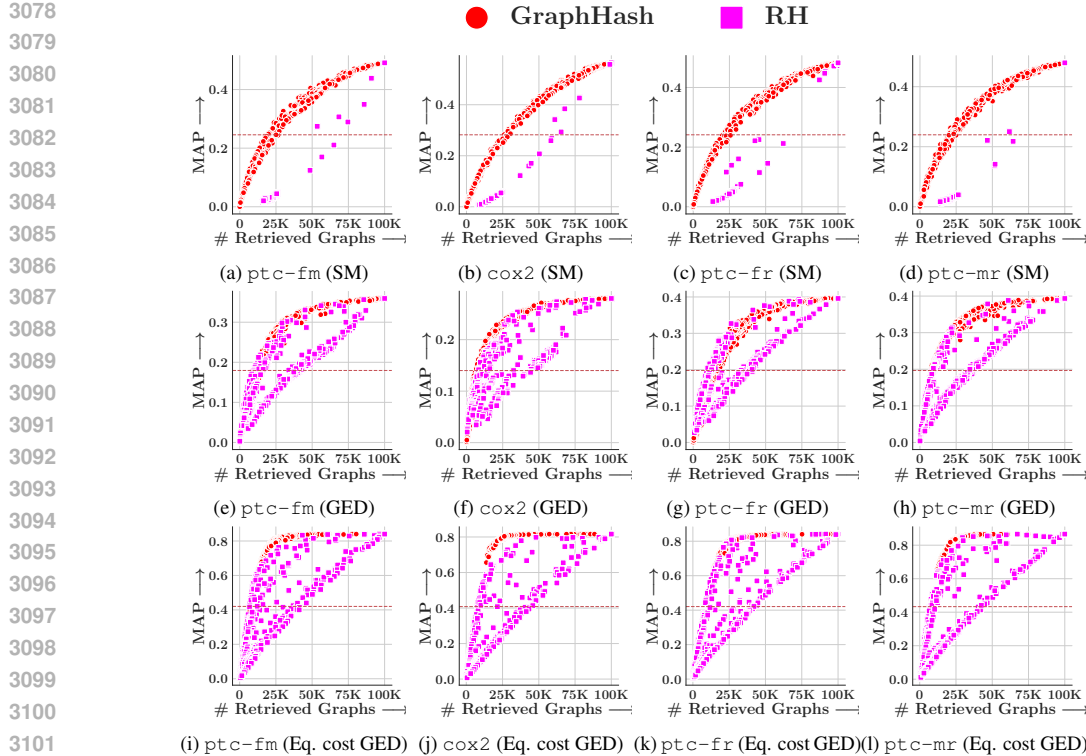


Figure 12: Trade-off between MAP and number of retrieved graphs taking all points. Top row: Subgraph Matching (SM); Middle row: GED; Bottom row: Equal cost GED ( $e_0 = 1$ ). Horizontal red line denotes 50% of exhaustive MAP.

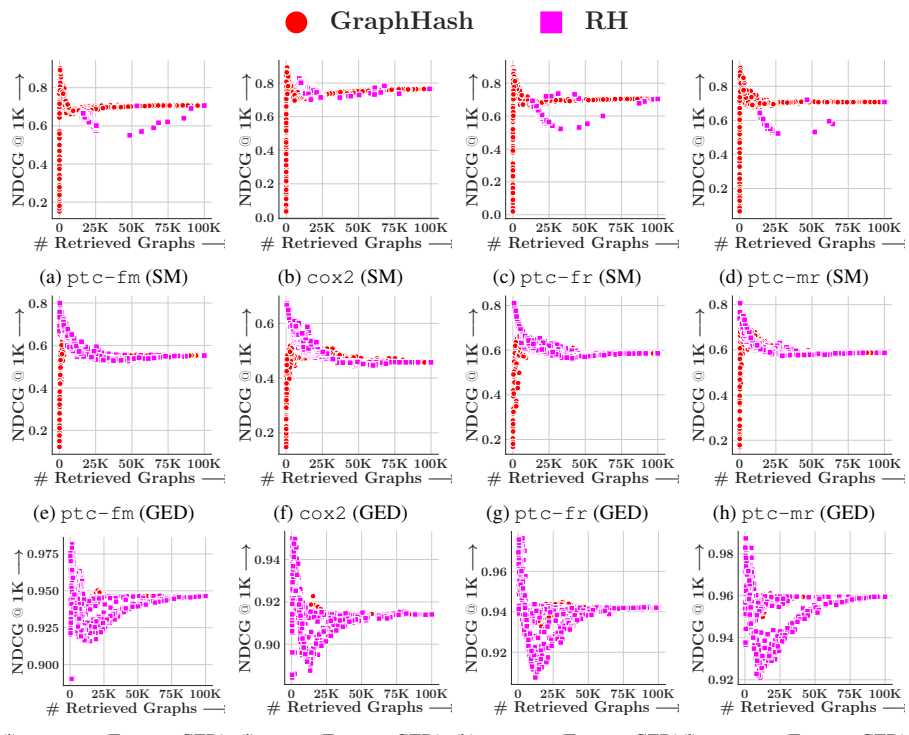
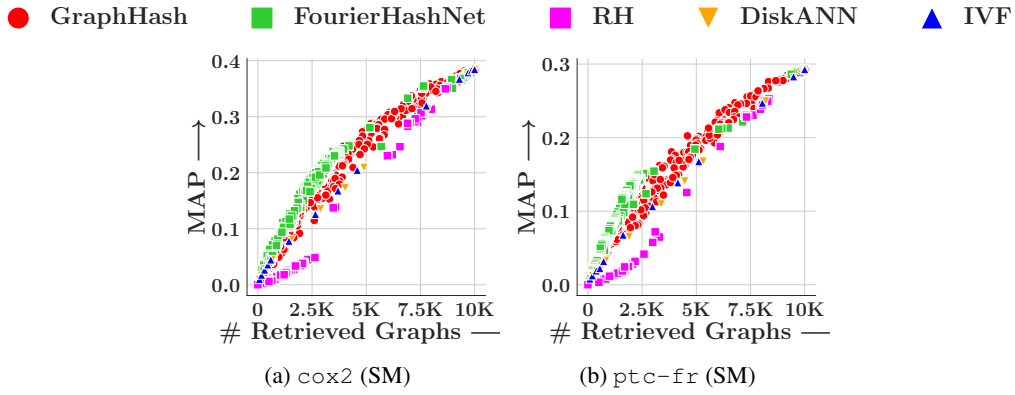


Figure 13: Trade-off between NDCG at 1000 and number of retrieved graphs taking all points. Top row: Subgraph Matching (SM); Middle row: GED; Bottom row: Equal cost GED ( $e_0 = 1$ ).

3132 H.2.4 EVALUATION ON LARGER GRAPHS  
3133

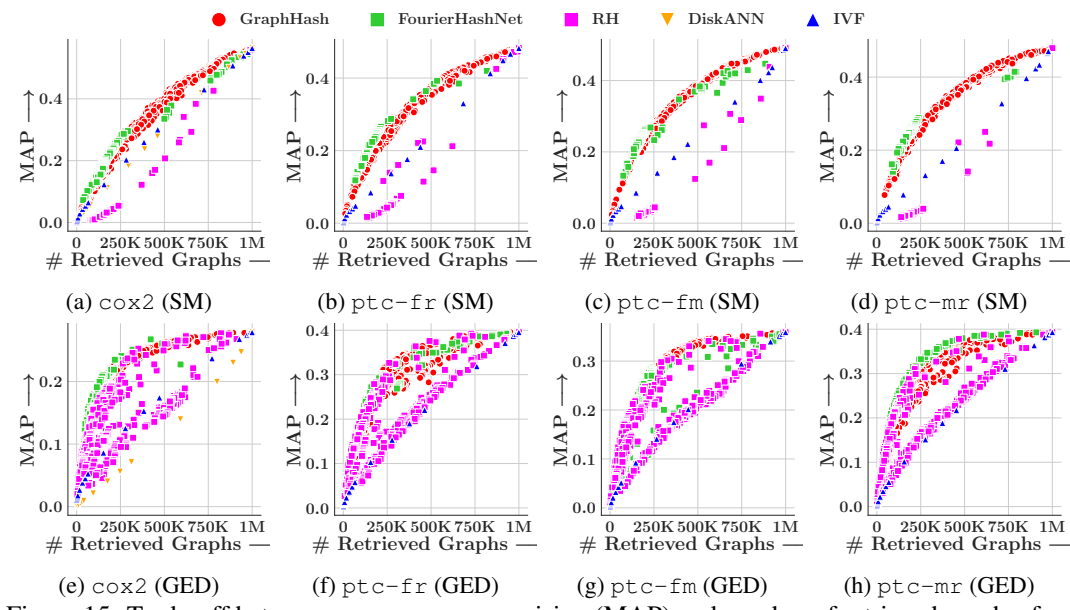
3134 We synthetically generate larger versions of `cox2` and `ptc-fr` by combining graphs in the original  
3135 datasets for the Subgraph Matching task. The gold relevance labels are approximated as the set of  
3136 graphs made up of relevant items of the original data. We generate  $10^4$  corpus items for either dataset,  
3137 and plot the tradeoff curves as in Figure 4. We observe that GRAPHHASH performs better than the  
3138 baselines in high accuracy regime



3152 Figure 14: Trade-off between mean average precision (MAP) of  
3153 GRAPHHASH, FourierHashNet (Roy et al., 2023), Random Hyperplane (RH) (Charikar, 2002; Indyk  
3154 et al., 1997), IVF (Douze et al., 2024) and DiskANN (Simhadri et al., 2023), across two datasets with  
3155 synthetically generated large graphs under Subgraph Matching supervision.  
3156

3157  
3158 H.2.5 EVALUATION ON LARGER CORPUS  
3159

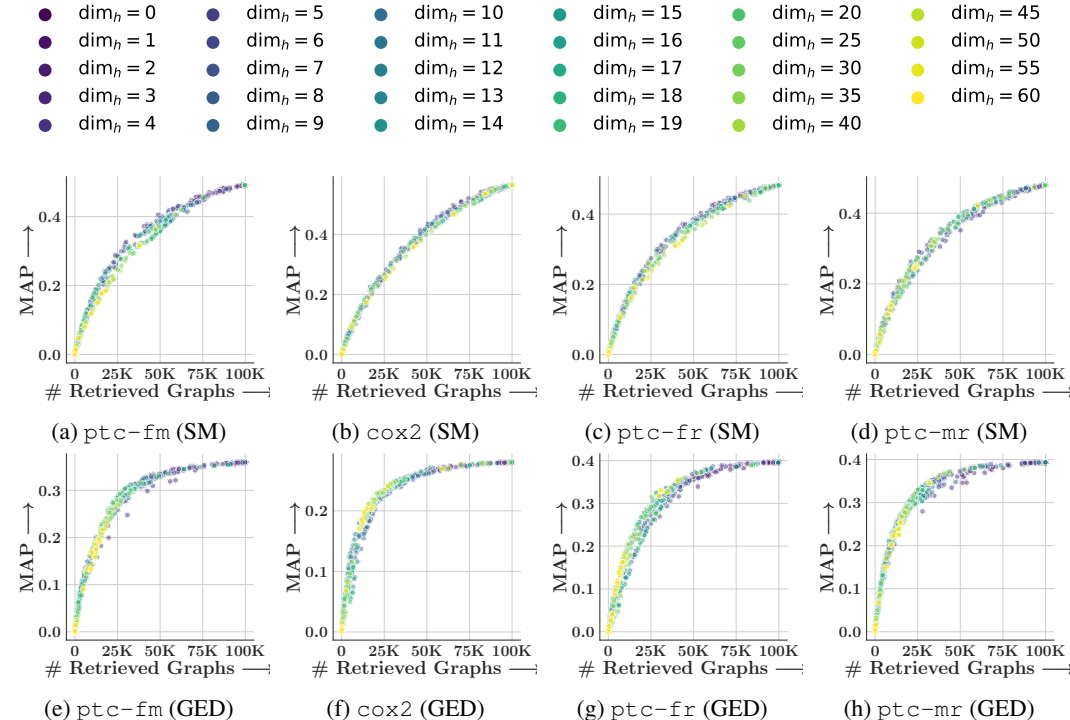
3160 In this set of experiments, we evaluate GRAPHHASH on a larger corpus of  $1M$  items.  
3161



3182 Figure 15: Trade-off between mean average precision (MAP) of  
3183 GRAPHHASH, FourierHashNet (Roy et al., 2023), Random Hyperplane (RH) (Charikar, 2002; Indyk  
3184 et al., 1997), IVF (Douze et al., 2024), and DiskANN (Simhadri et al., 2023) across all datasets for a  
3185 million sized corpus. Top row: Retrieval based on Subgraph Matching (SM); Bottom row: Retrieval  
based on GED

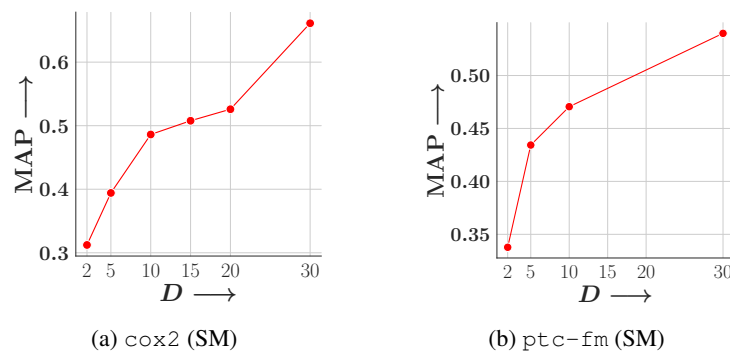
3186 H.2.6 ABLATION STUDIES  
3187

3188 **Ablation on  $\dim_h$**  Here, we present the trade-off curves for MAP versus number of retrieved  
3189 graphs for each choice of  $\dim_h$ , the size of the hashcode. The below tradeoff has been summarised  
3190 to Figure 5 in the main paper. Owing to the larger number of values of  $\dim_h$ , we use a colorscale for  
3191 the scatterplot.



3207 Figure 16: Trade-off between mean average precision (MAP) and number of retrieved graphs, for  
3208 GRAPHHASH for different values of the hashcode size  $\dim_h$

3209 **Ablation with  $D$**  Here, we perform experiments ablating the embedding dimension of the network,  
3210 and the number of hash tables used.

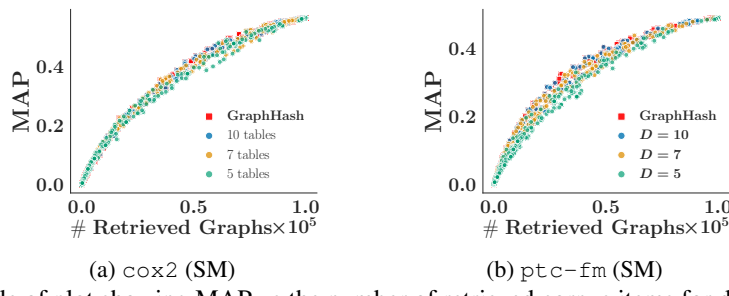


3211 Figure 17: The exhaustive MAP achieved by an embedding model trained on the node aligned loss  
3212 with respect to the embedding dimension of the model.

3213 We see that MAP increases monotonically with  $D$ , as is expected as the higher dimension allows for  
3214 richer feature representation without hitting the bottleneck in training requirements.

3215 **Ablation with number of hash tables** We also perform ablation over the number of hash tables.  
3216 Note that for GRAPHHASH the number of hash tables corresponds to the number of dimensions of

3240  
3241 the embedding utilised, which implies a monotone behavior in the performance. We seek to find if  
3242 the accuracy losses are comparatively low, which could help cut time and memory.  
3243



3244  
3245 Figure 18: Trade of plot showing MAP vs the number of retrieved corpus items for different variants  
3246 of GRAPHHASH that uses a different number of hash tables for retrieving results.  
3247

3248 We observe that the drop in performance is not too significant from 10 to 7, although it is noticeable  
3249 for 5. Ultimately, this vindicates our decision to use all 10 hash tables  
3250

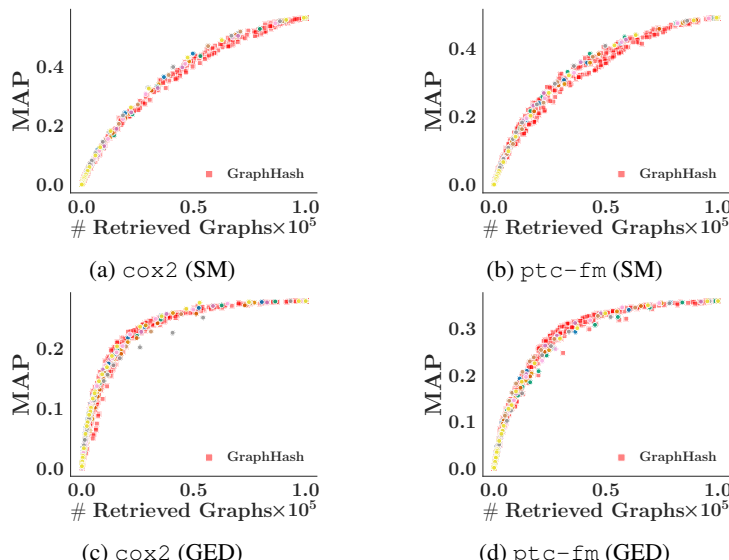
3251 **Stability of random hyperplane seeding** Next, we evaluate the stability of the random hyperplane  
3252 hashing scheme over multiple random seeds. In this setting, we set 10 different random seeds for  
3253 the hyperplanes, keeping the embeddings and fourier maps fixed. We then evaluate the retrieval  
3254 performance on the best hyperparameters found from GRAPHHASH.  
3255

3256 We report the mean and standard deviation in AUC over these 10 runs.  
3257

Dataset (Task)	Mean AUC	Std
ptc-fm (SM)	0.342685	0.006966
cox2 (SM)	0.369972	0.009179
ptc-fm (GED)	0.289546	0.007598
cox2 (GED)	0.238293	0.005878

3258 Table 19: Mean and standard deviation of AUC over 10 different random seeds for RH seeding.  
3259

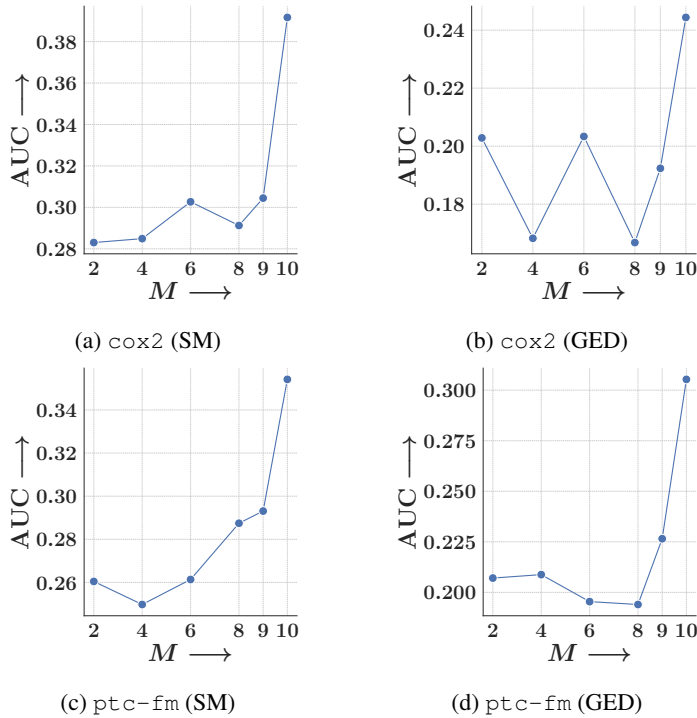
3260 We also plot the tradeoff curves for the different random seeds, contrasting their performance with  
3261 the final version of GRAPHHASH. Each color denotes a different seed.  
3262



3263 Figure 20: Tradeoff curves comparing GRAPHHASH (red) with different random seeds for Random  
3264 Hyperplane hashing across both tasks on cox2 and ptc-fm. Each color denotes a different seed.  
3265

3294 We observe that the variation in performance between different seeds is very minimal, as the different  
 3295 values coincide with the tradeoff trajectory of the best performing hyperparameters of GRAPHHASH.  
 3296

3297 **Stability of fourier map dimension  $\dim_T$**  We also ablate over the size of the fourier representation  
 3298  $\dim_T$ . In our formulation, we have reparameterized  $\dim_T = 4nM$ , where  $n$  is the size of the graphs.  
 3299 In our experiment we ablate over  $M$ .



3300  
 3301  
 3302  
 3303  
 3304  
 3305  
 3306  
 3307  
 3308  
 3309  
 3310  
 3311  
 3312  
 3313  
 3314  
 3315  
 3316  
 3317  
 3318  
 3319  
 3320  
 3321  
 3322  
 3323  
 3324  
 3325  
 3326  
 3327  
 3328  
 3329  
 3330  
 3331  
 3332  
 3333  
 3334  
 3335  
 3336  
 3337  
 3338  
 3339  
 3340  
 3341  
 3342  
 3343  
 3344  
 3345  
 3346  
 3347  
 Figure 21: Comparison of AUC of the MAP vs retrieval ratio curve for different values of the per-dimension-fourier frequencies  $M$ , across two datasets on both tasks.

3325 We compare the AUC generated by the tradeoff curve generated for each value of  $M$ . We observe a  
 3326 sharp decline in the performance when going down from 10 fourier frequencies per dimension.  
 3327

3348  
3349H.2.7 COMPARISON OF sim AND  $\text{sim}_d$ 3350  
3351  
3352  
3353

**Direct comparison of sim vs.  $\text{sim}_d$**  We compare the quality of the approximation by plotting the scatter plots of the scores obtained by sim and  $\text{sim}_d$  for all the datasets and tasks. Specifically, we compare the mean 1D score, *i.e.*  $\frac{1}{D} \sum_{i=1}^D \text{sim}_d^{(i)}$  against the true score sim scaled by  $\frac{1}{D}$ . For each  $G_c, G_q$  pair in the test set, we compute these two values and plot them.

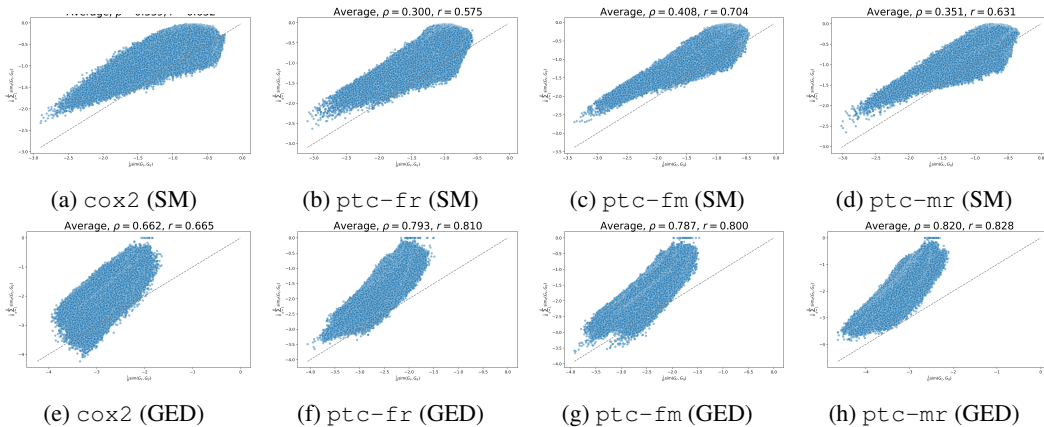
3354  
3355  
3356  
3357  
3358  
33593360  
3361  
3362  
3363  
3364  
3365  
3366

Figure 22: Scatter plots comparing the mean 1D similarity scores (y-axis) with the true similarity scores (x-axis) computed with sinkhorn iterations, for the (top) Subgraph Matching and (bottom) Graph Edit Distance task across different datasets.

3371  
3372  
3373  
3374  
3375

**Decay of  $|\text{sim}_d(G_c, G_q) - \text{sim}(G_c, G_q)|$  with increasing  $D$**  Next, we empirically validate the concentration result from Proposition 7 by plotting the average absolute error  $|\text{sim}_d(G_c, G_q) - \text{sim}(G_c, G_q)|$  over all pairs  $(G_c, G_q)$  in the test set as a function of  $D$ . We note that the deviation decreases with increasing  $D$ , confirming the result.

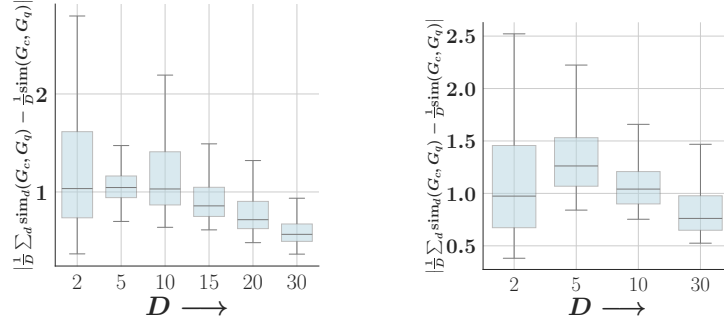
3376  
3377  
3378  
3379  
3380  
3381  
3382  
3383  
3384  
33853386  
3387  
3388  
3389

Figure 23: Boxplot of average absolute error  $|\frac{1}{D} \sum_d \text{sim}_d(G_c, G_q) - \frac{1}{D} \text{sim}(G_c, G_q)|$  as a function of  $D$  for the Subgraph Matching task on different datasets.

3390  
3391  
3392  
3393  
3394  
3395  
3396  
3397  
3398  
3399  
3400  
3401

3402  
3403

## H.2.8 EVALUATION OF LSH METHODS UNDER ALIGNED SCORING FUNCTIONS

3404  
3405  
3406  
3407  
3408

To ensure a fair comparison across LSH-based retrieval strategies, we evaluate each method using graph embeddings specifically trained to align with its intended scoring function. That is, while GRAPHHASH is evaluated under transport-based supervision, FourierHashNet and Random Hyperplane (RH) methods are applied on embeddings trained for hinge and cosine-based scoring, respectively.

3409  
3410  
3411

**GRAPHHASH: Transport-Based Scoring with GNN Embeddings.** For GRAPHHASH, we use node-level embeddings produced by a GNN encoder, trained using a pairwise ranking loss (Eq. (G.2)) based on the transport distance  $\Delta(G_c, G_q)$  (Eq. (1)).

3412  
3413  
3414

For the baselines that require a single-vector representation of graphs, we adopt the GEN architecture from (Li et al., 2019), which aggregates node embeddings into a global graph-level vector via mean pooling.

3415  
3416  
3417  
3418  
3419

**FourierHashNet: Hinge Distance over Aggregated Graph Embeddings (GEN + FourierHash-Net).** FourierHashNet is designed for asymmetric hinge-based distances over global graph embeddings. We apply it on GEN representations trained using the ranking loss in Eq. (G.2), where  $\text{rel}(G_c, G_q) = \|\mathbf{a}_q - \mathbf{a}_c\|_+$ , and  $\mathbf{a}_q, \mathbf{a}_c$  denote the pooled graph embeddings. Here,  $[\cdot]_+$  is the ReLU function.

3420  
3421  
3422  
3423

**RH: Cosine Similarity-Based Hashing (GEN + RH).** To align with RH’s reliance on cosine similarity, we again use GEN-pooled embeddings and train them with the ranking loss in Eq. (G.2), setting  $\text{rel}(G_c, G_q) = -\cos(\mathbf{a}_q, \mathbf{a}_c)$ . This setup ensures that the learned representations are optimized for RH’s angle-based locality-sensitive hashing.

3424  
3425  
3426  
3427

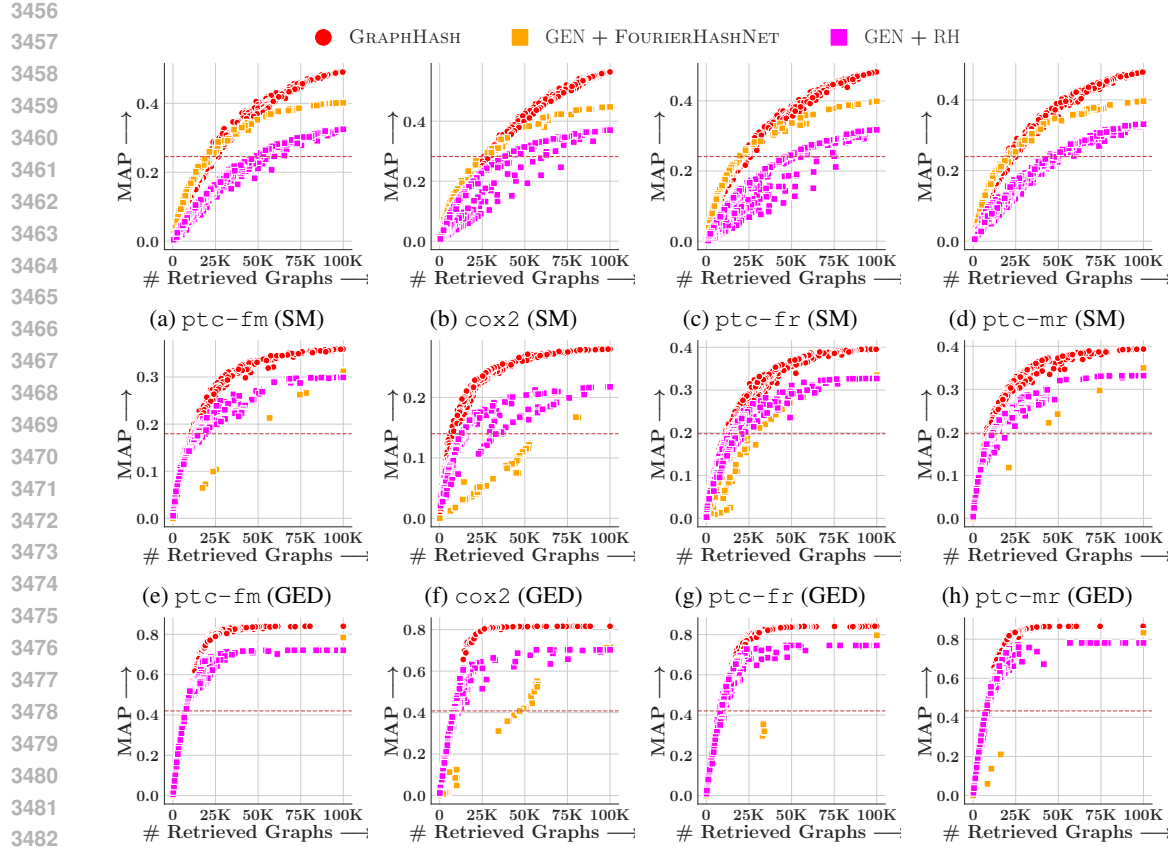
**Summary.** Each method is thus benchmarked under conditions it was designed for: transport distance with GRAPHHASH, hinge distance with FourierHashNet, and cosine similarity with RH. This isolates the performance of the retrieval mechanism from mismatches in training objectives or input embeddings.

3428  
3429

**Observations.** Figures 24 and 25 present retrieval performance across all datasets and supervision types. Figure 24 reports MAP trade-offs, while Figure 25 reports NDCG. We observe that:

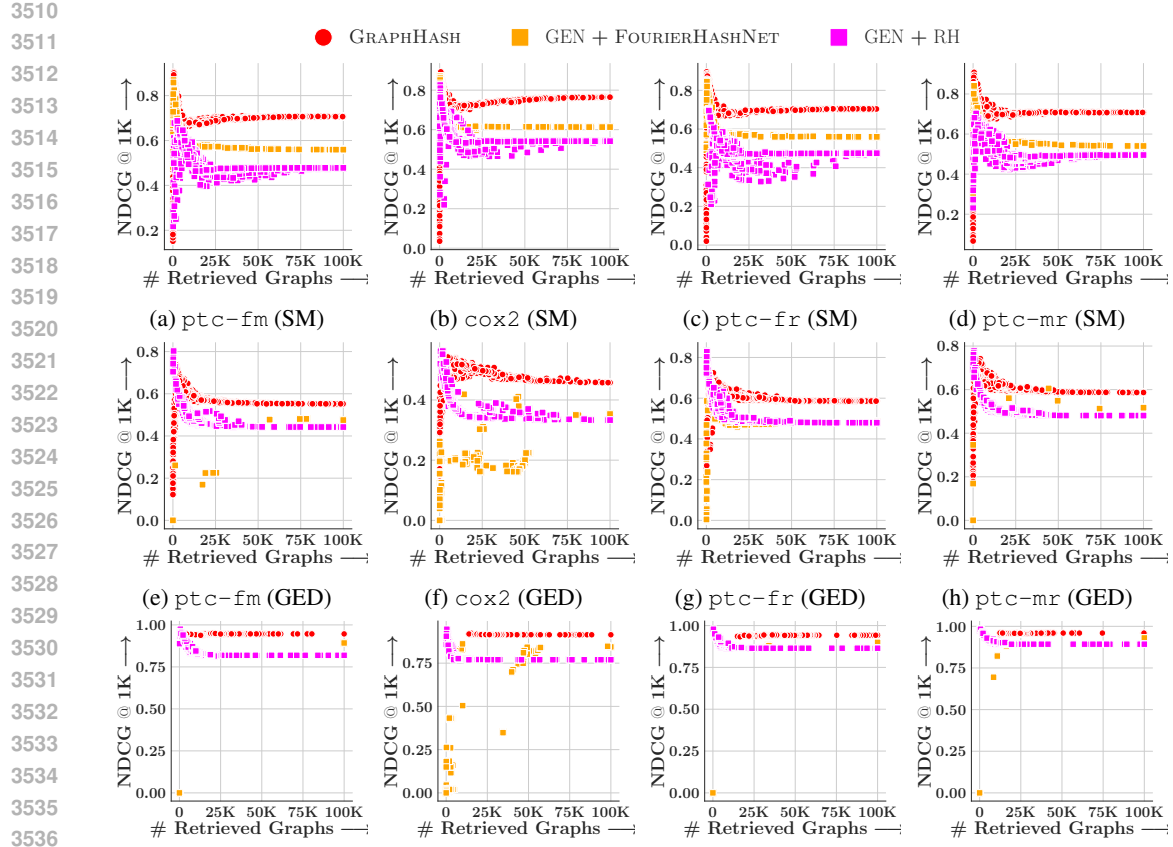
3430  
3431  
3432  
3433  
3434  
3435  
3436  
3437  
3438  
3439  
3440  
3441  
3442  
3443  
3444  
3445  
3446  
3447  
3448  
3449  
3450  
3451  
3452  
3453  
3454  
3455

1. **Exhaustive scores reveal superiority of transport-based supervision.** Across all datasets and similarity signals, GRAPHHASH consistently achieves higher exhaustive MAP and NDCG compared to both GEN + FourierHashNet and GEN + RH. This confirms that transport-based supervision captures a more powerful and fine-grained notion of graph relevance.
2. **RH shows significantly reduced variance when used with compatible supervision.** Unlike earlier results where RH was applied to transport-trained embeddings and exhibited high variability (Figure 4), the GEN + RH setup shows much smoother and more stable trade-offs. This emphasizes the importance of matching the embedding training signal to the retrieval method.
3. **FourierHashNet benefits from hinge-compatible embeddings.** When used with GEN-trained embeddings under hinge distance supervision, FourierHashNet exhibits broader coverage of the selectivity spectrum, yielding smoother MAP and NDCG trade-off curves. This again reinforces the value of scoring-function alignment between embedding training and LSH mechanism.
4. **Despite improvements, GRAPHHASH retains overall dominance.** Even though GEN-based variants show improved performance over their misaligned counterparts, they still fall short of GRAPHHASH in nearly all retrieval settings. This underscores the strength of the transport scoring model in both relevance estimation and downstream index quality.



(i) ptc-fm (Eq. cost GED) (j) cox2 (Eq. cost GED) (k) ptc-fr (Eq. cost GED)(l) ptc-mr (Eq. cost GED)

Figure 24: Trade-off between mean average precision (MAP) and number of retrieved graphs, for all the methods, *viz.*, GRAPHHASH, FourierHashNet (Roy et al., 2023) using GEN embeddings, Random Hyperplane (RH) (Charikar, 2002; Indyk et al., 1997) using GEN embeddings, across all datasets. Top row: Retrieval based on Subgraph Matching (SM); Middle row: Retrieval based on GED; Bottom row: Retrieval based on Equal cost GED ( $e_0 = 1$ ). Horizontal red line denotes 50% of exhaustive MAP. Our method shows a better trade-off than others in majority of the cases.



(i) ptc-fm (Eq. cost GED) (j) cox2 (Eq. cost GED) (k) ptc-fr (Eq. cost GED) (l) ptc-mr (Eq. cost GED)

Figure 25: Trade-off between NDCG at top 10000 and number of retrieved graphs, for all the methods, *viz.*, GRAPHHASH, FourierHashNet (Roy et al., 2023) using GEN embeddings, Random Hyperplane (RH) (Charikar, 2002; Indyk et al., 1997) using GEN embeddings, across all datasets. Top row: Retrieval based on Subgraph Matching (SM); Middle row: Retrieval based on GED; Bottom row: Retrieval based on Equal cost GED ( $e_{\bullet} = 1$ ). Our method shows a better trade-off than others in majority of the cases.